ANALYTICAL AND EXPERIMENTAL STUDY OF CRACKS EMANATING FROM AN ELLIPTICAL HOLE IN UNIDIRECTIONAL COMPOSITE MATERIAL

By

SAID ABDEL-MAABOUD KHALIL

A DISSERTATION PRESENTED TO THE GRADUATE SCHOOL
OF THE UNIVERSITY OF FLORIDA
IN PARTIAL FULFILLMENT OF THE REQUIREMENTS
FOR THE DEGREE OF DOCTOR OF PHILOSOPHY

UNIVERSITY OF FLORIDA

1984

Dedicated to

the loving memory of my father

and to

my mother, wife, and son

ACKNOWLEDGMENTS

The author would like to express his deep appreciation to all the members of his graduate committee for their assistance during the course of this research. Special thanks are extended to Dr. Chang-Tsan Sun, Chairman of the author's supervisory committee, for providing guidance, encouragement, and continuous support throughout the course of study.

Special thanks are extended to Dr. Lawrence E. Malvern, the co-chairman of the committee, for his many helpful comments and suggestions which aided the completion of this work. Thanks are also extended to Dr. U. H. Kurzweg, for his valuable advice and suggestions on the mathematical part.

Thanks are given to Dr. M. H. Clarkson and Dr. Robert Reed-Hill for their services on the committee. Special thanks are also extended to Dr. Robert L. Sierakowski, the previous co-chairman of the committee, for his financial support through the research assistantship in the Department of Engineering Sciences.

The author is particularly indebted to the Egyptian Ministry of Higher Education for the financial support of his graduate studies in the United States.

Again, special thanks go to Dr. Malvern for the financial support for the one-fourth time assistantship received in the last year of study.

Finally, the author wishes to thank his wife, his mother, and his late father for the encouragement, patience, understanding, and love that only a family can give.

TABLE OF CONTENTS

KEY TO SYMBOLS

The following list defines the principal symbols used in this dissertation and gives the sections where they are explained further. Other symbols are defined in context. Matrices are denoted by the symbols [ ] (for a rectangular matrix) and { } (for a column vector); $[\ ]^T$ indicates the transpose. Overbars ($\bar{\ }$) indicate a complex conjugate or a prescribed (known) value for specified quantities. Standard Cartesian tensor notation is used; repeated indices are to be summed, commas denote partial differentiation.

A: Area of the element (3.3.1; 3.3.2)

a_{ij}: The elastic constant for strain-stress matrix (2.1; 4.6; Appendix A)

$[B]$: Matrix relating strains and displacements (Appendix A)

$C_{ijk\ell}$, $[C]$: Constitutive (strain-stress) matrix (3.2; 3.3.1; 3.3.3; 3.3.4; 4.1)

e: Subscript or superscript indicating "element"

$E_{ijk\ell}$, $[E]$: Constitutive (stress-strain) matrix (3.1; 3.3.2; Appendix B)

G_{12}: Shear modulus (2.1; Appendix B)

$[K], [K^e]$: Super and regular element stiffness matrix (4.1; Appendix B)

$[L]$: Coefficient matrix for interpolation field variable (4.2; Appendix B)

m: Total number of elements (3.3.1; 3.3.2; 3.3.4)

n: Indicates the outward unit normal to the boundary (2.2)

n: Subscript indicates direction number (2.2), element number (3.3.1; 3.3.2; 2.3.4)

$\{q\}$: Vector of nodal field variables (displacements) for element (4.1; Appendix B)

r: Radial coordinate (4.2); superscript indicates "regular element" (3.3)

s: Natural coordinate for quadrilateral elements (3.3; 4.2); superscript indicates "singular element" (3.3.1; 3.3)

S: Interelement boundary surface (3.3; 3.3.1; 3.3.4)

S_σ, S_u: A portion of surface areas over which surface tractions or displacements are prescribed, respectively (3.1; 3.2; 3.3.1; 3.3.2; 3.3.3; 3.3.4)

$T_i, \{T\}$: Surface traction (3.1; 3.2)

u_i,{u}: Matrix for the displacement field in the element

$\tilde{u}_i$,{$\tilde{u}$}: Matrix for the interelement boundary displacement

V: General volume

x,y: Cartesian coordinates of two-dimensional elasticity

z, z_1, z_2: Complex variables (2.1; 4.2)

δ: Variational operator (3.1; 3.2); crack opening displacement (6.1)

θ: Angular coordinate

Θ: Angle between fiber direction and the x-axis (2.1) or fiber direction and loading axis (5.1, 7.2)

π_p, π_c: Total potential and complementary energy functionals (3.1; 3.2)

$(\pi_p)_m$: Modified potential energy functionals (3.3.1)

$(\pi_c)_m$: Modified complementary energy functionals (3.3.2)

σ_{ij},{σ}: Stress vector (2.1; 3.2;3.3.1)

τ_{xy}: Shear stress (2.1; 4.2)

ν_{12}: Poisson's ratio (2.1)

ν_i: The components of unit vector normal to the boundary where i=1,2 (3.1, 3.2) or i=x,y (4.2)

ϕ_1, ϕ_2: Airy stress functions (2.1; 4.2)

μ_1, μ_2: The roots of the characteristic equation (2.1; 4.2; 4.6)

β_1^*, β_2^*: The imaginary part of the roots μ_1, μ_2, respectively (2.1; 4.2; 4.5)

α_1^*, α_2^*: The real part of the roots μ_1, μ_2, respectively (2.1; 4.2; 4.5)

$\beta_j, \hat{\beta}_j$: The polynomial parameters for the stress functions (4.2; 4.5; 4.6)

$\varepsilon_{ij}, \{\varepsilon\}$: The symmetric strain tensor (3.1; 3.3.2; 3.3.3; Appendix B)

Abstract of Dissertation Presented to the Graduate School of the University of Florida in Partial Fulfillment of the Requirements for the Degree of Doctor of Philosophy

ANALYTICAL AND EXPERIMENTAL STUDY OF CRACKS EMANATING FROM AN ELLIPTICAL HOLE IN UNIDIRECTIONAL COMPOSITE MATERIAL

By

Said Abdel-Maaboud Khalil

December 1984

Chairman: C. T. Sun
Major Department: Engineering Sciences

This dissertation presents a fundamental study of stress fields around an elliptical hole, with and without cracks emanating from it, in unidirectional composite materials. The first part deals with the stress concentration factors. The second part discusses the stress intensity factors and energy release rate. Analytical study in the first part is based on the closed form of Savin's exact solution and the finite element solution (displacement model). Solutions of different anisotropic materials with different elliptical holes in shape and size are given.

The fracture mechanics part starts with a discussion of the application of different energy principles to the finite element technique. This discussion is followed by the

introduction of a new mathematical formulation of a finite element model. This model is based on the modified complementary energy principle in conjunction with the anisotropic elasticity and complex variable techniques.

Calculations of stress intensity factors for single mode and mixed mode fractures are included. Analytical and experimental evaluations of the strain energy release rate are determined. Analytical evaluation of the energy release rate is based on the finite element solution. The experimental part of this evaluation is based on the compliance calibration technique.

The finite element computer code developed here seems to offer accurate results in exceptionally efficient time. This code is capable of handling the two-dimensional fracture mechanics problem for isotropic and anisotropic cases with any number of cracks.

CHAPTER 1
INTRODUCTION

1.1 Motivation of the Research

The field of composite materials has experienced tremendous growth since the introduction of the so-called "advanced composites" in the early '60s. This growth has largely been the result of a desire to apply these high-strength and high-modulus but lightweight materials in air transportation systems and national defense as well as the automotive industry. This weight reduction factor should result in better energy conservation.

While the investigation and prediction of the elastic fracture behaviors of conventional engineering materials are fairly well documented and understood, the prediction of the fracture characteristics of anisotropic materials have presented engineers with some challenging problems.

Prediction of failure due to the presence of small cracks or flaws, especially in composite materials containing holes, has proven to be particularly difficult. Therefore, in order to overcome this difficulty we have to provide some reliable tools to serve engineering needs and to assess the safety of structural components. In making predictions of

this failure, we can facilitate the optimization of composite materials in terms of fracture mechanics parameters by estimating the high stresses near the crack tip.

Elastic fracture mechanics provides such tools to deal with these phenomena. A characterization of the crack with its local stress field by means of the stress intensity factor K_I, K_{II}, and K_{III} for different loading modes (to be discussed in the next section) can fulfill these needs.

Cracks emanating from holes represent one of the most common sources for catastropic failure. According to Karlsson and Backland [1], approximately one-third of all cracks were usually generated by high stress concentrations near the cutouts. In unidirectional composite materials, the location of these high stress concentrations not only depends on the type of load and the geometry of the hole, but also on the fiber orientation with respect to the geometric axes.

When attempting to analyze such a problem (especially with cracks) using an analytical method such as the conformal mapping technique to obtain an exact solution, we found that it was difficult to achieve. In more and more engineering situations today, it is necessary to obtain approximate numerical solutions to problems rather than exact closed-form solutions.

The finite element method is a powerful numerical analysis technique for obtaining approximate solutions to a

wide variety of engineering problems. This technique was first established in the early '60s. Since that time it has gained more popularity and recognition and has become an acceptable engineering analysis tool.

The desire to contribute to the further development of the finite element method was one motivation of this research. The necessity of analyzing the fracture mechanics problem in unidirectional reinforced composite material was the other motivation.

1.2 Fracture Mechanics: A Background Review

The field of fracture mechanics began in 1921 with the introduction of Griffith's theory [2]. This theory states that a crack will begin to propagate if the elastic energy released by its growth is greater than the energy required to create the fracture surfaces.

In 1958 Irwin extended Griffith's theory [2] into linear elastic fracture mechanics. He pointed out that there exist three kinematically admissible crack extension modes (Figure 1.1). The first mode is characterized by the motions of the crack surfaces that tend to separate symmetrically with respect to the plane occupied by the crack prior to deformation. It is called the opening mode (Mode I). The second mode concerns local deformation in which the crack surfaces glide over one another in opposite directions but

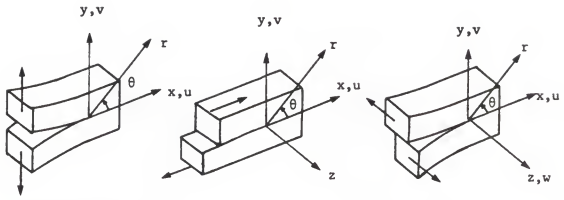

Mode I (Opening Mode) | Mode II (Sliding Mode) | Mode III (Tearing Mode)

Figure 1.1: Linear elastic fracture mechanics modes

in the same plane. It is called the sliding mode (Mode II). The final mode refers to the antiplane shear in which the movement of the crack surfaces can be related to the warping action of noncircular cylinders under torsion where the initially material points in one plane occupy different planes after deformation. It is called the tearing mode (Mode III). Each of these fracture modes has been mathematically modeled and well defined in terms of an important fracture parameter called the stress intensity factor (K). These stress intensity factors are the measure of the hypothetical elastic stress singularity at the crack tip, according to the classical theory of elasticity.

It is of considerable importance in many engineering problems to know the numerical value of the stress intensity factors, since there are critical values of K which determine whether or not the crack will propagate. In composite materials, sometimes the crack propagates in a different direction from the original crack direction. This leads us to the following brief discussion of some important fracture criteria.

The first approach is that of Sih and Chen [3] in which they formulate a strain energy density function, S, a measurement of the elastic energy field in the vicinity of a crack tip. This function, S, is a quadratic form of the Mode I and Mode II stress intensity factors and varies with the angle, θ, measured from the plane of the crack. It is then postulated that

1. Crack initiation will occur at the crack tip in a radial direction along which the strain energy density, S, is at a minimum.
2. The crack will begin to propagate when the density, S, reaches some critical value, S_{cr}, which is considered to be a material constant determined from experiment.

The second approach of fracture criteria is postulated as follows [4]:

1. The crack will propagate in the direction which causes the maximum energy release rate to occur.
2. The fracture will initiate when the release rate in that direction reaches a certain specified level.

The other approach to fracture criteria is to employ the method of compliance calibration to determine the strain energy release reate experimentally. This method will be discussed further in Chapter 6.

The critical value of the stress intensity factor is considered to be the fracture toughness. In spite of being considered as a material property in most of the conventional engineering materials, this fracture toughness is still a questionable property in composite materials.

Analysis of stress intensity factors at the crack tip has been the subject of many numerical applications. Some of these numerical schemes are methods including boundary collocation [5-7], conformal mapping [8], the analytical use of Green's function [9], and the finite element method. A literature review in the applications of the finite element method in fracture mechanics is introduced by Gallagher [10].

1.3 Objectives and Assumptions

The major goal of this research was to obtain a solution for the stresses near the crack tip for the problem of

cracks emanating from a hole in unidirectional fiber-reinforced composite materials. The secondary goal was that of developing a special finite element computer program to treat this crack tip singularity in an accurate and efficient way. The experimental verification for a simple case was the final goal.

The following considerations are the main basic assumptions throughout this research:

1. The composite materials are viewed from a macroscopic scale, i.e., to be characterized as homogeneous and rectilinearly anisotropic.
2. The stress singularities associated with the cracks are of the order $r^{-1/2}$, where r is the distance measured from the crack tip.
3. There are no thermal stresses or dynamic loading effects on the crack initiation.
4. There are small elastic strains during the deformation.
5. There is two-dimensional plane stress elasticity.

1.4 A Brief Review of Related Literatures

The increased demand for determining accurate predictions of stress fields in complex structures, such as the problem of cracks emanating from holes, has been the primary

concern for many investigators. This section will discuss some of the work related to that type of problem.

In 1956 Bowie [8] started one of the first analyses of this problem by solving the problem of equal cracks amanating from a circular hole in an isotropic infinite plate. The plate in his problem was subjected to uniaxial or biaxial stresses at infinity while the hole and crack boundaries were assumed to be free of tractions. His analysis was based on the conformal mapping of the inner star-cracked boundary onto a simple circle. Unfortunately, such a mapping for a realistic case of finite plate geometries would be extremely difficult to find. As cited in Oladimeji [11], the shortcoming of this method led Bowie in 1965 to apply a mapping-collocation technique to solve this problem for a finite sheet under uniaxial loading condition.

In 1971 Bowie and Freese [12] investigated the problem of a central crack in a rectangular sheet of orthotropic materials loaded under uniaxial tension. They extended the method of modified mapping-collocation, which was originally formulated for plane isotropic analysis, to solve the problem of plane anisotropy.

In 1971 Gandhi [7] treated the more general case of arbitrary orientations of the crack and the material principal symmetry axes relative to loading direction. He used the modified mapping-collocation technique to calculate the stress intensity factors for several orientations of cracks.

In 1974 Hsu [13] obtained the stress intensity factors at the root of a radial crack emanating from a circular hole in an infinite sheet, made of isotropic material, under inclined uniform tension. He used the Muskhelishvili formulation and the conformal mapping method in conjunction with the truncation technique to yield results for the combined mode fracture, K_I and K_{II}.

In 1980 Tirosh [14] used the energy release rate to predict the fracture strength of the central crack in unidirectional fiber-reinforced composite materials. He worked the problem of a crack in the fiber direction with the fiber direction being inclined to the loading direction. He then used mixed mode fracture analysis to solve for K_I and K_{II}.

In 1980 Wang and Yau [15] introduced an analytical study of cracks emanating from a circular hole in an off-axis unidirectional fiber-reinforced composite. They used the well-known path-independent J-integral for an arbitrary path which begins on one crack surface, encloses the crack tip, and terminates on the opposite surface of the crack.

1.5 Dissertation Overview and Contributions

The following areas have been investigated in detail throughout this work:

1. Review of Savin's classical solution.

2. Review of some variational principles and their applications to the finite element method.
3. Development of a new mathematical formulation in application of the finite element method to fracture mechanics.
4. An experimental verification of a simple case.

The first area covered in this work is a review of the classical elliptical problem (an elliptical hole in the center of an anisotropic infinite plate loaded under the state of simple tensile stress) which was solved in closed-form solution by Savin [16] in 1939. This solution is presented in Chapter 2. The objectives of this review are to achieve a full understanding of this analytical technique, which can lead to a similar formation in adapting a new numerical scheme. In addition, Savin's closed-form solution has been used for checking the numerical method for the problem of an elliptical hole in anisotropic media. The other reason for presenting this classical solution is to examine and compare the stress intensity factor in different composite materials under the same loading condition.

The second area covered is a review of some existing and available methods in variational principles (Chapter 3) and a discussion of their application in finite element

analysis. A review of the literature concerning such applications indicates that most of the work in this area falls into two main categories. One is for the characterization of fracture mechanics behavior in isotropic materials, where the presence of a single and/or a mixed mode is included. The other category involves the study of fracture mechanics in composite materials. In this category, the literature has emphasized a single mode loading and the case of orthotropic materials, when the material principal axes coincide with the geometrical axes, with the crack in one of the material principal directions. By comparison, mixed mode fracture and generally anisotropic behavior have received little attention.

In this work a new modified variational principle has been extended and presented in Chapter 4. This technique is then used to solve the problem of cracks emanating from a hole in a unidirectional fiber-reinforced composite. This mathematical formulation and finite element computer code, which is listed in Appendix E, are the main contributions of this work.

In Chapter 5 we present some results from Savin's solution (exact solution) and the finite element solution (approximate solution) for some practical problems.

In Chapter 6, an experimental program carried out to seek some comparison between the numerical prediction of

the energy release rate and its experimental evaluation for a simple case is discussed.

Finally, a discussion and conclusion is given in Chapter 7, in addition to some suggestions for further work and research related to this area.

CHAPTER 2
REVIEW OF CLASSICAL SOLUTION BY USING THE METHOD OF COMPLEX VARIABLES

The main purpose of this work is to study the problem of cracks emanating from an elliptical hole in a unidirectional fiber-reinforced composite material. We start from the general elasticity formulation of a related but simple problem. The problem is to determine the stresses in a homogeneous anisotropic plate weakened by an elliptical hole at the center of the plate subjected to the application of a uniform tension stress of intensity P at infinity.

The solution of this problem will be used as the datum line for checking the numerical program, when we apply it to such a simple case. The numerical program used in this research is to apply general elasticity theory in conjunction with the principle of minimum potential energy and the modified principle of minimum complementary energy to formulate a finite element technique.

The unidirectional composite material is considered as an orthotropic material. In general we have six independent constants when we apply Hook's law in a three-dimensional element. There are four independent constants for a two-dimensional problem which will be our case

of study. For the case when the fiber direction is not parallel to geometric axes, there are six elastic constants, which can be expressed in terms of the original four constants. Therefore, for the two-dimensional case there are only four independent material constants.

In this chapter the formulation of the elasticity problem using Savin's procedure [17] for the complex variables representation of the classical theory of elasticity will be discussed. Then the solution for the stress distribution in an infinitely large elastic plate with a traction-free elliptical hole under the state of simple tension at infinity in the direction of the X-axis is presented.

2.1 Formulation of the Problem

In this section all the fundamental elasticity equations to formulate the so-called "first fundamental problem" for anisotropic generalized plane stress will be stated.

We start from the generalized elasticity law (Hooke's law) for orthotropic media, referred to the symmetry axes,

$$\begin{Bmatrix} \varepsilon_1 \\ \varepsilon_2 \\ \gamma_{12} \end{Bmatrix} = \begin{bmatrix} S_{11} & S_{12} & 0 \\ S_{12} & S_{22} & 0 \\ 0 & 0 & S_{66} \end{bmatrix} \begin{Bmatrix} \sigma_1 \\ \sigma_2 \\ \tau_{12} \end{Bmatrix} \tag{2.1}$$

with four independent elastic constants S_{11}, S_{12}, S_{22}, and S_{66}, as mentioned before, where

$$S_{11} = 1/E_1, \quad S_{12} = -\nu_{12}/E_1,$$

$$S_{22} = 1/E_2, \quad S_{66} = 1/G_{12}$$

For the case that the fiber direction does not coincide with the geometric axes as shown in Figure 2.1, the following transformation is considered:

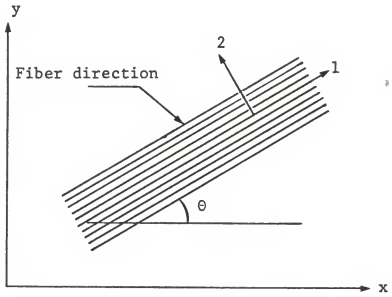

Figure 2.1: Fiber direction is inclined to x-axis by an angle θ

The transformation for the stresses between x-y axes and the 1-2 axes will be

$$\begin{Bmatrix} \sigma_x \\ \sigma_y \\ \tau_{xy} \end{Bmatrix} = \begin{bmatrix} \cos^2\theta & \sin^2\theta & -2\sin\theta & \cos\theta \\ \sin^2\theta & \cos^2\theta & 2\sin\theta & \cos\theta \\ \sin\theta\cos\theta & -\sin\theta\cos\theta & \cos^2\theta - & \sin^2\theta \end{bmatrix} \begin{Bmatrix} \sigma_1 \\ \sigma_2 \\ \tau_{12} \end{Bmatrix} \qquad (2.2)$$

Similarly, the transformation for the strains is given by the expression

$$\begin{Bmatrix} \varepsilon_x \\ \varepsilon_y \\ \frac{1}{2}\gamma_{xy} \end{Bmatrix} = \begin{bmatrix} \cos^2\theta & \sin^2\theta & -2\sin\theta & \cos\theta \\ \sin^2\theta & \cos^2\theta & 2\sin\theta & \cos\theta \\ \sin\theta\cos\theta & -\sin\theta\cos\theta & \cos^2\theta - & \sin^2\theta \end{bmatrix} \begin{Bmatrix} \varepsilon_1 \\ \varepsilon_2 \\ \frac{1}{2}\gamma_{12} \end{Bmatrix} \qquad (2.3)$$

Substitution of Equations (2.2) and (2.3) into Equation (2.1) gives the generalized plane-stress Hooke's Law referred to arbitrary X- and Y-axes,

$$\begin{Bmatrix} \varepsilon_x \\ \varepsilon_y \\ \gamma_{xy} \end{Bmatrix} = \begin{bmatrix} a_{11} & a_{12} & a_{16} \\ a_{12} & a_{22} & a_{26} \\ a_{16} & a_{26} & a_{66} \end{bmatrix} \begin{Bmatrix} \sigma_x \\ \sigma_y \\ \tau_{xy} \end{Bmatrix} \qquad (2.4)$$

Notice that the coefficients of the stress-strain matrix in this case are all nonzero, which is similar to

a generally anisotropic case, but these coefficients are not independent. The expressions of these coefficients in terms of the four basic constants will be given in Appendix A.

The stress components in a continuous elastic medium in a state of equilibrium, with no body force, satisfy the equations of equilibrium,

$$\frac{\partial \sigma_x}{\partial x} + \frac{\partial \tau_{xy}}{\partial y} = 0$$
$$\frac{\partial \tau_{yx}}{\partial x} + \frac{\partial \sigma_y}{\partial y} = 0 \tag{2.5}$$

In the case of small strains, the strain-displacement relations are

$$\varepsilon_x = \frac{\partial u_x}{\partial x}, \qquad \varepsilon_y = \frac{\partial u_y}{\partial y},$$
$$\varepsilon_{xy} = \frac{1}{2}\left(\frac{\partial u_x}{\partial y} + \frac{\partial u_y}{\partial x}\right) \tag{2.6}$$

With Equations (2.6) the displacement u_x and u_y can be eliminated to obtain the compatibility equation in terms of ε_x, ε_y, and γ_{xy}

$$\frac{\partial^2 \varepsilon_x}{\partial^2 y} + \frac{\partial^2 \varepsilon_y}{\partial^2 x} - 2\,\frac{\partial^2 \varepsilon_{xy}}{\partial y\,\partial x} = 0 \tag{2.7}$$

Substitution of Equation (2.4) into Equation (2.7) gives

$$\frac{\partial^2}{\partial y^2}\left(a_{11}\sigma_x + a_{12}\sigma_y + a_{16}\tau_{xy}\right)$$

$$+ \frac{\partial^2}{\partial x^2}\left(a_{12}\sigma_x + a_{22}\sigma_y + a_{26}\tau_{xy}\right)$$

$$- \frac{\partial^2}{\partial x\,\partial y}\left(a_{16}\sigma_x + a_{26}\sigma_y + a_{66}\tau_{xy}\right) = 0 \quad (2.8)$$

According to the theory of elasticity, any state of stress must satisfy equilibrium equations, compatibility equation, and boundary conditions. So, by making use of the Airy[1] stress function F(x,y),

$$\sigma_x = \frac{\partial^2 F}{\partial y^2}, \quad \sigma_y = \frac{\partial^2 F}{\partial x^2}, \quad \tau_{xy} = -\frac{\partial^2 F}{\partial x\,\partial y} \quad (2.9)$$

which automatically satisfies the equilibrium equations, and then substituting F(x,y) into the compatibility equation (2.8), we obtain

$$a_{22}\frac{\partial^4 F}{\partial x^4} - 2a_{26}\frac{\partial^4 F}{\partial x^2\,\partial y^2} + \left(2a_{12} + a_{66}\right)\frac{\partial^4 F}{\partial x^2\,\partial y^2}$$

$$- 2a_{16}\frac{\partial^4 F}{\partial x^2\,\partial y^2} + a_{11}\frac{\partial^4 F}{\partial y^4} = 0 \quad (2.10)$$

---

[1]As first noted by a British astronomer G. B. Airy in 1862.

which can be written in the following symbolic form

$$D_1 D_2 D_3 D_4 F(x,y) = 0$$

where

$$D_k = \frac{\partial}{\partial y} - \mu_k \frac{\partial}{\partial x}, \qquad k = 1, 2, 3, 4$$

and μ_k are the roots of the characteristic equation

$$a_{11}\mu^4 - 2a_{16}\mu^3 + \left(2a_{12} + a_{66}\right)\mu^2 - 2a_{26}\mu + a_{22} = 0 \tag{2.11}$$

On the basis of energy considerations, Lekhnitskii [18] showed that the roots of the above equation fall into one of the following cases:

Case 1

The roots are pairwise different

$$\mu_1 = \alpha_1^* + i\beta_1^* \quad \text{and} \quad \mu_2 = \alpha_2^* + i\beta_2^* \tag{2.12a}$$

Case 2

The roots are pairwise equal

$$\mu_1 = \mu_2 = \mu = \alpha^* + i\beta^* \tag{2.12b}$$

where α_1^*, α_2^*, β_1^*, and β_2^* are real constants and $i = \sqrt{-1}$.

In general, the stress function $F(x,y)$ can be expressed by two arbitrary analytical functions $\phi_1(z_1)$, $\phi_2(z_2)$ as follows:

Case 1

We have $z_1 = x + \mu_1 y$, $z_2 = x + \mu_2 y$

$$F(x,y) = 2\,\mathrm{Re}[\phi_1(z_1) + \phi_2(z_2)] \tag{2.13a}$$

Case 2

We have $z_1 = z_2 = x + \mu y$

$$F(x,y) = 2\,\mathrm{Re}[\phi_1(z_1) + \bar{z}\phi_2(z_2)] \tag{2.13b}$$

where Re denotes the real part of the complex variables and the superbar ($\bar{\ }$) indicates complex conjugate. Now let

$$\phi_k(z_k) = \frac{\partial F(z_k)}{\partial z_k}, \qquad k=1,2 \tag{2.13c}$$

Substituting (2.13a) into (2.9), we get

$$\begin{aligned}
\sigma_x(x,y) &= 2\mathrm{Re}\left(\frac{\partial \phi_1(z_1)}{\partial z_1}\mu_1^2 + \frac{\partial \phi_2(z_2)}{\partial z_2}\mu_2^2\right) \\
\sigma_y(x,y) &= 2\mathrm{Re}\left(\frac{\partial \phi_1(z_1)}{\partial z_1} + \frac{\partial \phi_2(z_2)}{\partial z_2}\right) \\
\tau_{xy}(x,y) &= -\,2\mathrm{Re}\left(\frac{\partial \phi_1(z_1)}{\partial z_1}\mu_1 + \frac{\partial \phi_2(z_2)}{\partial z_2}\mu_2\right)
\end{aligned} \tag{2.14}$$

Substitution of Equation (2.14) into (2.4) and integration of the resulting equation leads to the following expression for the displacements u and v in x and y directions, respectively,

$$u = 2\mathrm{Re}[P_1\phi_1(z_1) + P_2\phi_2(z_2)] - y\beta_r + \beta_u$$
$$v = 2\mathrm{Re}[r_1\phi_1(z_1) + r_2\phi_2(z_2)] + x\beta_r + \beta_v \qquad (2.15)$$

where the quantities P_j, r_j ($j=1,2$) are defined by

$$P_j = a_{11}\mu_j^2 + a_{12} - a_{16}\mu_j \qquad j=1,2$$
$$r_j = (a_{12}\mu_j^2 + a_{22} - a_{26}\mu_j)/\mu_j \qquad j=1,2 \qquad (2.16)$$

and the additional terms $(-y\beta_r + \beta_u)$ and $(x\beta_r + \beta_v)$ of Equation (2.15) are expressions of the rigid body motion of the body. The coefficient, β_r, is linked to the rotation of the body, while β_u and β_v are linked to the translation of the body in x and y directions, respectively.

2.2 The Boundary Conditions

The stress function F(x,y) must satisfy certain boundary conditions on the contour of the investigated area. Let the component of the traction vector in the x-direction be X_n and in the y-direction be Y_n as shown in Figure 2.2, then

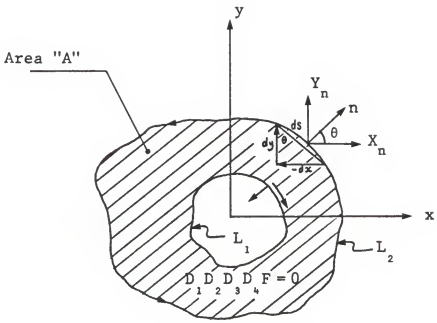

Figure 2.2: Multiply connected region

$$X_n = \sigma_x \cos\theta + \tau_{xy} \sin\theta$$
$$Y_n = \tau_{xy} \cos\theta + \sigma_y \sin\theta \qquad (2.17)$$

From Figure 2.2, we get

$$\cos\theta = dy/dS \ , \qquad \sin\theta = -dx/dS$$

Substituting the above values for $\sin\theta$ and $\cos\theta$ into Equation (2.17) and using Equation (2.9), we get

$$X_n = \frac{\partial^2 F}{\partial y^2}\frac{dy}{dS} + \frac{\partial^2 F}{\partial x\,\partial y}\frac{dx}{dS} = \frac{d}{dS}\left(\frac{\partial F}{\partial y}\right)$$
$$Y_n = -\frac{\partial^2 F}{\partial x\,\partial y}\frac{dy}{dS} - \frac{\partial^2 F}{\partial x^2}\frac{dx}{dS} = -\frac{d}{dS}\left(\frac{\partial F}{\partial x}\right) \qquad (2.18)$$

By integrating Equations (2.18) with respect to S, we get

$$\frac{\partial F}{\partial x} = -\int_0^S Y_n \, dS + c_1 , \quad \frac{\partial F}{\partial y} = \int_0^S X_n \, dS + c_2 \tag{2.19}$$

where c_1 and c_2 are arbitrary real constants. By substituting Equation (2.13) into Equation (2.18), we get

$$2\mathrm{Re}[\Phi_1(z_1) + \Phi_2(z_2)] = \mp \int_0^S Y_n \, dS + c_1 = f_1$$
$$2\mathrm{Re}[\mu_1 \Phi_1(z_1) + \mu_2 \Phi_2(z_2)] = \mp \int_0^S X_n \, dS + c_2 = f_2 \tag{2.20}$$

where the upper sign corresponds to the outer boundary L_2 and the lower sign corresponds to the inner boundary L_1, and the functions Φ_k are as defined in Equation (2.13c).

2.3 Solution of the Problem

In this section we shall discuss the solution of the problem of an elliptical hole in an anisotropic plate under unidirectional tensile stress. We have seen from Equation (2.20) that the solution of the fundamental equation (2.10) of the theory of elasticity in a region which given traction boundary conditions on the boundary of the region was reduced to the determination of two analytical functions $\Phi_1(z_1)$, and $\Phi_2(z_2)$ in the region for given boundary values of Φ_1 and Φ_2 on the boundary of the investigated area.

Let us assume the two analytical functions to be in the form

$$\Phi_1(z_1) = A_1 z_1 + \phi_1^{\circ}(z_1)$$
$$\Phi_2(z_2) = A_2 z_2 + \phi_2^{\circ}(z_2) \tag{2.21}$$

where $A_1 = B_1^* + iC_1^*$ and $A_2 = B_2^* + iC_2^*$ are two complex constants to be determined from the boundary condition at infinity; and $\phi_1^{\circ}(z_1)$, $\phi_2^{\circ}(z_2)$ are two single-valued functions which can be expressed in the form of Laurent's series.

We insert Equations (2.21) into Equations (2.14) and evaluate at infinity, where the components of the external stresses are

$$\sigma_x = P, \qquad \sigma_y = 0, \qquad \tau_{xy} = 0 \tag{2.22}$$

By carrying out this substitution, we obtain the following linear system of equations (three equations with four unknowns):

$$2\mathrm{Re}[\mu_1^2(B_1^* + iC_1^*) + \mu_2^2(B_2^* + iC_2^*)] = P$$
$$2\mathrm{Re}[(B_1^* + iC_1^*) + (B_2^* + iC_2^*)] = 0 \tag{2.23}$$
$$-2\mathrm{Re}[\mu_1(B_1^* + iC_1^*) + \mu_2(B_2^* + iC_2^*)] = 0$$

In order to find a solution, one of the unknown B_1^*, C_1^*, B_2^*, and C_2^* has to be chosen arbitrarily. So, let us choose

$C_1^* = 0$ and solve the system of Equations (2.23) to get

$$B_1^* = P/\{2[(\alpha_2^* - \alpha_1^*)^2 + (\beta_2^{*2} - \beta_2^{*2})]\}$$

$$B_2^* = -P/\{2[(\alpha_2^* - \alpha_1^*) + (\beta_2^{*2} - \beta_1^{*2})]\} = - B_1^*$$

$$C_2^* = P(\alpha_1^* - \alpha_2^*)/\{2\beta_2^*[(\alpha_2^* - \alpha_1^*)^2 + (\beta_2^{*2} - \beta_1^{*2})]\} = (\alpha_1^* - \alpha_2^*)B_1^*/\beta_2^* \tag{2.24}$$

Thus, Equation (2.21) becomes

$$\Phi_1(z_1) = B_1^* z_1 + \phi_1^\circ(z_1)$$

$$\Phi_2(z_2) = B_1^* w\, z_2 + \phi_2^\circ(z_2) \tag{2.25}$$

where

$$w = - 1 + i\,\frac{\alpha_1^* - \alpha_2^*}{\beta_2^*}$$

After substituting Equation (2.25) into (2.20), evaluating at the inner boundary, and taking into consideration that the contour of the hole is stress free, i.e., $f_1 = f_2 = 0$, we can write

$$2\mathrm{Re}[\phi_1^{\circ}(z_1) + \phi_2^{\circ}(z_2)] = f_1^{\circ}(\theta)$$

$$2\mathrm{Re}[\mu_1\phi_1^{\circ}(z_1) + \mu_2\phi_2^{\circ}(z_2)] = f_2^{\circ}(\theta) \tag{2.26}$$

where

$$f_1^{\circ}(\theta) = -B_1^{*}2\mathrm{Re}[z_1 + w\, z_2]$$

$$f_2^{\circ}(\theta) = -B_1^{*}2\mathrm{Re}[\mu_1 z_1 + \mu_2 w\, z_2] \tag{2.27}$$

After substituting Equations (2.25) into the stress formulas of Equations (2.14), using the value of B_1^{*} from Equation (2.24) and simplifying, we obtain the following formulas for σ_x, σ_y, and τ_{xy}

$$\sigma_x = P + 2\mathrm{Re}\left[\mu_1^2\frac{\partial\phi_1^{\circ}(z_1)}{\partial z_1} + \mu_2^2\frac{\partial\phi_2^{\circ}(z_2)}{\partial z_2}\right]$$

$$\sigma_y = 2\mathrm{Re}\left[\frac{\partial\phi_1^{\circ}(z_1)}{\partial z_1} + \frac{\partial\phi_2^{\circ}(z_2)}{\partial z_2}\right] \tag{2.28}$$

$$\tau_{xy} = -2\mathrm{Re}\left[\mu_1\frac{\partial\phi_1^{\circ}(z_1)}{\partial z_1} + \mu_2\frac{\partial\phi_2^{\circ}(z_2)}{\partial z_2}\right]$$

By making use of the well-known Schwartz formula [19], which determines a holomorphic function inside a

circular region in terms of a continuous real function on its boundary, then a solution of Equation (2.25) can be determined. Using Muskhelishvili's notation [19], we can write the Schwartz formula as

$$F(\zeta) = \frac{1}{2\pi i} \int_{\gamma} U(\theta) \frac{\sigma + \zeta}{\sigma - \zeta} \frac{d\sigma}{\sigma} + i\alpha_0 \qquad (2.29)$$

where $U(\theta)$ is the real part of $F(\zeta)$ evaluated on the contour γ of the unit circle $|\zeta| = 1$, and α_0 is some real constant.

To use this formula in the case of the elliptical hole, a mapping function has to be introduced. It is known from the theory of functions of a complex variable that the mapping of an area A, consisting of the outside of an elliptical hole, onto the inside of a unit circle, can be obtained by means of the function

$$z = \omega(\zeta) = \frac{1}{2}\left[(a - b)\zeta + (a + b)\frac{1}{\zeta}\right] \qquad (2.30)$$

where $z = x + iy$, $\zeta = \xi + i\eta$, and a,b are the semi-axes of the ellipse.

We introduce two additional complex planes z_1 and z_2 related to the z-plane by affine transformation $z_1 = x + \mu_1 y$, $z_2 = x + \mu_2 y$, where μ_1 and μ_2 are as defined in Equation (2.12a). The known mapping function $z = \omega(\zeta)$ then formulates the functions which give a conformal mapping of the z_1- and z_2-planes onto the interior of the unit circle.

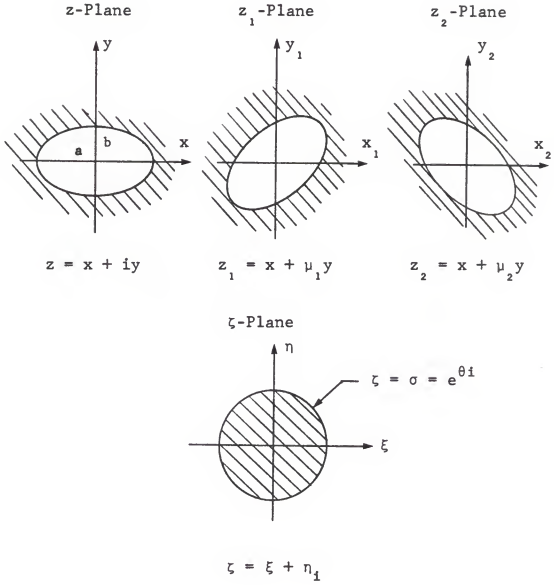

The planes z_1 and z_2 are obtained from z-plane by means of an affine transformation where

for the z_1-plane: $x_1 = x + \alpha_1^* y, \quad y_1 = \beta_1^* y$

for the z_2-plane: $x_2 = x + \alpha_2^* y, \quad y_2 = \beta_2^* y$

$$\mu_1 = \alpha_1^* + i\beta_1^* \qquad \mu_2 = \alpha_2^* + i\beta_2^*$$

Figure 2.3: Mapping the outside of an elliptical hole, on the inside of a unit circle

$$z_1 = \omega_1(\zeta) = \frac{1}{2}\left[(a + i\mu_1 b)\zeta + (a - i\mu_1 b)\frac{1}{\zeta}\right]$$
$$z_2 = \omega_2(\zeta) = \frac{1}{2}\left[(a + i\mu_2 b)\zeta + (a - i\mu_2 b)\frac{1}{\zeta}\right] \tag{2.31}$$

Substituting Equation (2.31) into Equation (2.27), we obtain the expressions for the continuous real functions evaluated on the contour of the unit circle

$$f_1^{\circ}(\theta) = - B_1^{*}2\mathrm{Re}[Z_1 + w Z_2]$$
$$f_2^{\circ}(\theta) = - B_1^{*}2\mathrm{Re}[\mu_1 Z_1 + w\mu_2 Z_2] \tag{2.32}$$

where

$$Z_1 = \frac{1}{2}(a + i\mu_1 b)\sigma + \frac{1}{2}(a - i\mu_1 b)\frac{1}{\sigma}$$

$$Z_2 = \frac{1}{2}(a + i\mu_2 b)\sigma + \frac{1}{2}(a - i\mu_2 b)\frac{1}{\sigma}$$

Using the complex conjugate method to separate the real and imaginary parts of Equation (2.31) and carrying out algebraic details, we obtain the following expression:

$$f_1^{\circ}(\theta) = - \frac{1}{2} B_1^{*}k_1/\sigma$$
$$f_2^{\circ}(\theta) = - \frac{1}{2} P\, b\sigma i + k_2/\sigma \tag{2.33}$$

where k_1 and k_2 are two complex constants.

By using the Schwartz formula, Equation (2.29), and taking into consideration that

$$\int_{\gamma} \sigma \frac{\sigma + \xi}{\sigma - \xi} \frac{d\sigma}{\sigma} = 4\pi i\xi \; ; \qquad \int_{\gamma} \frac{1}{\sigma} \frac{\sigma + \xi}{\sigma - \xi} \frac{d\sigma}{\sigma} = 0$$

we obtain, with the help of Equations (2.13), (2.26), and (2.29), expressions for the two analytical functions $\phi_1^\circ, \phi_2^\circ$ in the ζ-plane:

$$\phi_1^\circ(\zeta) = - \frac{i}{2(\mu_1 - \mu_2)} \frac{P}{b} \zeta \tag{2.34}$$

$$\phi_2^\circ(\zeta) = + \frac{i}{2(\mu_1 - \mu_2)} \frac{P}{b} \zeta \tag{2.35}$$

Let us go back to the original z_1- and z_2-planes. We invert the transformation of Equation (2.31) to give

$$\zeta = \frac{a - i\mu_1 b}{z_1 + \sqrt{z_1^2 - (a^2 + \mu_1^2 b^2)}} \tag{2.36}$$

$$\zeta = \frac{a - i\mu_2 b}{z_2 + \sqrt{z_2^2 - (a^2 + \mu_2 b^2)}} \tag{2.37}$$

and then, inserting for ζ its value from Equation (2.36) into Equation (2.34), and the value from Equation (2.37) into Equation (2.35), gives

$$\phi_1^{\circ}(z_1) = -\frac{i\,P\,b}{2(\mu_1 - \mu_2)} \frac{a - i\mu_1 b}{z_1 + \sqrt{z_1^2 - (a^2 + \mu_1^2 b^2)}}$$

$$\phi_2^{\circ}(z_2) = \frac{i\,P\,b}{2(\mu_1 - \mu_2)} \frac{a - i\mu_2 b}{z_2 + \sqrt{z_2^2 - (a^2 + \mu_2^2 b^2)}} \qquad (2.38)$$

By differentiating the functions of Equation (2.38), we obtain

$$\frac{\partial \phi_1^{\circ}(z_1)}{\partial z_1} = -\frac{i\,P\,b\,F_1^*}{2(\mu_1 - \mu_2)(a + i\mu_1 b)}$$

$$\frac{\partial \phi_2^{\circ}(z_2)}{\partial z_2} = \frac{i\,P\,b\,F_2^*}{2(\mu_1 - \mu_2)(a + i\mu_1 b)} \qquad (2.39)$$

where

$$F_1^* = 1 - \frac{z_1}{\sqrt{z_1^2 - (a^2 + \mu_1^2 b^2)}}$$

$$F_2^* = 1 - \frac{z_2}{\sqrt{z_2^2 - (a^2 + \mu_2^2 b^2)}}$$

Substituting Equation (2.39) into the stress formula (2.28), yields the general expression for the stress components in Cartesian coordinates

$$\sigma_x(x,y) = P\left\{1 + b \cdot \mathrm{Im}\left[\frac{1}{\mu_1 - \mu_2}\left(\frac{\mu_1^2 F_1^*}{a + i\mu_1 b} - \frac{\mu_2^2 F_2^*}{a + i\mu_2 b}\right)\right]\right\}$$

$$\sigma_y(x,y) = P\,B \cdot \mathrm{Im}\left[\frac{1}{\mu_1 - \mu_2}\left(\frac{F_1^*}{a + i\mu_1 b} - \frac{F_2^*}{a + i\mu_2 b}\right)\right] \qquad (2.40)$$

$$\tau_{xy}(x,y) = -P\,b \cdot \mathrm{Im}\left[\frac{1}{\mu_1 - \mu_2}\left(\frac{\mu_1 F_1^*}{a + i\mu_1 b} - \frac{\mu_2 F_2^*}{a + i\mu_2 b}\right)\right]$$

where Im denotes the imaginary part of a complex variable. Since it is assumed that no external forces act on the contour of the elliptical hole, then the normal stress and the shear stress on that contour should vanish. The only remaining stress component in the normal-tangential coordinate directions will be the internal normal stress acting on planes perpendicular to the tangential direction. To obtain a clear picture of the changes of this stress due to anisotropy, it is necessary to transfer the components of the stresses in Equation (2.40) to elliptical coordinates by using the following transformation [21]:

$$\sigma_\xi = \frac{1}{2}(\sigma_x + \sigma_y) + \frac{1}{2}(\sigma_x - \sigma_y)\cos 2\alpha + \tau_{xy}\sin 2\alpha$$

$$\sigma_\eta = \frac{1}{2}(\sigma_x + \sigma_y) - \frac{1}{2}(\sigma_x - \sigma_y)\cos 2\alpha - \tau_{xy}\sin 2\alpha \qquad (2.41)$$

$$\tau_{\xi\eta} = -\frac{1}{2}(\sigma_x - \sigma_y)\sin 2\alpha + \tau_{xy}\cos 2\alpha$$

where ξ and ζ are the normal and the tangential axes to elliptic boundary and θ is the angle between the x-axis and the normal to elliptic boundary as indicated in Figure 2.4, where

$$\tan \alpha = \frac{b}{a} \tan \theta \tag{2.42}$$

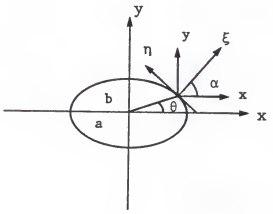

Figure 2.4: Coordinate system for elliptic hole.

To achieve this objective we introduce the parametric form of the elliptical contour

$$x = a \cos \theta \ , \qquad y = b \sin \theta \tag{2.43}$$

and calculate the components of stresses σ_x, σ_y, and τ_{xy} as functions of θ on the contour before using the transformation of Equation (2.41).

CHAPTER 3
ENERGY PRINCIPLES AND FINITE-ELEMENT MODEL

The main purpose of this chapter is to review the fundamental bases of many existing finite element procedures. It is worthwhile to examine how the energy approaches in variational principles play such important roles in obtaining approximate elasticity solutions to boundary value problems. These variational principles are based on the concept of a certain integral expression (π). When this expression has a stationary value ($\delta\pi = 0$), the remaining elasticity requirements are satisfied, thus giving a complete solution.

A traditional application of the energy principles to structural analysis is the Rayleigh-Ritz method, in which a single trial function is constructed to approximate either the displacements or stresses, depending upon the functional to be used. Since this trial function must span the entire structure, it often becomes lengthy and complicated—an inconvenient aspect. In an attempt to overcome this drawback, the finite element method uses several trial functions, each usually simple, and each defined over only a portion of the structure. This piecewise estimation is the essence of the finite element method. If the estimation pieces

"finite elements" are then properly joined, a satisfactory approximation can be expected.

There are two classical basic variational principles in structural mechanics. They are based upon the following principles:

1. Potential energy principle
2. Complementary energy principle

The other energy principles have been generated from the previous ones, in the form of modified and/or mixed energy formulations. Some of the other energy principles will be discussed later in this chapter.

3.1 Potential Energy Principle

To introduce this principle we start from the potential energy functional (π_p) as given by

$$\pi_p = U + V \tag{3.1}$$

where U is the internal strain energy and V is the potential energy functional of external work done by the applied loads. Then, a definition of the principle of potential energy can be given, as stated by Desai and Abel [22]:

> Of all possible displacement configurations a body can assume which satisfy compatibility and the constraints or kinematic boundary conditions, the configuration satisfying equilibrium makes the potential energy assume a minimum value. (p. 58)

Here it is important to note that variations of displacements are taken while forces and stresses are assumed constant. Thus, $\delta\pi_p = \delta U + \delta V = 0$, and it is minimal if $\delta^2\pi_p > 0$. In order to base a solution on this principle, the potential energy functional is defined as a function of the displacements and strains in the following fashion (with no body force):

$$\pi_p = \int_V \frac{1}{2} E_{ijk\ell}\, \epsilon_{ij}\, \epsilon_{k\ell}\, dV - \int_{S_\sigma} \bar{T}_i\, u_i\, dS \qquad (3.2)$$

where the volume integral represents the work of internal strain energy U, and the variation of the surface integral represents the external work done by the specified surface traction ($\bar{T}_i$) (therefore potential energy lost) during displacements δu_i. Then, provided that the compatibility conditions are enforced by choosing a continuous function for the displacement field, the equilibrium conditions are an automatic consequence of the stationary condition $\delta\pi_p = 0$.

The finite element model formed from this theorem is identified as the conventional finite element displacement model. It is considered the most predominant finite element model to have been used in structure analysis. It provides a simple yet accurate method for many engineering applications.

This model will be used and referred to as the regular finite element model when we apply it to the fracture mechanics aspect of a general elasticity problem in

Chapter 4. The mathematical derivation of that regular finite element formulation will be given in Appendix B.

3.2 Complementary Energy Principle

Analogous to the potential energy theorem, the total complementary energy functional (π_c) is defined as

$$\pi_c = U^* + V^* \tag{3.3}$$

where U^* is the complementary strain energy and V^* is the complementary energy functional of boundary forces acting through prescribed displacements. The principle can be stated as in Desai and Abel [22]:

> Of all possible force and stress states which satisfy equilibrium and the stress boundary conditions, the state satisfying compatibility makes the complementary energy assume a minimum value. (p. 59)

Thus, $\delta\pi_c = \delta U^* + \delta V^* = 0$, and π_c is a minimum if $\delta^2\pi_c > 0$.

In a manner similar to that of potential energy, the complementary energy function is defined as a function of stresses and tractions while displacements are assumed constant.

The total complementary energy is expressed as

$$\pi_c = \int_V \frac{1}{2} C_{ijk\ell}\, \sigma_{ij}\, \sigma_{k\ell}\, dV - \int_{S_u} T_i\, \bar{u}_i\, dS \tag{3.4}$$

In this expression the volume integral contains the complementary strain energy (strain energy expressed as a function

of the stresses) while the variation of the second integral represents the external complementary work done by the tractions on the specified displacements. As long as the equilibrium conditions are ensured ($\sigma_{ij,j} = 0$ for no body forces) the compatibility conditions are implicitly contained in the statements of stationary condition $\delta\pi_c = 0$. The finite element model based on this theorem has been classified and identified as an equilibrium model.

Here the primary variable is the stress field, which is assumed to satisfy exactly the equilibrium conditions, while compatibility is approximated by the variational principle; this leads to better results for stresses than for displacements. Since for many engineering purposes a knowledge of stress distribution is the desired result and the displacements are of secondary interest, this model has advantages in engineering applications. However, this complementary energy method has had limited success compared with the potential energy method. This limited success is due to the difficulty in establishing an assumed stress distribution which exactly satisfies the equilibrium conditions and which is still expressible in terms of a convenient set of nodal quantities.

3.3 Modified Energy Principles and Hybrid Models

The finite element procedures based upon conventional energy principles (displacement and equilibrium models)

have met some difficulties [23] when elements of different types (bars, beams, plates) or different forms (second and third order polynomials) are joined together. These difficulties have been encountered in satisfying the required conditions on interelement continuity. For instance, in a crack problem the elasticity solution near the crack tip indicates a region of high stress gradients, with the stress becoming singular at the crack tip. This known solution can be used to construct special functions for elements around the crack tip. Meanwhile, regular polynomials are used for the other elements in regions where the stress gradients are not so high. As evident in Figure 3.1, when a singular and a regular element are adjacent, discontinuities are bound to occur between the elements.

A basic extension of the compatible and equilibrium models is needed to handle such cases. In order to simply construct the different trial functions, it is necessary to relax the troublesome continuity requirements. In removing these requirements from their explicit status, some action must be taken to reinstate continuity at least by some approximate matching procedure. This can be accomplished by introducing the modified energy principles. Several matching procedures, between the boundary of the singular cracked and the adjacent regular elements, have been discussed and summarized by Spiering and de Pater [24].

The Lagrange multiplier concept is considered as one of the possibilities to deal with such constraints in variational problem. To ascertain its usefulness, assume that a functional (π) is subject to the constraint condition:

$$\text{on S:} \quad \phi(x_i) = 0$$

An augmented functional (π_{Aug}) can then be formed:

$$\pi_{Aug} = \pi - \int_S \lambda_i \, \phi(x_i) \, dS \tag{3.5}$$

where the Lagrange multipliers (λ_i) are functions of the surface coordinates. Once the variation of the augmented functional has been carried out, the physical definition of the multiplier can be determined.

This new approach in finite element method, which involves independent approximations of interior and boundary variables, is generally called the hybrid formulation.

3.3.1 Modified Complementary Energy Principle (Hybrid Stress)

The modified complementary energy principle $(\pi_c)_m$ can be formulated by introducing the traction reciprocity conditions as equations of constraint and employing the Lagrange multiplier concept; that is, in the finite element method, the equilibrium must be maintained for the surface

tractions T_i, defined by $T_i = \sigma_{ij}\ \nu_j$ across the interelement boundaries. Let two neighboring elements s and r be isolated (Figure 3.1b) and consider the boundary traction components $T_i^s(S)$ and $T_i^r(S)$ $(i = 1,2)$ over the respective sides of the common boundary AB for the two dimension case. The equilibrium conditions at the interelement boundary are given by

$$T_i^s(S) + T_i^r(S) = 0 \qquad (i = 1,2) \tag{3.6}$$

Equation (3.6) may be considered as the condition of the constraint and can be introduced by including Lagrange multiplier terms

$$\int_{AB} \lambda_i(S)\,[T_i^s(S) + T_i^r(S)]\ dS \tag{3.7}$$

or

$$\int_{AB} \lambda_i\ T_i\ dS\Big|_s + \int_{AB} \lambda_i\ T_i\ dS\Big|_r$$

The Lagrange multipliers λ_i, which are functions of the surface coordinates, are to be treated as additional variables.

When all the interelement boundaries in each element n have been considered, the modified complementary energy functional may be written as follows, where S_n is the sum of all the parts of the element boundary which are interelement

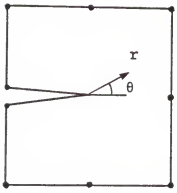

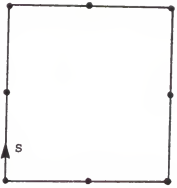

Singular element (s) Regular element (r)

$u^s = a_1 + a_2\sqrt{r} + a_3 r$ $u^r = b_1 + b_2 s + b_3 s^2$

a. Inter-element boundary displacement for the assumed displacement hybrid model

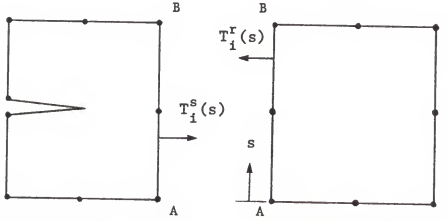

Singular element (s) Regular element (r)

$$T_i^s(s) + T_i^r(s) = 0 \qquad i=1,2$$

b. Inter-element boundary traction for the assumed stress hybrid model

Figure 3.1: Matching regular and singular elements

boundaries and S_{u_n} is the part of the element boundary that is an external boundary part of the element boundary on which displacements $\bar{u}_i$ are specified

$$(\pi_c)_m = \sum_{n=1}^{M} \left\{ \int_{A_n} \frac{1}{2} c_{ijk\ell}\, \sigma_{ij}\, \sigma_{k\ell}\, dA - \int_{S_n} \lambda_i\, T_i\, dS - \int_{S_{u_n}} T_i\, \bar{u}_i\, dS \right\} \tag{3.8}$$

Then, by taking the variation of the functional $(\pi_c)_m$ with respect to σ_{ij} and λ_i, this variation enforces equilibrium and defines the multipliers λ_i as the displacements $\tilde{u}_i$ along the interelement boundary. This modified principle then becomes a two-field principle, that is, an assumed stress field within the element and an independent assumed displacement on its boundary.

Finally, since the hybrid method relies on assumed boundary displacements, the prescribed boundary stress no longer constitutes a restrained boundary condition. In this case the functional $(\pi_c)_m$ can be written more conveniently as [25]

$$(\pi_c)_m = \sum_{n=1}^{M} \int_{A_n} \frac{1}{2} c_{ijk\ell}\, \sigma_{ij}\, \sigma_{k\ell}\, dA - \int_{\partial A_n} T_i\, \tilde{u}_i\, dS + \int_{S_{\sigma_n}} \bar{T}_i\, \tilde{u}_i\, dS \tag{3.9}$$

where $\partial A_n = S_n + S_{\sigma_n} + S_{u_n}$ is the entire boundary for the element number n, and

$$\tilde{u}_i = \bar{u}_i \qquad \text{on } S_{u_n} \tag{3.10}$$

and

$$T_i = \bar{T}_i \qquad \text{on } S_{\sigma_n} \tag{3.11}$$

3.3.2 Modified Potential Energy Principle (Hybrid Displacement)

In applying the variational principle of minimum potential energy to finite element analysis, the assumed displacement function needs to be continuous within each individual element A_n, but not across the interelement boundary of A_n. This interelement boundary discontinuity (see Figure 3.1a) can be relaxed by introducing the Lagrange multipliers, λ_i, as a constraint condition on the interelement boundary displacement. The potential energy functional is therefore modified and a new functional can be written

$$(\pi_p)_m = \sum_{n=1}^{M} \left[\pi_p - \int_{S_{AB}} \lambda_i \, (S)[(u_i)^s - (u_i)^r] \, dS \right] \tag{3.12}$$

Following the same line of thought, the variational principle enforces compatibility and defines the physical meaning of the multiplier (λ_i) as the interelement boundary tractions $\tilde{T}_i$ [26].

$$(\pi_p)_m = \sum_{n=1}^{M} \left\{ \int_{A_n} \frac{1}{2} E_{ijk\ell}\, \varepsilon_{ij}\, \varepsilon_{k\ell}\, dA - \int_{\partial A_n} \tilde{T}_i\, \tilde{u}_i\, dS + \int_{S_{u_n}} T_i\, \bar{u}_i\, dS \right\} \tag{3.13}$$

where u_i represent the smooth continuous displacements within A_n and the displacements $\tilde{u}_i$ represent the boundary displacements on the ∂A_n (the total boundary of A_n).

An important characteristic of the displacement hybrid variational functional is that the boundary displacement field $\tilde{u}_i$ and the displacement field u_i in the interior of the body are separate and distinct [27].

3.3.3 Reissner's Variational Principle (Mixed Method)

Reissner's functional (π_R) is one of the known mixed variational principles. It attempts to treat both compatibility and equilibrium conditions with equal respect. This functional is developed by noting that if the stresses and the strains satisfy the constitutive relations, then

$$\int_V \sigma_{ij}\, \varepsilon_{ij}\, dV = \int_V \frac{1}{2} E_{ijk\ell}\, \varepsilon_{ij}\, \varepsilon_{k\ell}\, dV + \int_V \frac{1}{2} C_{ijk\ell}\, \sigma_{ij}\, \sigma_{k\ell}\, dV \tag{3.14}$$

Using this relation, the complementary energy (in the form of stress energy) can be brought into the potential energy functional:

$$\pi_{pc} = \int_V \sigma_{ij}\, \varepsilon_{ij}\, dV - \int_V \frac{1}{2}\, C_{ijk\ell}\, \sigma_{ij}\, \sigma_{k\ell}\, dV - \int_{S_\sigma} \bar{T}_i\, u_i\, dS \tag{3.15}$$

The displacements are still the only variables since the strains and the stresses are determined from them. The stresses become the second set of variables by relaxing the compatibility conditions both along the boundary and in the interior using Lagrange multipliers. Introducing these as constraints, the functional can then be modified [22]

$$\pi_R = \pi_{pc} - \int_V \tilde{\sigma}_{ij} \left[\varepsilon_{ij} - \frac{1}{2}\,(u_{i,j} + u_{j,i})\right] dV$$

$$- \int_{S_u} \tilde{T}_i\, [u_i - \bar{u}_i]\, dS \tag{3.16}$$

where the Lagrange multipliers, $\tilde{\sigma}_{ij}$ and $\tilde{T}_i$, become the actual stresses and boundary tractions, respectively. Here the constitutive relations are the only equations of elasticity that have been satisfied exactly; all others are approximated by the variational procedure.

3.3.4 Mixed Modified Energy Principle (Day's Model)

This type of the modified energy principles has been introduced by Day [22] in 1981. He employed both the modified potential and modified complementary energy principles simultaneously, so the displacements and stresses in the continuum can be treated in a more equal basis. That was accomplished by describing the continuum with two independent fields, a compatible displacement field, and an equilibrating stress field. Then he determined some additional terms to be added to the functional in order to treat the problem of interelement boundary discontinuity in both displacements and tractions. The final form of this functional becomes

$$\pi_D = \sum_{n=1}^{M} \left\{ \int_{V_n} \frac{1}{2} E_{ijk\ell}\, \epsilon_{ij}\, \epsilon_{k\ell}\, dV - \int_{V_n} \frac{1}{2} C_{ijk\ell}\, \sigma_{ij}\, \sigma_{k\ell}\, dV \right.$$

$$- \int_{S_{\sigma_n}} u_i\, [2\bar{T}_i - T_i]\, dS + \int_{S_{u_n}} T_i\, [2\bar{u}_i - u_i]\, dS$$

$$\left. + \int_{S_n} T_i\, \tilde{u}_i\, dS \right\} \qquad (3.17)$$

For more details and the proof of this method see reference [23].

3.4 Summary and Comparison

The various finite element formulations discussed above in this chapter will be summarized in Table 3.1 as given by Day [23].

The main differences lie in the manner in which the governing equations of elasticity are handled. They may be either exactly satisfied by the assumed trial functions or may be approximated by use of the variational principle.

Table 3.1: Summary of finite element formulations

Model	Variational Principle	Variables	Compatibility Conditions		Equilibrium Conditions	
			Internal	External	Internal	External
Compatible	π_p	In V: u_i	Exact	Exact	Approximate	Approximate
Equilibrium	π_c	In V: σ_{ij}	Approximate	Approximate	Exact	Exact
Hybrid Displacement	$(\pi_p)_m$	In V: u_i On S: T_i	Exact	Approximate	Approximate	Approximate
Hybrid Stress	$(\pi_c)_m$	In V: σ_{ij} On S: u_i	Approximate	Approximate	Exact	Approximate
Mixed: Reissner	π_R	In V: u_i In V: σ_{ij}	Approximate	Approximate	Approximate	Approximate
Mixed: Day	π_D	In V: u_i In V: σ_{ij}	Exact	Approximate	Exact	Approximate

CHAPTER 4
DEVELOPMENT OF A STRESS-HYBRID SINGULARITY SUPER FINITE ELEMENT

In Chapter 3 we discussed some details of the various aspects of the energy principles and their application in forming different types of finite element models. In this chapter, the stress-hybrid model will be extended and developed in order to treat the fracture behavior in composite materials and, in general, anisotropic materials.

4.1 Brief Outline of the Method Used

In the analysis that follows, the development of a stress-hybrid singularity super-element, which can be utilized to model the behavior of a sharp crack in a rectilinearly (homogeneous) anisotropic plane, will be undertaken.

The concept of super-element was first developed in 1973 by Tong, Pian, and Larsy [28] for isotropic materials. Later, in 1977, Tong [29] extended the application to orthotropic material in which the axes of orthotropic symmetry are either parallel to or perpendicular to the geometrical axes of the plate. Here, in this study, we expanded the concept of super-element further to the case of an orthotropic material with its axes of material symmetry making some angle θ with one of the geometrical axes of the plate.

In Section 4.2 a full explanation of the mathematical formulation is given. The stress functions $\phi_1(\xi_1)$ and $\phi_2(\xi_2)$ of Section 3.2 are expressed in a slightly different way from that which is stated in reference [29]. Both the stress intensity factors in Section 4.5 and the strain energy release rate in Section 4.5 were computed using the finite element computer code developed.

Using the same notation as Tong, Pian, and Larsy [28], and implementing both the divergence theorem and the equilibrium condition on the complementary energy functional leads from the expression of Equation (3.8) to the following variational functional (in matrix form) see Appendix D, where now π denotes the complementary energy functional for the single element.

$$\pi = \int_{\partial A} \{T\}^T \{\tilde{u}\}\, dS - \frac{1}{2} \int_{\partial A} \{T\}^T \{u\}\, dS \qquad (4.1)$$

in which

$$T_i = \sigma_{ij}\, \nu_j \qquad \text{on } \partial A \qquad (4.2)$$

$$(u_{i,j} + u_{j,i})/2 = C_{ijk\ell}\, \sigma_{k\ell} \qquad \text{in } A \qquad (4.3)$$

where the vectors $\{T\}$, $\{u\}$, and $\{\tilde{u}\}$ can be approximated by

$$\{T\} = [R]\{\beta\} \tag{4.4a}$$

$$\{u\} = [U]\{\beta\} \tag{4.4b}$$

$$\{\tilde{u}\} = [L]\{q\} \tag{4.4c}$$

in which [R], [U], and [L] are matrices defining the assumed functional relationships; {β} and {q} are vectors of unknown coefficients.

A substitution of Equations (4.4) into Equation (4.1) yields

$$\pi = \{\beta\}^T[G]\{q\} - \frac{1}{2}\{\beta\}^T[H]\{\beta\} \tag{4.5}$$

in which

$$[G] = \int_{\partial A} [R]^T[L]\, dS \tag{4.6}$$

and

$$[H] = \frac{1}{2}\int_{\partial A} ([R]^T[U] + [U]^T[R])\, dS \tag{4.7}$$

By applying the stationary condition on Equation (4.5) one can determine {β} and then eliminate {β} from Equation (4.5). Thus,

$$0 = \frac{\partial \pi}{\partial \beta} = [G]\{q\} - [H]\{\beta\}$$

gives

$$\{\beta\} = [H]^{-1}\,[G]\{q\} \tag{4.8}$$

and by substituting Equation (4.8) into Equation (4.5), one obtains

$$\pi = \{q\}^T[G]^T[H]^{-1}[G]\{q\} - \frac{1}{2}\{q\}^T[G]^T[H]^{-1}[H][H]^{-1}[G]\{q\}$$

or

$$\pi = \frac{1}{2}\{q\}^T[K]\{q\} \tag{4.9}$$

where

$$[K] = [G]^T[H]^{-1}[G] \tag{4.10}$$

is the element stiffness matrix for the super-element as given by Tong, Pian, and Larsy [28].

Now, in order to calculate the components of this super-element stiffness matrix [K], the matrices [G] and [H] have to be obtained first. A special mathematical treatment based on the theory of anisotropic plates in conjunction with the theory of elastic fracture mechanics has to be undertaken.

In the next section this mathematical formulation will be presented in detail, and then it will be programmed later in the form of a special subroutine to compute the

super-element stiffness matrix [K]. A proper connection of this subroutine to the main program is required in order to produce the global stiffness matrix. This stiffness matrix then can be applied to the total assembled structure.

4.2 Mathematical Formulation of Super-Element Stiffness Matrix

In the following derivation, the value of the complex variables z_1 and z_2 will be based on Case 1 of Equation (2.12a), Chapter 2, where the roots of the characteristic equation (2.11) are pairwise different

$$\begin{aligned} z &= x + i\,y \\ z_1 &= x + \mu_1 y \\ z_2 &= x + \mu_2 y \end{aligned} \tag{4.11}$$

Since the nature of the crack tip singularity is that the displacement field is proportional to the square root of the distance measured from the crack tip, and the stress field is proportional to the inverse of this square root distance, then the proper choiceof a mapping function to account for this singularity in the ξ-plane (see Figure 4.1) is

$$z_j = w(\xi_j) = \xi_j^2 \tag{4.12}$$

Now Lekhnitskii's representation of the stress function [18] can be utilized to express the components of stresses, displacements, and boundary conditions of Equations (2.14), (2.15), and (2.20) in terms of thenew transformed ξ-plane as follows:

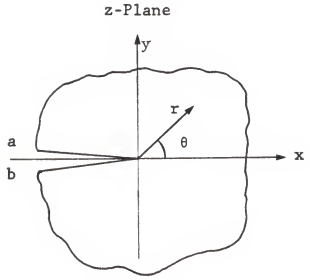

a. Sharp crack is assumed to lie on the negative portion of the complex z-plane with crack tip at $z = 0$

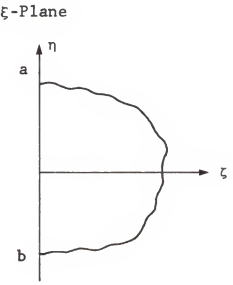

b. The crack lies on the imaginary axis of the transformed ξ-plane

Figure 4.1: Mapping of the crack region

(1) For stresses

$$\sigma_x = \mathrm{Re}[\mu_1^2\phi_1'(\xi_1)/\xi_1 + \mu_2^2\phi_2'(\xi_2)/\xi_2]$$

$$\sigma_y = \mathrm{Re}[\phi_1'(\xi_1)/\xi_1 + \phi_2'(\xi_2)/\xi_2] \qquad (4.13)$$

$$\tau_{xy} = -\mathrm{Re}[\mu_1\phi_1'(\xi_1)/\xi_1 + \mu_2\phi_2'(\xi_2)/\xi_2]$$

(2) For displacements (with no rigid body motion)

$$u = 2\,\mathrm{Re}[p_1\phi_1(\xi_1) + p_2\phi_2(\xi_2)]$$

$$v = 2\,\mathrm{Re}[q_1\phi_1(\xi_1) + q_2\phi_2(\xi_2)] \qquad (4.14$$

(3) For boundary conditions

$$2\,\mathrm{Re}[\phi_1(\xi_1) + \phi_2(\xi_2)] = f_1^*$$

$$2\,\mathrm{Re}[\mu_1\phi_1(\xi_1) + \mu_2\phi_2(\xi_2)] = f_2^* \qquad (4.15)$$

As we can see from Equation (4.11) and the assumption of the crack which is to be laid on the negative portion of the real axis of the z-plane (see Figure 4.1), $z = z_1 = z_2$ on the crack surface; therefore, the complex variables ξ, ξ_1, ξ_2 will also coincide on the crack surface; otherwise ξ_1 and ξ_2 are found to be distinct and can be calculated.

Assuming that the functions $\phi_1(\xi_1)$ and $\phi_2(\xi_2)$ of Equations (4.13), (4.14), and (4.15) are properly analytic,

a simple polynomial can be used in approximating their functional representations. The values of ϕ_1 and ϕ_2 can therefore be approximated by

$$\phi_1(\xi_1) = \sum_{j=1}^{n} b_j \xi_1^j ; \quad \phi_2(\xi_2) = \sum_{j=1}^{n} \hat{b}_j \xi_2^j \qquad (4.16)$$

in which b and $\hat{b}_j$ are the complex constants

$$b_j = \beta_j + i\beta_{j+n}$$

(nonsymmetric case)

$$\hat{b}_j = \hat{\beta}_j + i\hat{\beta}_{j+n}$$

or (4.17)

$$b_j = \beta_j ; \quad \hat{b}_j = \hat{\beta}_j \quad \text{(symmetric case)}$$

It will be assumed that the surface of the crack is stress free. Thus, $\overline{T}_x = \overline{T}_y = 0$, and it follows from Equation (2.20) that $f_1 = f_2 = 0$.

Substituting Equation (4.16) into Equation (4.15) and using Equation (4.17) yields

$$\sum_{j=1}^{n} \mathrm{Re}[b_j \xi_1^j + \hat{b}_j \xi_2^j] = 0$$

$$\sum_{j=1}^{n} \mathrm{Re}[\mu_1 b_j \xi_1^j + \mu_2 \hat{b}_j \xi_2^j] = 0 \qquad (4.18)$$

from which it is only necessary to satisfy

$$\begin{aligned} &\mathrm{Re}[b_j \xi_1^j + \hat{b}_j \xi_2^j] = 0 \\ &\mathrm{Re}[\mu_1 b_j \xi_1^j + \mu_1 \hat{b}_j \xi_2^j] = 0 \end{aligned} \tag{4.19}$$

for each j in order to assure satisfaction of the traction free condition on each crack surface.

Returning to Equation (4.11) and introducing the polar coordinates, r_k, θ_k, one can express z_k as

$$z_k = r_k e^{i\theta_k} \qquad \text{for } k=1,2 \tag{4.20}$$

where

$$\begin{aligned} r_k &= [(x + \alpha_k^* y)^2 + (\beta_k^* y)^2]^{1/2} \\ \theta_k &= \tan^{-1} [\beta_k^* y/(x + \alpha_k^* y)] \end{aligned} \tag{4.21}$$

Thus, it is not difficult to express ξ_k from Equation (4.12) in terms of the polar coordinates; hence

$$\xi_k^j = r_k^{j/2}[\cos (j\theta_k/2) + i \sin (j\theta_k/2)]$$

Along the crack surface $r_k = |x|$, $\theta = \pi$

$$\xi_1^j = \xi_2^j = |x|^{j/2}[\cos (j\pi/2) + i \sin (j\pi/2)] \tag{4.22}$$

Substituting Equation (4.22) into Equation (4.19) gives

$$\mathrm{Re}\{(\beta_j + i\beta_{j+n} + \hat{\beta}_j + i\hat{\beta}_{j+n})|x|^{j/2}[\cos(j\pi/2) + i\sin(j\pi/2)]\} = 0$$

$$\mathrm{Re}\{[\mu_1(\beta_j + i\beta_{j+n}) + \mu_2(\hat{\beta}_j + i\hat{\beta}_{j+n})]|x|^{j/2}[\cos(j\pi/2) + i\sin(j\pi/2)]\} = 0$$

or

$$(\beta_j + \hat{\beta}_j)\cos(j\pi/2) - (\beta_{j+n} + \hat{\beta}_{j+n})\sin(j\pi/2) = 0 \qquad (4.23a)$$

$$(\alpha_1^*\beta_j - \beta_1^*\beta_{j+n} + \alpha_2^*\hat{\beta}_j - \beta_2^*\hat{\beta}_{j+n})\cos(j\pi/2) - (\beta_1^*\beta_j + \alpha_1^*\beta_{j+n} + \beta_2^*\hat{\beta}_j + \alpha_2^*\hat{\beta}_{j+n})\sin(j\pi/2) = 0 \qquad (4.23b)$$

By solving Equations (4.23) for the real coefficient $\hat{\beta}_j$ and $\hat{\beta}_{j+n}$ in terms of β_j and β_{j+n}, we can find a relation between $\phi_1(\xi_1)$ and $\phi_2(\xi_2)$ to guarantee a stress-free condition along the entire length of the crack face. Thus, the following relations can be obtained:

$$\hat{\beta}_j = M_{11j}\beta_j + M_{12j}\beta_{n+j}$$

$$\hat{\beta}_{j+n} = M_{21j}\beta_j + M_{22j}\beta_{n+j} \tag{4.24}$$

in which

$$M_{11j} = -\beta_1^*/\beta_2^* , \quad M_{12j} = (\alpha_2^* - \alpha_1^*)/\beta_2^*$$

for odd j

$$M_{21j} = 0 , \quad M_{22j} = -1$$

and (4.25)

$$M_{11j} = -1 , \quad M_{12j} = 0 ,$$

for even j

$$M_{21j} = (\alpha_1^* - \alpha_2^*)/\beta_2^* , \quad M_{22j} = -\beta_1^*/\beta_2^*$$

Thus, the two analytical stress functions of Equation (4.16) will become

$$\phi_1(\xi_1) = \sum_{j=1}^{n} (\beta_j + i\beta_{j+n})\xi_1^j$$

(4.26)

$$\phi_2(\xi_2) = \sum_{j=1}^{n} [(M_{11j}\beta_j + M_{12j}\beta_{n+j}) + i(M_{21j}\beta_j + M_{22j}\beta_{n+j})]\xi_2^j$$

Substituting the above value of stress functions from Equation (4.26) into the stress equation (4.13), we obtain

$$\sigma_x = \sum_{j=1}^{2n} A_j(\xi_1,\xi_2)\beta_j$$

$$\sigma_y = \sum_{j=1}^{2n} B_j(\xi_1,\xi_2)\beta_j \qquad (4.27)$$

$$\tau_{xy} = \sum_{j=1}^{2n} C_j(\xi_1,\xi_2)\beta_j$$

where

$$A_j = j\ \mathrm{Re}[\mu_1^2\xi_1^{j-2} + \mu_2^2(M_{11j} + i\ M_{21j})\xi_2^{j-2}]$$

$$A_{j+n} = j\ \mathrm{Re}[i\mu_1^2\xi_1^{j-2} + \mu_2^2(M_{12j} + i\ M_{22j})\xi_2^{j-2}]$$

$$B_j = j\ \mathrm{Re}[\xi_1^{j-2} + (M_{11j} + i\ M_{21j})\xi_2^{j-2}]$$

$$B_{j+n} = j\ \mathrm{Re}[i\xi_1^{j-2} + (M_{12j} + i\ M_{22j})\xi_2^{j-2}]$$

$$C_j = -\ j\ \mathrm{Re}[\mu_1\xi_1^{j-2} + \mu_2(M_{11j} + i\ M_{21j})\xi_2^{j-2}]$$

$$C_{j+n} = -\ j\ \mathrm{Re}[i\mu_1\xi_1^{j-2} + \mu_2(M_{12j} + i\ M_{22j})\xi_2^{j-2}]$$

A similar substitution of Equation (4.26) into the displacement equation (4.14) produces

$$u = \sum_{j=1}^{2n} f_j(\xi_1, \xi_2)\beta_j$$

$$v = \sum_{j=1}^{2n} g_j(\xi_1, \xi_2)\beta_j \qquad (4.28)$$

where

$$f_j(\xi_1, \xi_2) = 2\,\mathrm{Re}[p_1\xi_1^j + p_2(M_{11j} + i\,M_{21j})\xi_2^j]$$

$$f_{j+n}(\xi_1, \xi_2) = 2\,\mathrm{Re}[i\,p_1\xi_1^j + p_2(M_{12j} + i\,M_{22j})\xi_2^j]$$

$$g_j(\xi_1, \xi_2) = 2\,\mathrm{Re}[q_1\xi_1^j + q_2(M_{11j} + i\,M_{21j})\xi_2^j]$$

$$g_{j+n}(\xi_1, \xi_2) = 2\,\mathrm{Re}[i\,q_1\xi_1^j + q_2(M_{12j} + i\,M_{22j})\xi_2^j]$$

The integrations to determine [H] and [G] for the particular geometry of Figure 4.2 become

$$\{\beta\}^T[H]\{\beta\} = \int_{\partial A} \{T\}^T\{u\}\,dS$$

$$= \int_B^C + \int_D^F + \int_G^H \nu_x(\sigma_x u + \tau_{xy} v)\,dS + \int_C^D$$

$$+ \int_F^G \nu_y(\tau_{xy} u + \sigma_y v)\,dS \qquad (4.29)$$

$$\{\beta\}^T[G]\{q\} = \int_{\partial A} \{T\}^T\{\tilde{u}\}\, dS$$

$$= \int_B^C + \int_D^F + \int_G^H \nu_x(\sigma_x\tilde{u} + \tau_{xy}\tilde{v})\, dS + \int_C^D$$

$$+ \int_F^G \nu_y(\tau_{xy}\tilde{u} + \sigma_x\tilde{v})\, dS \qquad (4.30)$$

where

$$\sigma_x u = \frac{1}{2} \sum_{j,k=1}^{n} (A_j f_k + A_k f_j)\beta_j\beta_k$$

$$\tau_{xy} v = \frac{1}{2} \sum_{j,k=1}^{n} (C_j g_k + C_k g_j)\beta_j\beta_k$$

$$\tau_{xy} u = \frac{1}{2} \sum_{j,k=1}^{n} (C_j f_k + C_k f_j)\beta_j\beta_k$$

$$\sigma_y v = \frac{1}{2} \sum_{j,k=1}^{n} (B_j g_k + B_k g_j)\beta_j\beta_k$$

In applying Equation (4.30) the boundary displacement vector $\{\tilde{u}\}$ will be expressed in terms of the element nodal displacement vector $\{q\}$ by the following relation

$$\{\tilde{u}\} = [L]\{q\} \qquad (4.31)$$

where [L] is a matrix of properly selected shape functions defined along the element boundary. The [L] matrix is chosen such that when the corresponding nodal displacements

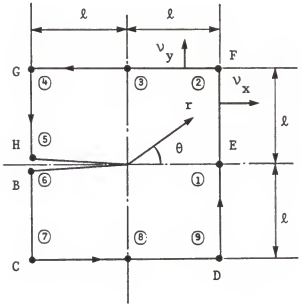

Figure 4.2: Nine-node super-element

of the adjacent elements are matched, $\tilde{u}$ is the same for the two different kinds of elements over their common boundaries. In this case, the standard elements are assumed to be four-node quadrilaterals possessing four corner nodes for each element. Since these elements possess a linear displacement along the element boundaries, it is necessary to require a linear variation of the boundary displacement field $\{\tilde{u}\}$ [Equation (4.31)] along the sides of the singular element

(Figure 4.2) in order to insure compatibility between the two element types. Therefore one can assume the following:

$L_{11} = L_{22} = 1 - S/\ell$; $L_{12} = L_{24} = S/\ell$; all other $L_{ij} = 0$ and $q_j = \{u_P \quad v_P \quad u_{P+1} \quad v_{P+1}\}$ between nodes P and nodes P+1, where ℓ is the distance between the two nodes, $(u_P; v_P)$ is the value of $\tilde{u}$ at node P, and S is the distance measured from node P.

4.3 Numerical Integration

The evaluation of the integrals involved in the stiffness matrices was accomplished using numerical integration. In this regard, it is noted that the type and order of integration used represents a critical decision, as a method must be chosen which uses a minimum number of integration points and achieves an acceptable level of accuracy. The method used here in formulating the super-element stiffness matrix was a 5X5 Gaussian quadrature procedure; the method for the formulation of the regular element stiffness matrix was a 3X3 Gaussian quadrature. These choices seem to offer the best compromise between accuracy and economy. That is, the stress intensity factor K_I (opening mode) for the first example used by Tong, Pian, and Larsy [28] was obtained exactly in CPU time 0.51 seconds, compared to 1.7 seconds on an IBM 370/165 in that reference. For the other example of that study [28] the exact values of K_I

and K_{II} (shear mode) were obtained using the same number of degrees of freedom with only 1.15 seconds of CPU time compared to 2.5 seconds; i.e., we established a 100 percent accuracy with more than 50 percent reduction in computation time for both cases studied in that reference.

4.4 Convergence Characteristics of the Method

In any acceptable numerical formulation, the numerical solution must converge and tend toward the exact solution of the problem. For the finite element method, the pure models (regular stress and displacement models) are based strictly on the energy theorems, which are not only stationary principles but are also minimum principles. This allows bounds to be put on the strain energy. The compatible (displacement) model will always provide an upper bound to the true stiffness of the structure. In other words, the stiffness coefficients for a given displacement model have magnitudes higher than those for the exact solution. Thus, under a given load, the simulated structure deforms less than the actual structure. It follows that the approximate displacement solution will converge to the exact solution from below: that is, we obtain lower bounds to the true solution [22]. The equilibrium (stress) model is just the opposite, always being too flexible, and gives an upper bound [30].

In the hybrid formulations, the relaxing of the continuity requirements, by introducing the Lagrange multiplier, does alter the convergence characteristics. As a consequence, neither monotonic convergence nor determination of lower or upper bounds can be achieved. However, all hybrid formulations possess a solution that lies between the limits [30] such as shown in Figure 4.3.

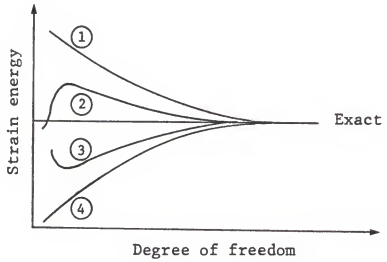

1. Equilibrium (monotonic)
2. Hybrid (nonmonotonic)
3. Hybrid (nonmonotonic)
4. Compatible (monotonic)

Figure 4.3: Convergence of strain energy with the mesh refinement

In this study we chose the interpolation function [L] of Equation (4.31) to be of the linear type because it is well recognized, in signular elasticity problems, that the rate of solution convergence is generally independent of the order of polynomials used for interpolation functions in element formulation [31]. That is, the use of higher-order elements does not necessarily improve the rate of convergence of the numerical solution. In fact, the rate of convergence of the finite element solution is governed by the order of the singularity rather than the order of the polynomial used for the interpolation function. In addition, simplicity and less computer time can be gained.

4.5 Stress Intensity Factors

As previously derived by Sih, Paris, and Irwin [32], the stress intensity factors, K_I and K_{II}, for plane generally anisotropic media near the crack-tip region can be evaluated from the formulas

$$K_I + K_{II}/\mu_2 = -\sqrt{2}(\mu_1 - \mu_2)/\mu_2 \lim_{\xi_1 \to 0} \phi_1'(\xi_1) \tag{4.32}$$

and

$$K_I + K_{II}/\mu_1 = \sqrt{2}(\mu_1 - \mu_2)/\mu_1 \lim_{\xi_2 \to 0} \phi_2'(\xi_2) \tag{4.33}$$

where from Equation (4.9) we obtain

$$\lim_{\xi_1 \to 0} \phi_1'(\xi_1) = b_1 \quad \text{and} \quad \lim_{\xi_2 \to 0} \phi_2'(\xi_2) = \hat{b}_1$$

and from Equations (4.15a) and (4.15b) when j=1, we get

$$\hat{\beta}_{n+1} = - \beta_{n+j} \tag{4.34}$$

$$\hat{\beta}_1 = [(\alpha_2^* - \alpha_1^*)\beta_{n+1} - \beta_1^*\beta_1]/\beta_2^* \tag{4.35}$$

Now Equations (4.32) and (4.33) become

$$K_I + K_{II}/\mu_2 = - \sqrt{2}[(\mu_1 - \mu_2)/\mu_2]b_1 \tag{4.36}$$

$$K_I + K_{II}/\mu_1 = \sqrt{2}[(\mu_1 - \mu_2)/\mu_1]\hat{b}_1 \tag{4.37}$$

Solving the above two equations for K_{II}, we obtain

$$K_{II} = - \sqrt{2}(\mu_2\hat{b}_1 + \mu_1 b_1) \tag{4.38}$$

Substituting Equation (4.38) into Equation (4.36), we get

$$K_I = \sqrt{2}(b_1 + \hat{b}_1) \tag{4.39}$$

Since K_I is a real quantity (the stress intensity factor for the crack opening mode) only the real part of the right-hand side of Equation (4.39) will be considered, i.e.,

$$K_I = \sqrt{2}\ (\beta_1 + \hat{\beta}_1) \tag{4.40}$$

and by using Equation (4.35) to eliminate $\hat{\beta}_1$ from Equation (4.40), a direct expression for K_I can be obtained

$$K_I = \sqrt{2}\ [(1 - \beta_1^*/\beta_2^*)\beta_1 + (\alpha_2^* - \alpha_1^*)\beta_{n+1}/\beta_2^*] \tag{4.41}$$

To evaluate K_{II}, the same procedure can be followed by considering only the real part of Equation (4.38) which is to be evaluated after the replacement of the roots μ_1 and μ_2 by their complex expressions from Equation (2.12a), i.e.,

$$K_{II} = -\sqrt{2}\ \mathrm{Re}[(\alpha_2^* + i\beta_2^*)(\hat{\beta}_1 + i\hat{\beta}_{n+1}) + (\alpha_1^* + i\beta_1^*)(\beta_1 + i\beta_{n+1})]$$

$$= -\sqrt{2}\ (\alpha_2^*\hat{\beta}_1 - \beta_2^*\hat{\beta}_{n+1} + \alpha_1^*\beta_1 - \beta_1^*\beta_{n+1})$$

By eliminating $\hat{\beta}_1$ and $\hat{\beta}_{n+1}$ and using Equations (4.34) and (4.35), a direct expression for K_{II} can be obtained

$$K_{II} = -\sqrt{2}\ \{(\alpha_1^* - \alpha_2^*\beta_1^*/\beta_2^*)\beta_1 + [\beta_2^* - \beta_1^* + \alpha_2^*(\alpha_2^* - \alpha_1^*)/\beta_2^*]\beta_{n+1} \tag{4.42}$$

Thus, once the value of the parameters β_1 and β_{n+1} have been computed, the stress intensity factors, in mode I and mode II, can be calculated directly from the preceding equations.

In the case of isotropic material, the roots of the characteristic equation are equal to $\sqrt{-1}$, i.e., $\mu_1 = \mu_2 = i$; in that case it is clear that this value cannot be applied directly to Equations (4.32) and (4.33), but it must be approached in the limit as a small difference Δ, i.e., when Δ approaches zero in which

$$\mu_1 = i\,, \qquad \mu_2 = (1 + \Delta)i$$

or

$$\beta_1^* = 1\,, \qquad \beta_2^* = 1 + \Delta\,, \quad \text{and} \quad \alpha_1^* = \alpha_2^* = 0 \qquad (4.43)$$

By substituting Equation (4.43) into both Equations (4.41) and (4.42) and taking the limit on Δ in each equation, and considering a symmetric deformation ($\beta_{n+1} = 0$) and single fracture mode behavior, we obtain

From Equation (4.41): $\quad K_I = \sqrt{2}\ \beta_1$

From Equation (4.42): $\quad K_{II} = 0$

which are the well-known formulas of the stress intensity factor for the case of a single opening mode in an isotropic material [2].

4.6 Strain Energy Release Rate

Although stress intensity factors K_I and K_{II} describe details of a stress field near the crack-tip, the critical strain energy release rate G_{cr} at the beginning of crack propagation is also of a significant interest. It is a quantity physically measurable in experiments and methematically well defined. In addition, it can be viewed as the portion of the work performed by the external loads during crack extension that goes into failure of the material per unit area of crack growth.

Sih, Paris, and Irwin [32] studied the energy release rates for the case of more than one mode present at crack-tip in generally anisotropic media. They determined that this energy can be evaluated from the following formulae:

$$J_1 = \frac{1}{2}\pi\, K_I\, a_{22}\, \mathrm{Im}\{[K_I(\mu_1 + \mu_2) + K_{II}]/\mu_1\mu_2\}$$

$$J_2 = \frac{1}{2}\pi\, K_{II}\, a_{11}\, \mathrm{Im}[K_{II}(\mu_1 + \mu_2) + K_I\mu_1\mu_2] \qquad (4.44)$$

and

$$G = J_1 + J_2$$

For the special case of orthotropic material with the crack being on one plane of elastic symmetry Equation (4.44) can be reduced to the following form:

$$J_1 = \pi K_I^2 \{[(a_{22}/a_{11})^{1/2} + (2\,a_{12} + a_{66})/2\,a_{11}]\,a_{11}\,a_{22}/2\}^{1/2}$$

(4.45)

$$J_2 = \pi K_{II}^2 [(a_{22}/a_{11})^{1/2} + (2\,a_{12} + a_{66})/2\,a_{11}]^{1/2} a_{11}/\sqrt{2}$$

where the values of a_{11}, a_{22}, a_{12}, and a_{66} can be found in Appendix A.

4.7 Stress and Displacement near the Crack Tip

After calculating the stress intensity factors K_I and K_{II} (opening and shear modes, respectively) from Section 4.5, the stresses and displacements in the vicinity of the crack tip can be easily obtained using the corresponding mode equations which are stated in Appendix C for both generally anisotropic and isotropic cases.

Here we notice that in the orthotropic case the stress distributions and the displacement field near the crack tip depend not only on K_I and/or K_{II} as in the isotropic cases but also depend on the material properties and the material symmetry axis with respect to geometric axes.

CHAPTER 5

RESULTS OF ANALYTICAL AND NUMERICAL TECHNIQUES

This chapter will discuss results in two parts. The first will be the application of Savin's analytical solution to some practical problems in unidirectional composite materials, mainly glass/epoxy and graphite/epoxy, both widely used in aircraft and military industries. The plane stress field will be determined for thin plates of these materials with the presence of either a circular hole or an elliptical hole. Three different elliptical holes will be discussed in terms of the aspect ratio of major to minor axis.

The second part of this chapter will discuss the numerical solution for the fracture mechanics problem. Stress intensity factors obtained by finite element solution will be compared to other solutions obtained by different techniques using the same assumptions.

5.1 Stress-Concentration Factors

The problem of stress concentrations around openings in an anisotropic plate was one of primary concern to many investigators [33]. Since the establishment of the commercial use of composite materials in the early 1960s, it has

become vary important to analyze the prediction of failure due to these high stress concentrations.

In order to apply any of the proposed failure criteria for composite materials, the stress distributions due to the external load before failure have to be determined first. Because of the limited scope of this study, investigation of these failure criteria will not be discussed here. All results of stress distributions around an opening to be given here are obtained by applying the theory of elasticity according to the formulation discussed in Chapter 2 under the assumption that failure has not yet occurred.

The elastic properties used for calculation of these stresses in graphite/epoxy are given here as in Collazo's study [34]:

$E_1 = 128$ GPa $\quad (20 \times 10^6$ psi)

$E_2 = 11$ GPa $\quad (1.6 \times 10^6$ psi)

$G_{12} = 6.4$ PGa $\quad (0.93 \times 10^6$ psi)

$\nu_{12} = 0.38$

The fiber volume fraction is approximately 63 percent. The elastic properties for the glass/epoxy composite will be given in Chapter 6, where this composite is used for the experimental part of this study.

Stress concentrations will be discussed for four different hole shapes, two different fiber materials, and five different fiber orientation angles with respect to the loading direction. In all following figures, which contain stress-concentration factor vs the coordinate angle θ, we use the symbol $\diamond$ for the corresponding isotropic case, and the symbols $\boxdot$, $\odot$, $\triangle$, +, and x to stand for the different fiber orientation angles 0°, 30°, 45°, 60°, and 90°, respectively. Both the fiber orientation angle Θ and the coordinate angle θ (abscissa in figures) for calculating stresses are measured counterclockwise from the loading direction. Hereafter, we will discuss the stress-concentration factor for four different cases, one circular and three different elliptical holes.

5.1.1 The Circular Hole

The stress concentrations around the circular hole in glass/epoxy and graphite/epoxy composite plates subjected to axial load (P) are calculated for different fiber orientation angles. Figure 5.1 shows the stress concentrations around the circular hole in plates made of glass/epoxy each of which has different fiber orientations, while Figure 5.2 shows the stress concentrations for the same fiber orientation but for plates made of graphite/epoxy composite. In both figures and the following figures, the case of isotropic material which corresponds to same hole

size, shape, and loading condition is also presented for comparison. For example in either Figures 5.1 or 5.2, the maximum value of the stress-concentration factor for a circular hole in an isotropic material occurs at 90° and has a value of 3, which is well-known in the theory of elasticity [21]. Since the maximum stress concentrations and their location angles are different depending on the fiber material and the fiber orientation angle, Table 5.1 presents a numerical value for the maximum stress-concentration factor $(\sigma_\theta/P)_{max}$ and its location (angle θ^*) on the circular contour of the hole for each fiber orientation angle and for the two fiber materials.

The effect of fiber orientations on the maximum stress-concentration factor and on its location are shown in Figure 5.3 and 5.4, respectively, for glass/epoxy and graphite/epoxy composite materials.

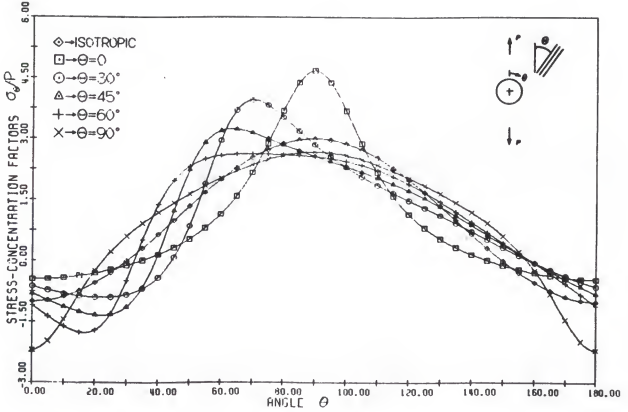

Figure 5.1: Stress-concentrations around a circular hole for glass/epoxy with different fiber orientations

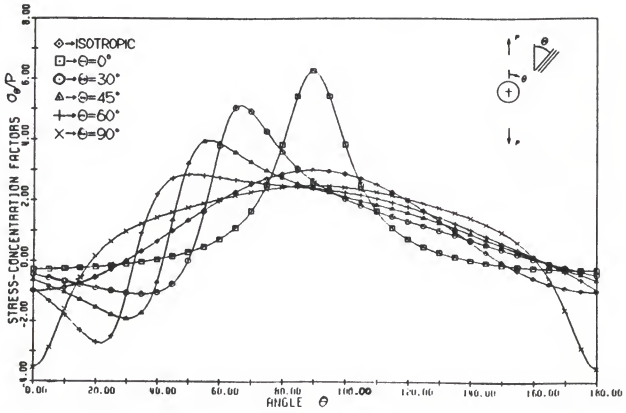

Figure 5.2: Stress-concentrations around a circular hole for graphite/epoxy with different fiber orientations

Table 5.1: Maximum stress-concentration factors for a circular hole

Fiber orientation θ (deg)	Glass/Epoxy $(\sigma_\theta/P)_{max}$	Glass/Epoxy θ^* (deg)	Graphite/Epoxy $(\sigma_\theta/P)_{max}$	Graphite/Epoxy θ^* (deg)
0	4.680	90	6.274	90
30	3.953	70	5.131	67
45	3.241	63	3.989	57
60	2.626	70	2.870	51
90	2.674	90	2.492	90

Note: For the case of isotropic materials $(\sigma_\theta/P)_{max} = 3.0$ and $\theta^* = 90^\circ$

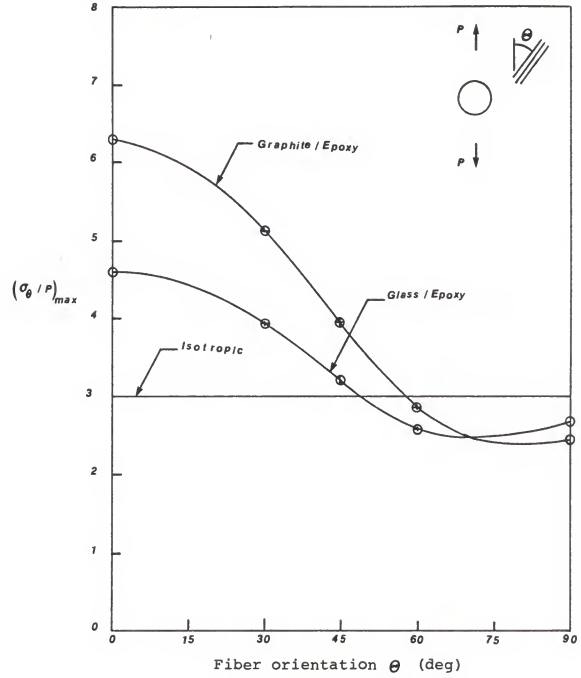

Figure 5.3: Maximum stress-concentration factor vs direction of fiber orientation for a circular hole

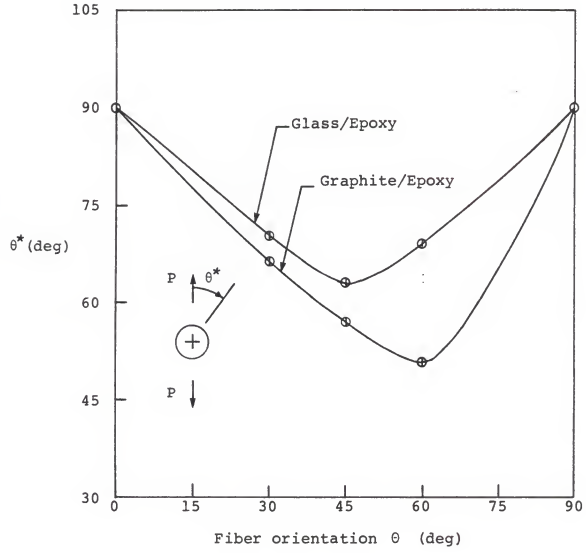

Figure 5.4: Location of the maximum stress-concentration vs direction of fiber orientation for a circular hole

5.1.2 The Elliptical Hole with Aspect Ratio a/b = 3

The stress concentrations around the hole for the two fiber materials and the five fiber orientation angles in this case are calculated and presented in Figure 5.5 and 5.6 for glass/epoxy and graphite/epoxy, respectively.

Table 5.2 presents the numerical value of the maximum stress-concentration factor $(\sigma_\eta/P)_{max}$ and its location (angle θ^*) on the elliptical contour of the hole for each fiber orientation angle and for the two fiber materials.

The effect of fiber orientations on the maximum stress-concentration factor and on its location are shown in Figures 5.7 and 5.8, respectively, for glass/epoxy and graphite/epoxy composite materials.

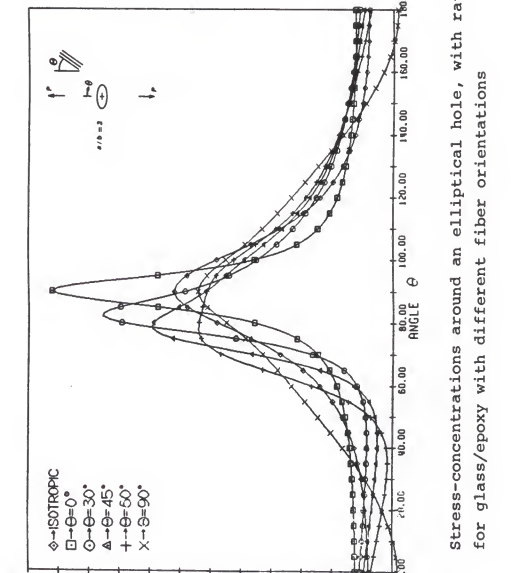

Figure 5.5: Stress-concentrations around an elliptical hole, with ratio $a/b = 3$, for glass/epoxy with different fiber orientations

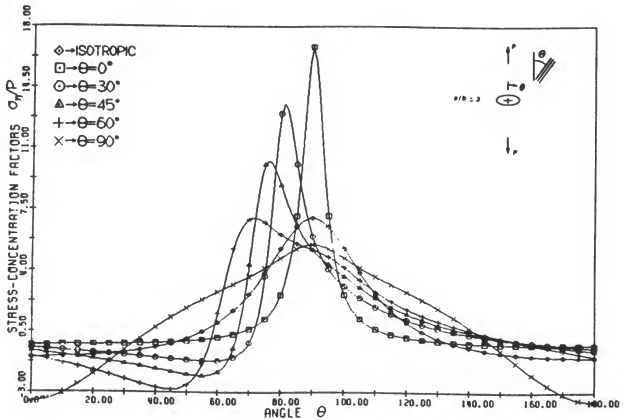

Figure 5.6: Stress-concentrations around an elliptical hole, with ratio a/b = 3, for graphite/epoxy with different fiber orientations

Table 5.2: Maximum stress-concentration factors for an elliptical hole with ratio a/b = 3.0

Fiber orientation θ (deg)	Glass/Epoxy $(\sigma_\eta/P)_{max}$	Glass/Epoxy θ^* (deg)	Graphite/Epoxy $(\sigma_\eta/P)_{max}$	Graphite/Epoxy θ^* (deg)
0	12.041	90	16.822	90
30	9.706	81	13.565	81
45	7.927	79	10.300	76
60	6.014	78	7.016	71
90	6.220	90	5.475	90

Note: For the case of isotropic materials $(\sigma_\eta/P)_{max} = 7.0$ and $\theta^* = 90.0°$

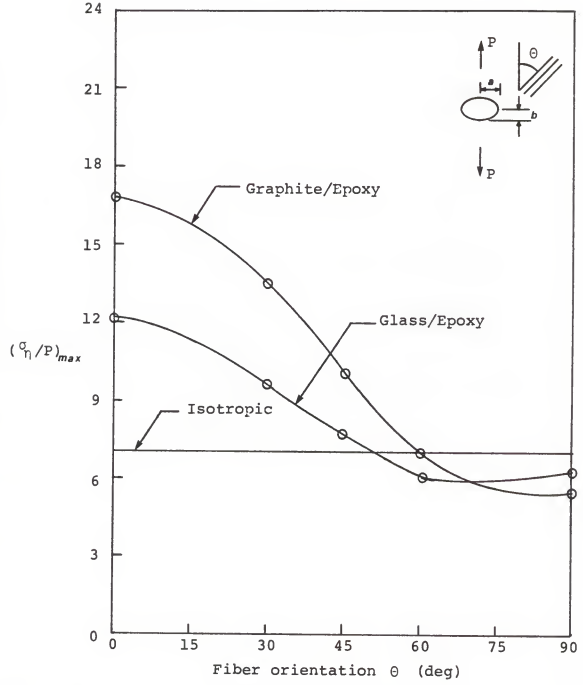

Figure 5.7: Maximum stress-concentration factor vs direction of fiber orientation for an elliptical hole, a/b = 3

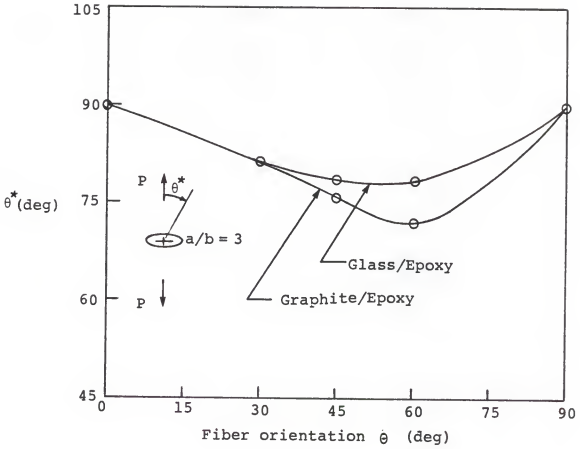

Figure 5.8: Location of the maximum stress-concentration vs direction of fiber orientation for an elliptical hole, a/b = 3

5.1.3 The Elliptical Hole with Aspect Ratio a/b = 9

The stress concentrations around the hole for the two fiber materials and the five fiber orientation angles in this case are calculated and presented in Figure 5.9 and 5.10 for glass/epoxy and graphite/epoxy, respectively.

Table 5.3 presents the numerical value of the maximum stress-concentration factor $(\sigma_\eta/P)_{max}$ and its location (angle θ^*) on the elliptical contour of the hole for each fiber orientation angle and for the two fiber materials.

The effect of fiber orientations on the maximum stress-concentration factor and on its location are shown in Figures 5.11 and 5.12, respectively, for glass/epoxy and graphite/epoxy composite materials.

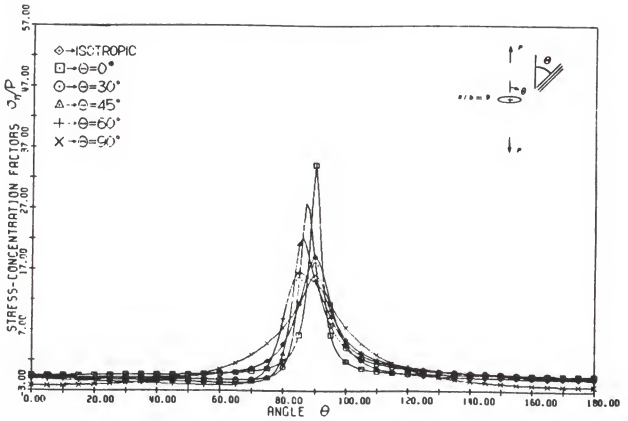

Figure 5.9: Stress-concentrations around an elliptical hole, with ratio a/b = 9, for glass/epoxy with different fiber orientations

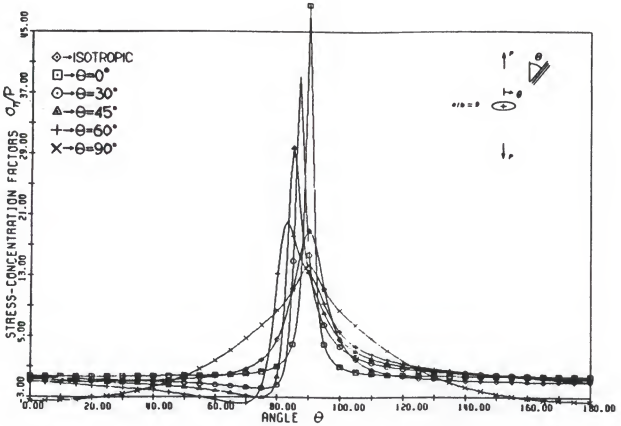

Figure 5.10: Stress-concentrations around an elliptical hole, with ratio a/b = 9, for graphite/epoxy with different fiber orientations

Table 5.3: Maximum stress-concentration factors for an elliptical hole with ratio a/b = 9

Fiber orientation θ (deg)	Glass/Epoxy $(\sigma_\eta/P)_{max}$	Glass/Epoxy θ^* (deg)	Graphite/Epoxy $(\sigma_\eta/P)_{max}$	Graphite/Epoxy θ^* (deg)
0	34.122	90	48.469	90
30	27.898	87	39.179	87
45	22.293	86	29.872	85
60	15.632	88	20.184	83
90	16.066	90	14.426	90

Note: For the case of isotropic materials $(\sigma_\eta/P)_{max} = 19.0$ and $\theta^* = 90^\circ$

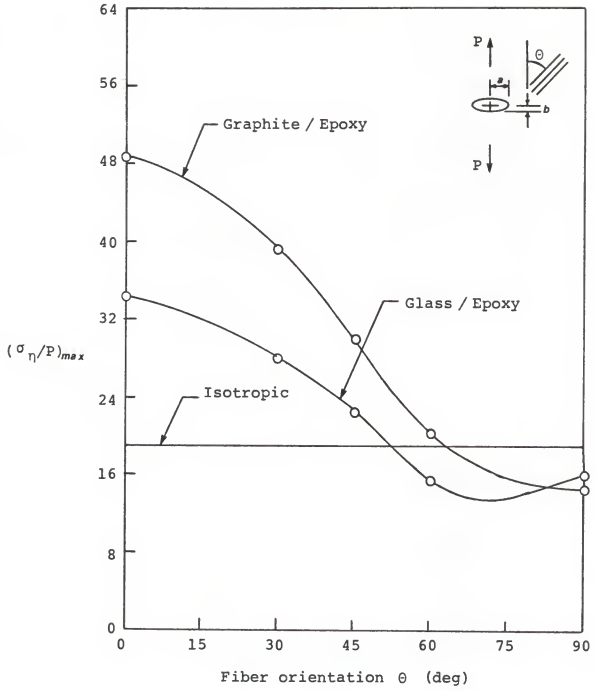

Figure 5.11: Maximum stress-concentration factor vs direction of fiber orientation for an elliptical hole, a/b = 9

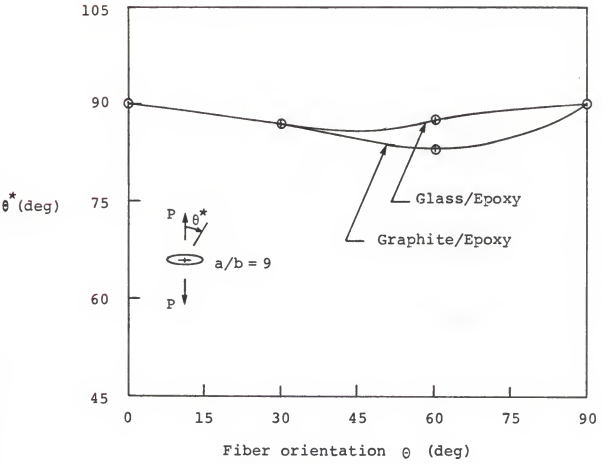

Figure 5.12: Location of the maximum stress-concentration vs direction of fiber orientation for an elliptical hole, a/b = 9

5.1.4 The Elliptical Hole with Aspect Ratio a/b = 20

The stress concentrations around the hole for the two fiber materials and the five fiber orientation angles in this case are calculated and presented in Figures 5.13 and 5.14 for glass/epoxy and graphite/epoxy, respectively.

Table 5.4 presents the numerical value of the maximum stress-concentration factor $(\sigma_\eta/P)_{max}$ and its location (angle θ^*) on the elliptical contour of the hole for each fiber orientation angle and for the two fiber materials.

The effect of fiber orientations on the maximum stress-concentration factor and on its location are shown in Figure 5.15 and 5.16, respectively, for glass/epoxy and graphite/epoxy composite materials.

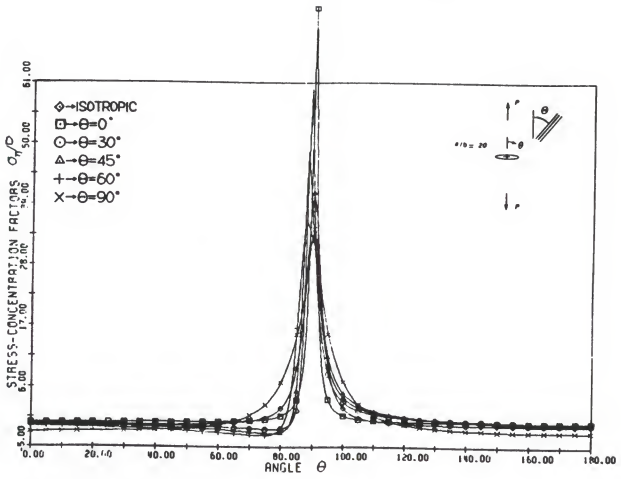

Figure 5.13: Stress-concentrations around an elliptical hole, with ratio a/b = 20, for glass/epoxy with different fiber orientations

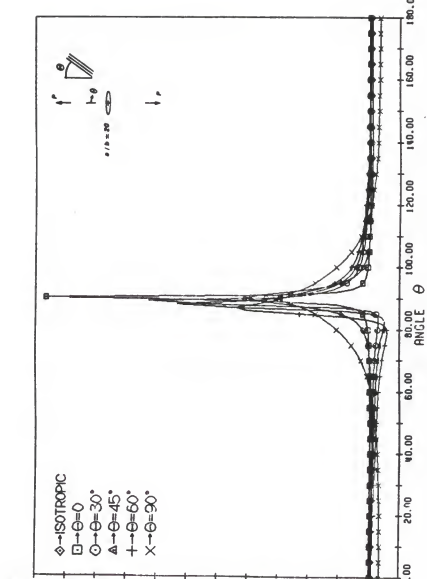

Figure 5.14: Stress-concentrations around an elliptical hole, with ratio a/b = 20, for graphite/epoxy with different fiber orientations

Table 5.4: Maximum stress-concentration factor for an elliptical hole with ratio a/b = 20

Fiber orientation θ (deg)	Glass/Epoxy		Graphite/Epoxy	
	$(\sigma_\eta/P)_{max}$	θ^* (deg)	$(\sigma_\eta/P)_{max}$	θ^* (deg)
0	74.603	90	106.483	90
30	59.951	89	72.795	89
45	48.576	88	63.407	88
60	35.687	88	44.003	87
90	34.479	90	30.835	90

Note: For the case of isotropic materials $(\sigma_\eta/P)_{max} = 41.0$ and $\theta^* = 90^\circ$

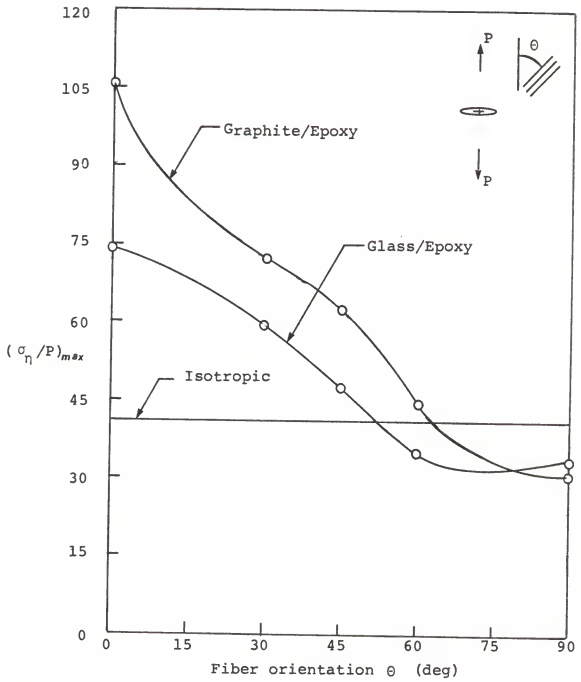

Figure 5.15: Maximum stress-concentration factor vs direction of fiber orientation for an elliptical hole, a/b = 20

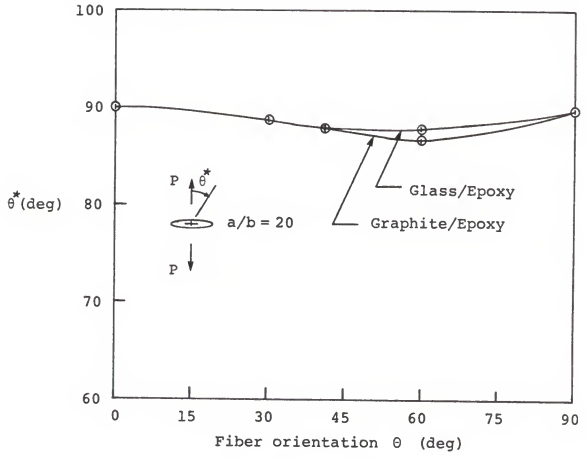

Figure 5.16: Location of the maximum stress-concentration vs direction of fiber orientation for an elliptical hole, a/b = 20

5.1.5 Effect of Aspect Ratio on Stress-Concentrations

The maximum value of stress-concentration factors vs the aspect ratios of the elliptical hole (a/b) are shown in Figure 5.17 and 5.18 for glass/epoxy and graphite/epoxy, respectively. A linear variation of the maximum stress-concentration factor and the aspect ratio has been noticed for the last two figures for all fiber orientation angles as well as for the isotropic case. This linear variation concludes what is known in the field of fracture mechanics as the stress singularity near crack tip, where this stress concentration factor reaches infinity as the aspect ratio of the elliptical hole goes to infinity, in other words as the minor axes of the ellipse becomes zero (the case of slit or sharp crack).

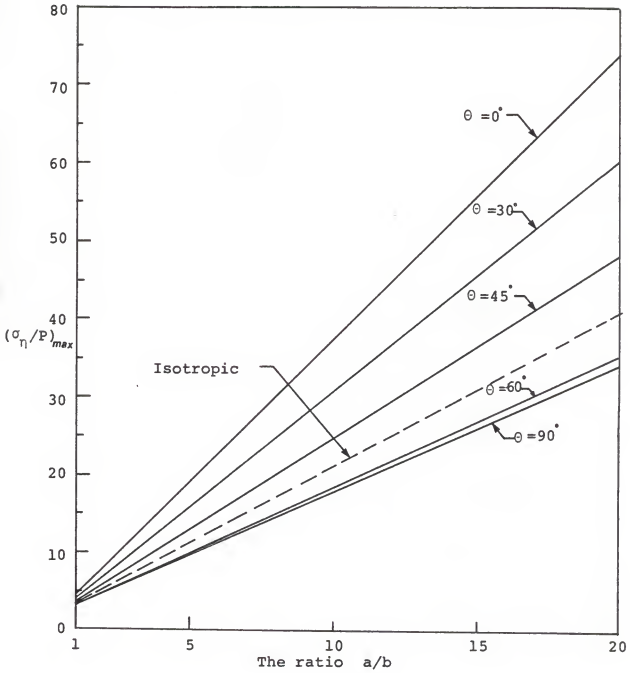

Figure 5.17: Maximum stress-concentration factor vs aspect ratio a/b of elliptical hole for glass/epoxy

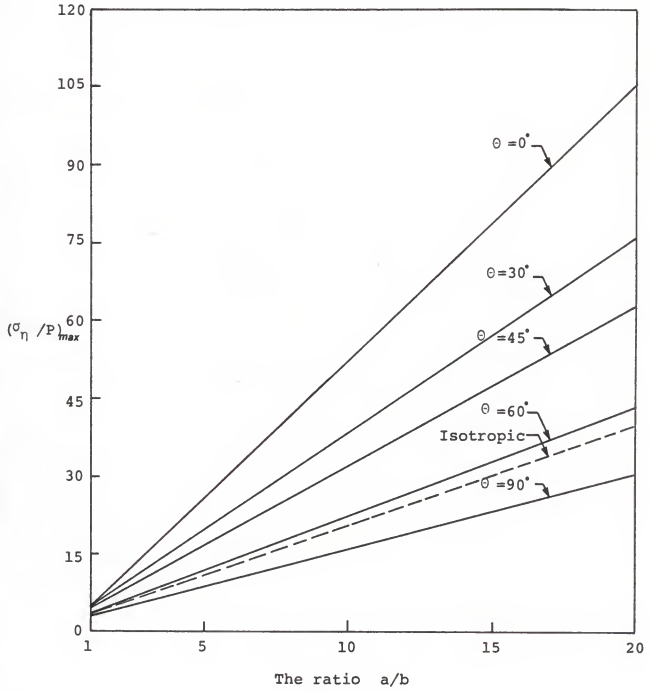

Figure 5.18: Maximum stress-concentration factor vs aspect ratio a/b of elliptical hale for graphite/epoxy

5.2 Stress Intensity Factors

After developing the finite element computer program which is based on the stress-hybrid model, the author chose some numerical examples which were based on different techniques such as the boundary collocation method. Two numerical examples were taken from Gandhi's study [7] and analyzed according to the finite element procedure. The first one has a central inclined crack with 45° to loading axis with the fiber direction parallel to the loading direction. The second one is exactly the same as the first one except that the fiber direction is perpendicular to the loading direction. Figure 5.19 shows a computer mesh of the plate with the singularity elements at each side of the crack tip.

The stress intensity factors obtained from the finite element computer code give the following result:

$$K_I = 0.4561 \qquad K_{II} = 0.6223 \tag{5.1}$$

Comparing to the values obtained from the boundary collection method in reference [7]

$$K_I = 0.6 \qquad K_{II} = 0.56 \tag{5.2}$$

we notice here some differences which will be discussed at the end of this section.

In the other numerical example where the fiber direction is perpendicular to the loading direction, the finite element result gives

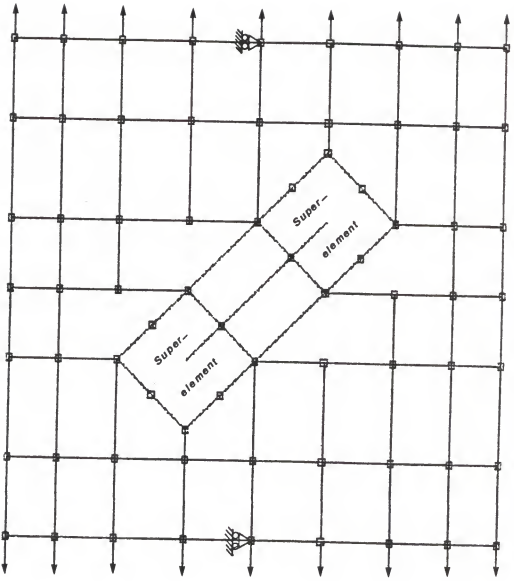

Figure 5.19: Mesh plot before deformation

$$K_I = 0.3825 \qquad K_{II} = 0.5669 \qquad (5.3)$$

Comparing this to the values obtained from reference [7],

$$K_I = 0.64 \qquad K_{II} = 0.61 \qquad (5.4)$$

indicates also some difference in the evaluation of these stress intensity factors.

Examination of Gandhi's results [7], Equations (5.2) and (5.4) for both cases, shows that the value of the stress intensity factor be obtained for the opening mode seems to have no large difference between these two cases in spite of having a large difference in the fiber orientations. For the first case the fiber direction is parallel to the loading direction and for the second case the fiber direction is perpendicular to the loading direction. In addition, the first case should produce stronger material in the loading direction than the other case. That means stress intensity factor K_I should have a higher value than the second case, which is predicted from the results obtained by our finite element method. Figure 5.20 indicates a computer mesh plot of the plate after deformation. This figure also shows that the central crack starts to open due to the external applied load. These crack displacements were magnified about 100 times larger than the actual displacement in order to see the shape of such deformations on the plot.

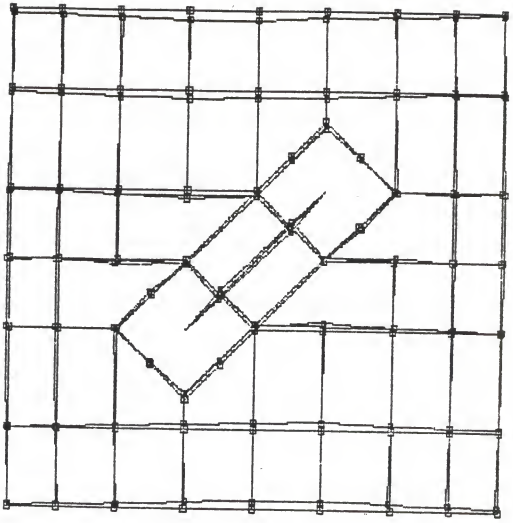

Figure 5.20: Mesh plot after deformation

CHAPTER 6
EXPERIMENTAL PROGRAM

The first section of this chapter will discuss the method used in the experimental part of this study as well as the formula used and its limitation. The other section will present some details on the material, type, and size of specimen used in addition to manufacturing and machining processes. Finally, a description of the fixture and mounting procedure will be given.

6.1 Theoretical Background

The experimental program was designed to provide some data which can be used in evaluating the strain energy release rate G based on compliance. This method is also known as the K-calibration technique. In particular, the program was intended to compare an experimental evaluation of G with an analytical calculation of G based on the stress intensity factors which were calculated from the stress-hybrid singularity super finite element (see Section 4.6). This comparison leads to full confidence in the principles discussed previously.

This compliance calibration technique is widely used in determining the fracture toughness of isotropic materials. This method is not valid for orthotropic materials when the

crack does not advance along the original crack direction. This is because the compliance calibration technique is based on the principle of linear fracture mechanics, which assumes in advance that the crack grows along its original direction. Because of the above restriction, this experimental verification was carried out for a special case of two symmetric cracks emanating from a circular hole in a direction parallel to the fiber direction. The fiber direction was chosen to be perpendicular to the loading direction in order to produce a single mode fracture (opening mode), so that one could measure the crack opening displacement (COD) in an accurate and more direct way by using the COD-extensometer.

The theoretical expression for the critical strain energy release rate using the compliance calibration method is given by the relation [35]

$$G_{cr} = \frac{1}{2} \frac{P^2_{max}}{t} \frac{d\lambda}{da} \tag{6.1}$$

where (a-d/2) is the original crack length and λ is the compliance of the specimen, which is defined as the inverse of the slope of the P-δ curve. A polynomial curve was fitted to the λ vs. a/w data and the slope $d\lambda/da$ was determined as a function of a/w. The energy release rate was then obtained from Equation (6.1).

6.2 Experimental Procedures

6.2.1 Specimen Preparation

All specimens were cut from two rectangular 30.5 cm x 30.5 cm plates of unidirectional composite materials. This composite material was manufactured from glass-epoxy which was supplied in prepreg Scotchply-1003 tape rolls by the 3M Company (Minnestoa Mining and Manufacturing Company). The two rectangular plates were laid up in one direction using 15 plies to form one lamina each. They were pressurized and cured in an autoclave using the prepreg supplier's recommendation for the curing cycle procedure. For more details on manufacturing processes and a description of experimental equipment see Collazo's study in reference [34]. The elastic constants for unidirectional Scotch ply glass-epoxy are the following [34]:

$E_1 = 40.0$ GPa $\quad (5.8 \times 10^6$ psi)

$E_2 = 8.27$ GPa $\quad (1.2 \times 10^6$ psi)

$G_{12} = 4.14$ GPa $\quad (0.6 \times 10^6$ psi)

$\nu_{12} = 0.26$

Six identical specimens were cut and machined from each plate to produce a specimen size of 300 mm x 42 mm. Each specimen was weakened by drilling a 10.66 mm diameter hole

in the center of the specimen. Two symmetric cracks were initiated at the center of the specimen on the hole boundary using a jeweler's saw. Some specimens suffered some degree of delamination near the hole on the crack side of the specimen where the drill exited, while the center cracks all exhibited some degree of deviation from a straight line due to wandering of the saw blade.

All twelve specimens cut from the two plates were identical in all dimensions and fiber orientation except for the ratio of the crack length to specimen width, which was nominally 0.3, 0.4, 0.5, 0.6, 0.7, and 0.8 for the six specimens, respectively. For illustration of all specimen dimensions see Figure 6.1 The other six specimens were prepared with the same crack length to specimen width ratios; thus, there were two identical specimens from each type. All specimens had an average thickness of about 3.25 mm and the fiber volume fractions for the plates were determined to be approximately 50 percent.

6.2.2 Test and Procedures

All specimens were ramp loaded by friction grips (see Figure 6.2) and tested at room temperature and a constant extension rate of 0.02 mm per second to the maximum load P_{max}. Each test was stopped shortly after reaching the maximum load, which corresponded to the beginning of crack propagation. The COD versus load was

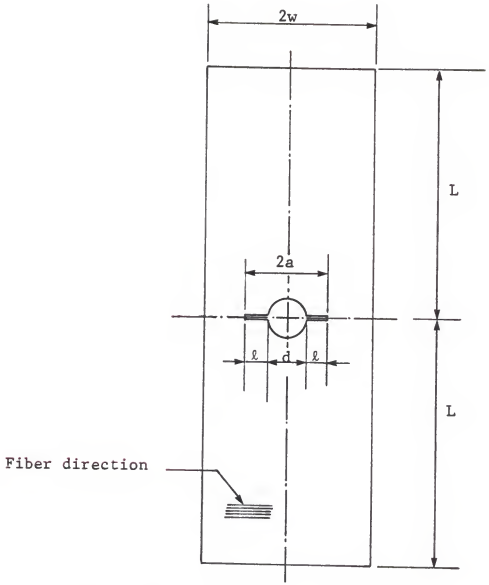

w = 21.0 mm; L = 150 mm; d = 10.66 mm;
a/w = 0.3, 0.4, 0.5, 0.6, 0.7, 0.8

Figure 6.1: A test specimen with all dimensions

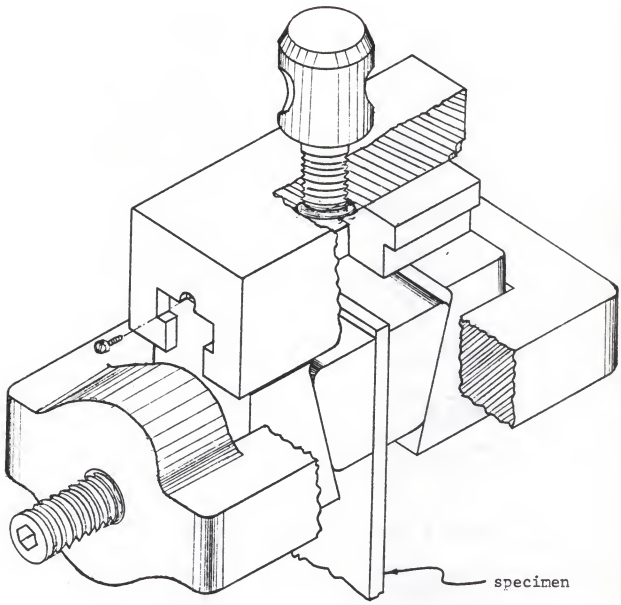

Figure 6.2: A specimen mounted by friction grips

recorded for all specimens by using an extensometer (MTS Model 632.02C-20), which was mounted on the center of the specimen by a special fixture (see Figure 6.3). This fixture was designed to attach the extensometer on the specimen and to allow it to be aligned centrally on the vertical axes of the specimen for better recording of COD. Figure 6.4 shows the tension specimen with extensometer attached, mounted on the Material Testing System (MTS) testing machine. The applied load and the corresponding displacement of the extensometer were recorded continuously on an x,y-plotter (Omnigraphic 2000; Houston Instruments). A typical load versus COD curve for the specimen having $a/w = 0.5$ is shown in Figure 6.5. The load which causes incipient crack growth is defined as P_{max} and the corresponding COD is the maximum crack opening displacement. The inverse of the slope of the linear portion of the load versus COD is known as the compliance, λ, of the load versus COD curve. For each specimen, data of P_{max} and λ were recorded.

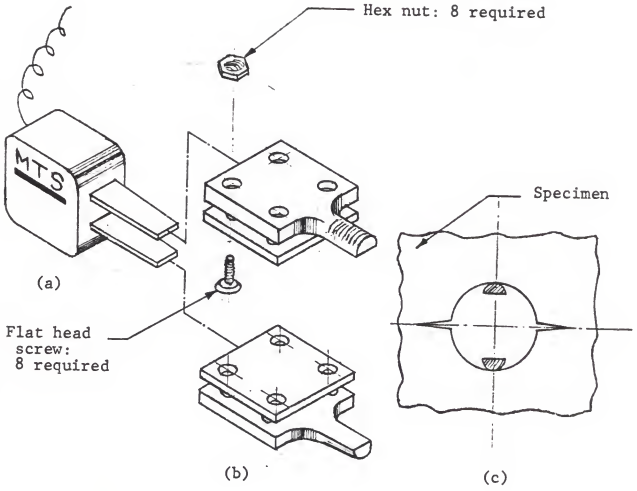

(a) MTS extensometer Model 632.02C-20
(b) Fixture assembly
(c) Front view of the fixture inside the hole

Figure 6.3: Extensometer and fixture assembly

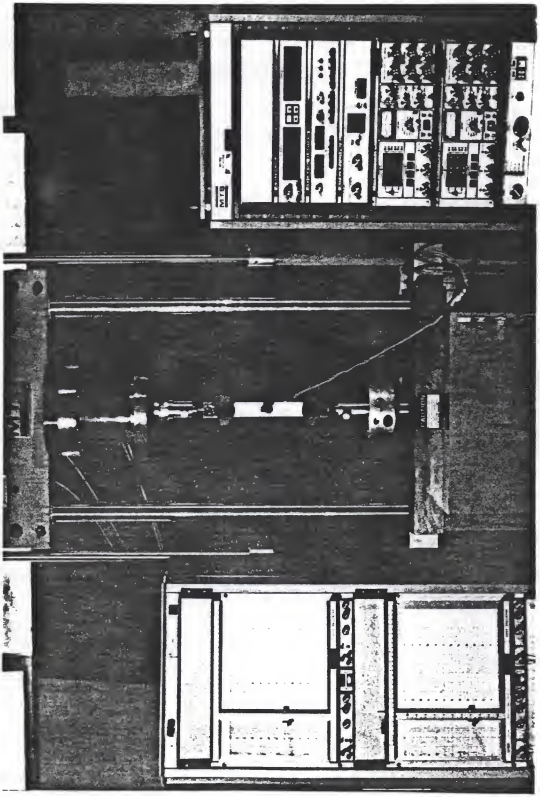

Figure 6.4: Photographic picture of MTS testing machine

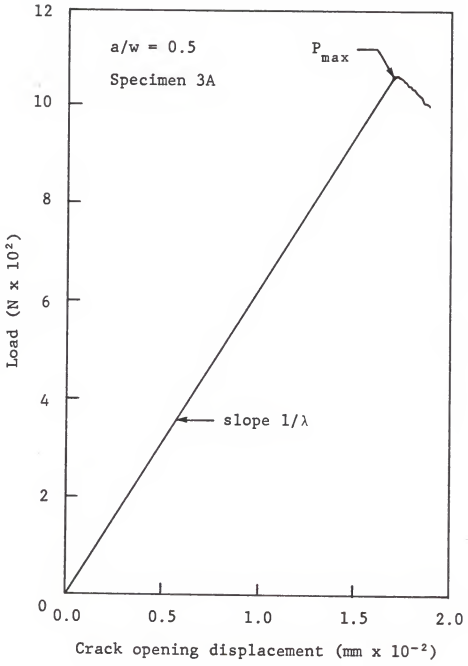

Figure 6.5: A typical load vs. crack opening displacement

CHAPTER 7
EXPERIMENTAL RESULTS, CONCLUSIONS, AND RECOMMENDATIONS

This chapter will present the test results of glass/epoxy specimens to determine the critical strain energy release rate. These results will then be compared to the numerical results obtained from the finite element computer program. Stress intensity factors and the energy release rate will be obtained for the case of a plate with two symmetrical cracks emanating from a circular hole in unidirectional reinforced-fiber composite materials.

Finally, an overall conclusion for the two main parts of this work (stresses around an opening with and without cracks) will be given. The last section will be mainly for stating some suggestions and recommendations for future work related to this topic.

7.1 Experimental Results

All twelve test specimens were loaded on the MTS testing machine to failure. Figure 7.1 shows a typical photograph of a specimen and all other attachments. A typical record of all specimens, including their initial crack-length to width ratio (a/w), the compliance λ, the derivative $d\lambda/d(a/w)$, and the critical energy release

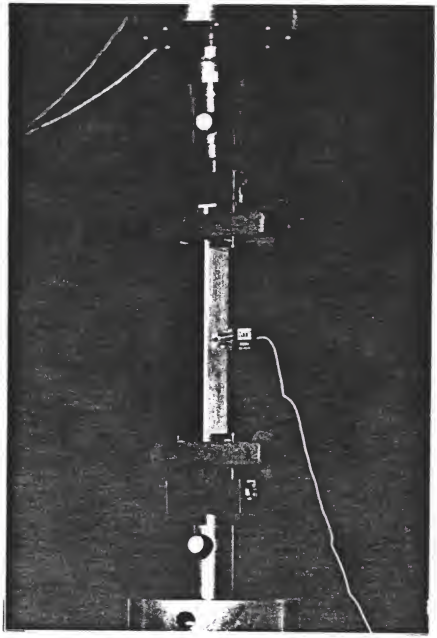

Figure 7.1: A typical photograph illustrating a specimen, fixture, and extensometer all mounted on MTS testing machine

rate per unit area of crack surface growth G_{cr} ($N \cdot M/m^2$ = N/m), all of which have been tabulated in Table 7.1.

A set of cubic polynomials (quasi-Hermite spline) in a form of mathematical library subroutine [36] was used to interpolate a set of experimental points from the compliance vs. initial a/w data. This quasi-Hermite spline produces a continuous first derivative of the compliance $d\lambda/d(a/w)$. This first derivative was evaluated at each initial crack/width ratio. Then, using Equation (6.1), the critical energy release rate at each initial crack/width ratio, a/w, can be obtained as in Table 7.1.

Data obtained from the experimental evaluation of compliance were scattered above and below the curve as is indicated in Figure 7.2. Therefore, the average value of these data was used to fit the compliance curve, even though this average seems not to be accurate enough, because it was obtained from only two specimens. Generally, these experimental results give us some confidence about the predicted value of G_{cr} from the analytical method. The experimental value for the critical energy release rate for glass/epoxy was determined, for the case of a/w = 0.5, to be 18.3 N/m where its calculated value is 39.90 N/m. This difference between analytical and experimental evaluation was expected for three reasons. First is the small number of specimens used. Second is the difficulty

Table 7.1: Experimental data and results for obtaining energy release rates

Specimen Number	a/w	P_{max} (N)	λ (mm/N x 10^{-5})	Thickness (mm)	$d\lambda/d(a/w)$ (mm/N x 10^{-5})	G (N/mm x 10^{-1})
1A	0.3	1,305.40	1.29	3.35	1.384	0.076
1B	0.3	1,176.00	1.33	3.25		
2A	0.4	1,244.68	1.32	3.23	3.428	0.166
2B	0.4	1,078.77	2.00	3.31		
3A	0.5	1,033.60	1.65	3.37	4.833	0.183
3B	0.5	1,024.60	2.20	3.35		
4A	0.6	915.75	2.33	3.45	9.129	0.260
4B	0.6	890.7	2.65	3.37		
5A	0.7	727.7	4.50	3.32	15.548	0.288
5B	0.7	647.8	5.00	3.20		
6A	0.8	581.5	5.50	3.42	26.087	0.298
6B	0.8	560.0	6.50	3.36		

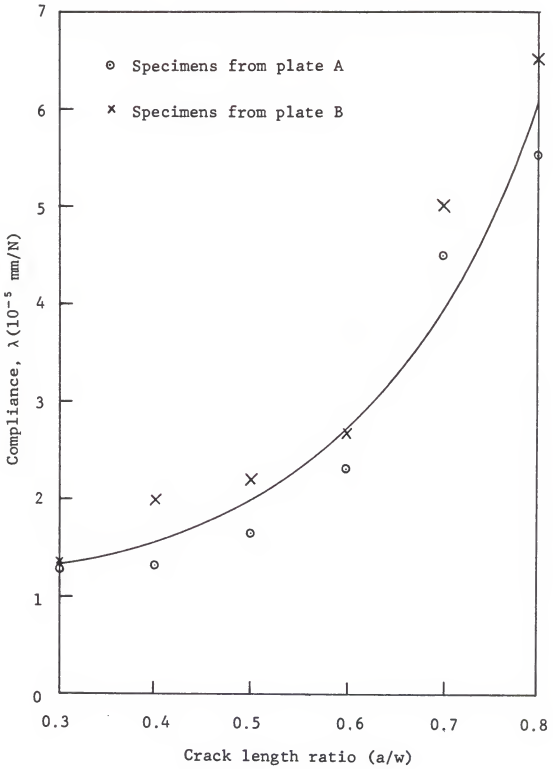

Figure 7.2: Compliance λ vs. a/w plot

of producing identical specimens due to manufacturing and machining all specimens manually in the laboratory. The third reason is the difficulty of producing a sharp crack tip as in the theoretical analysis.

7.2 Analytical Results

To produce some numerical results we chose the case of two initial symmetric cracks perpendicular to the loading direction and emanating from a circular hole with ratio $a/w = 0.5$, for five different fiber orientations with respect to the loading axis. In the case where the fiber direction angle is 0° or 90°, the calculation of the stress intensity factors and the energy release rate were carried out for one quarter of the specimens. This quarter was divided into 29 quadrilateral isoparametric elements, one being the singular-super element, where the stress singularity near the crack tip has been treated by using the hybrid stress model discussed in Chapter 4. The total number of degrees of freedom was 81; Figure 7.3 shows a computer plot mesh for this case. Calculations have been carried out for glass/epoxy and graphite/epoxy composite materials.

For a case where the fiber direction makes some angle with the loading direction, we considered the full specimen mesh, because there was no material or geometric symmetry. The specimen was divided into 114 quadrilateral

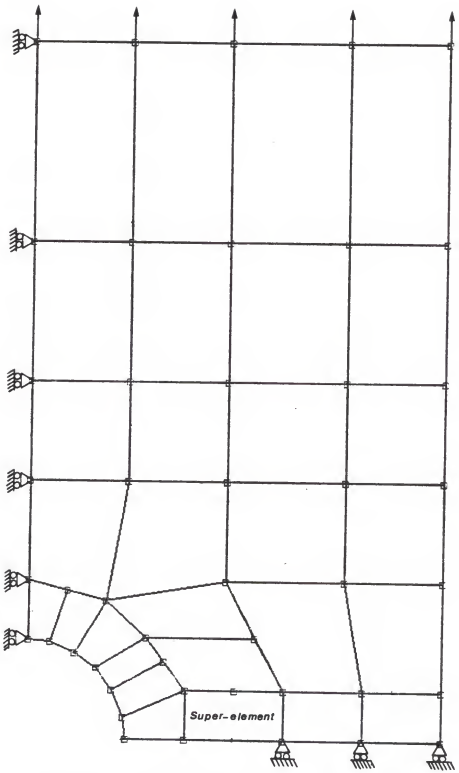

Figure 7.3: Mesh for one quarter specimen (symmetric case), a/w = 0.5

isoparametric elements, two of which were singular-super elements, one for each crack tip. The total number of degrees of freedom was 322. Computer mesh plots for the full specimen before and after deformation are shown in Figures 7.4 and 7.5, respectively.

All results obtained by the finite element computer program are tabulated in Tables 7.1 and 7.2 for glass/epoxy and graphite/epoxy composite materials, respectively. Figure 7.6 shows the result of K_I and K_{II} with different fiber orientations for glass/epoxy composite material, as given by Equations (4.41) and (4.42) of Section 4.5. Figure 7.7 shows the results of calculation of strain energy release rate for glass/epoxy having different fiber orientations, as given by Equation (4.44) of Section 4.6.

7.3 Overall Conclusions and Remarks

7.3.1 Stress Concentration Factors

Based on the analytical solution discussed in Chapter 2, the results shown in Figures 5.1 through 5.18 and Tables 5.1 through 5.4, we make the following remarks regarding the stress concentration near holes in unidirectional fiber-reinforced composite materials:

1. The maximum value of stress concentration depends on the stiffness of the composite.
2. The location of this maximum value depends on the fiber orientation, fiber material, and loading direction.

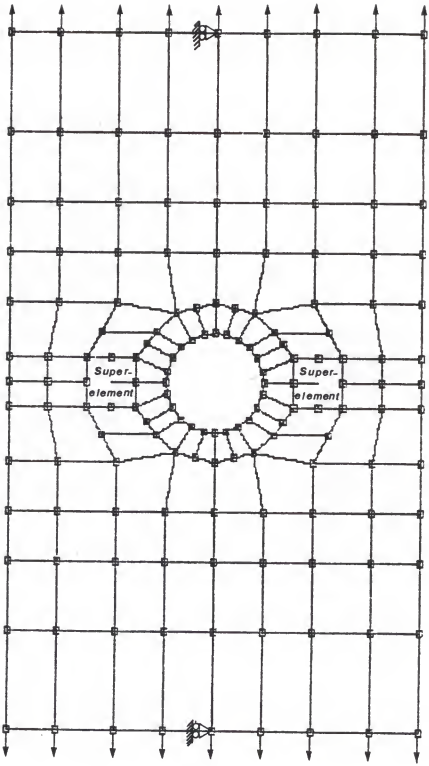

Figure 7.4: Full specimen mesh before deformation (nonsymmetric case), a/w = 0.5

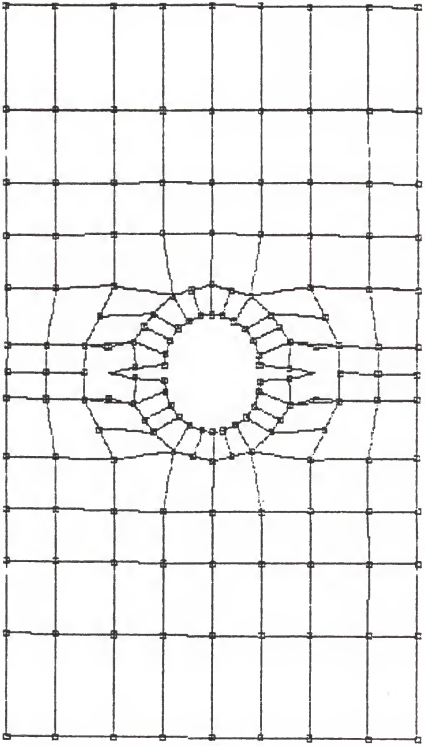

Figure 7.5: Full specimen mesh after deformation (nonsymmetric case), a/w = 0.5

Table 7.2: Analytical results for K_I, K_{II}, and G

Fiber Orientation θ (degree)	$K_I \times 10^{-5}$ $(MN/m^2)\sqrt{m}$	$K_{II} \times 10^{-5}$ $(MN/m^2)\sqrt{m}$	G (N/m)
0	9.07	0.00	261.20
20	3.62	7.30	156.00
45	1.03	6.35	84.27
60	3.24	4.04	44.94
90	5.26	0.00	39.90

Note: These results obtained from the finite element computer program for the case of unidirectional glass/epoxy composite material

Table 7.3: Analytical results for K_I, K_{II}, and G

Fiber Orientation θ (degree)	$K_I \times 10^{-5}$ $(MN/m^2)\sqrt{m}$	$K_{II} \times 10^{-5}$ $(MN/m^2)\sqrt{m}$	G (N/m)
0	9.57	0.00	194.90
90	3.92	0.00	9.22

Note: These results obtained from the finite element computer program for the case of unidirectional graphite/epoxy (symmetric case)

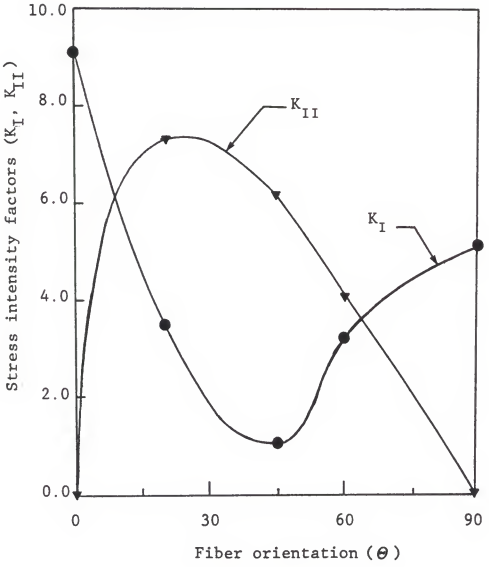

Figure 7.6: Stress intensity factors vs. fiber orientation for two symmetric cracks emanating from a circular hole in unidirectional glass/epoxy (a/w = 0.5)

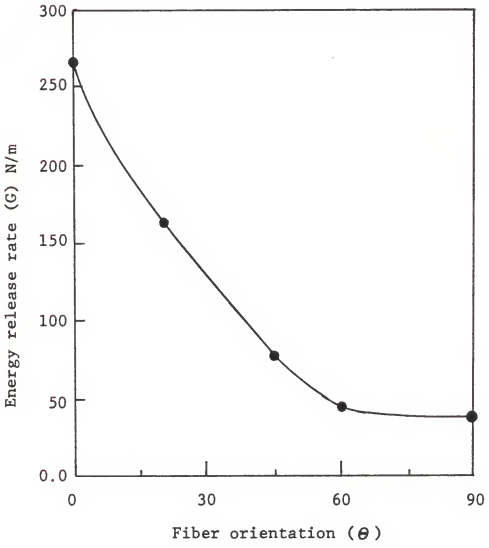

Figure 7.7: Energy release rate vs. fiber orientation for glass/epoxy (a/w = 0.5)

3. The maximum stress can be reduced by changing the fiber direction with respect to loading direction.
4. The shape and size of the hole also has a large effect on stresses. For example, a hole of a circular shape causes less stress than an elliptical shape with the major axis perpendicular to the loading axis.
5. When the value of the aspect ratio a/b for the elliptical hole increases, the location of maximum stress-concentration becomes more independent from both fiber orientation and fiber material for the same loading direction.
6. As the aspect ratio (a/b) increases, the maximum stress-concentration factor increases linearly for glass/epoxy and graphite/epoxy composite materials. The same is also true for the isotropic case.

7.3.2 Stress Intensity Factors

The stress intensity factor for the opening mode with the fiber direction parallel to the loading direction has a higher value than the value for the case with the fiber direction perpendicular to the loading direction. On

the other hand, uncracked material in the first case with the fibers parallel to the loading direction, is considered to be much stronger than in the other case.

The same argument holds for the energy release rate, where we have a higher value for the case of fiber direction being parallel to the loading direction. In comparing the single mode fracture behavior between the two different composite materials studied, we find that the graphite/epoxy composite gives a lower stress intensity factor and a lower energy release rate than glass/epoxy. This means that a composite material made of graphite/epoxy offers more fracture resistance than a composite material made of glass/epoxy.

In the mixed-mode fracture behavior, the fracture failure takes place because of a combination of two stress intensity factors, K_I and K_{II}. In the analytical results of Figure 7.6, we find that the stress intensity factor of the shear mode decreases as the fiber direction angle θ increases. But increasing this angle reduces the strength of the material in the loading direction. So, it seems impossible to optimize K_I and K_{II} at the same time. Obviously, there is a trade-off between K_I and K_{II}, depending upon the loading direction and design requirements.

7.4 Recommendations for Future Study

There are two distinct areas in which future research can be carried out. The first deals with the failure criteria and the location of failure stresses due to the high stress-concentrations near holes in composite materials. In addition, a study of the effects of the stacking sequence, and the type of material and loading condition on the fracture properties of a laminate, will make a valuable contribution to engineering design.

The second general area of future research is to study the stress intensity factors using different finite element models based on one of the mixed energy approaches discussed in Chapter 3 and then compare its results with the results obtained from the approach studied here. Another possible continuation of this work is to extend the technique adopted in this dissertation to three-dimensional elasticity and then solve the fracture mechanics problem. A special treatment has to be added into the code in order to seek a solution when we have pairwise equal roots, such as were obtained by solving the characteristic equation (2.11) of Chapter 2.

One final recommendation is to study the order of the stress singularity near the crack tip for different composites and its effect on the evaluation of stress intensity factors near the crack tip.

APPENDICES

APPENDIX A
ELASTIC COEFFICIENTS FOR GENERAL ORTHOTROPIC MATERIALS

The coefficients of the stress-strain matrix a_{ij} of Equation (2.4) can be written as follows [18, 37]:

$$a_{11} = \cos^4\theta/E_1 + (1/G_{12} - 2\nu_{12}/E_1)\sin^2\theta\cos^2\theta + \sin^4\theta/E_2$$

$$a_{12} = -\nu_{12}(\sin^4\theta + \cos^4\theta)/E_1 + (1/E_1 + 1/E_2 - 1/G_{12})\sin^2\theta\cos^2\theta$$

$$a_{22} = \sin^4\theta/E_1 + (1/G_{12} - 2\nu_{12}/E_1)\sin^2\theta\cos^2\theta + \cos^4\theta/E_2$$

$$a_{16} = (2/E_1 + 2\nu_{12}/E_1 - 1/G_{12})\sin\theta\cos^3\theta - (2/E_2 + 2\nu_{12}/E_1 - 1/G_{12})\sin^3\theta\cos\theta$$

$$a_{26} = (2/E_1 + 2\nu_{12}/E_1 - 1/G_{12})\sin^3\theta\cos\theta - (2/E_2 + 2\nu_{12}/E_1 - 1/G_{12})\sin\theta\cos^3\theta$$

$$a_{66} = (4/E_1 + 4/E_2 + 8\nu_{12}/E_1 - 2/G_{12}) \sin^2\theta \cos^2\theta$$

$$+ (\sin^4\theta + \cos^4\theta)/G_{12}$$

where θ is the angle between the fiber direction and the x-axis (see Figure 2.1). All the above coefficients are expressed in terms of just four independent material constants E_1, E_2, ν_{12}, and G_{12}.

APPENDIX B
THE MATHEMATICAL FORMULATION OF THE CONVENTIONAL FINITE ELEMENT (DISPLACEMENT MODEL)

For the finite element displacement model, the governing equilibrium equations can be obtained by minimizing the total potential energy functional of the system. The total potential energy functional (π) can be expressed as previously stated in Equation (3.2)

$$\pi_p = \int_V \frac{1}{2} E_{ijk\ell} \epsilon_{ij} \epsilon_{k\ell} \, dV - \int_{S_\sigma} \bar{T}_i u_i \, dS \qquad (B.1)$$

or in matrix notation

$$\pi_p = \int_V \frac{1}{2} \{\epsilon\}^T [E] \{\epsilon\} \, dV - \int_{S_\sigma} \{u\}^T \{\bar{T}\} \, dS \qquad (B.2)$$

In the finite element displacement method, the displacement is assumed to have unknown values only at the nodal points, so that the variations within any element are described in terms of the nodal values by means of interpolation function. Thus,

$$\{\bar{u}\} = [L] \{q^e\} \qquad (B.3)$$

where [L] is the set of interpolation functions termed shape functions and $\{q^e\}$ is the vector of nodal displacements of the element. The strains within the element can be expressed in terms of element nodal displacement as

$$\{\varepsilon\} = [B]\{q^e\} \tag{B.4}$$

where [B] is the strain matrix generally composed of derivatives of the shape functions. If we assume that the total volume V is divided into M discrete elements and the element shape functions have been chosen so that no singularities exist in the integrands of the functional, the total functional of potential energy of the continuum can be expressed as the sum of the functional contributions of the individual element. Thus,

$$\pi_e(u,v) = \sum_{e=1}^{M} \pi_e(u,v) \tag{B.5}$$

where $\pi_e(u,v)$ represents the potential energy functional of an element e which can be written

$$\pi_e(u,v) = \frac{1}{2} \int_{V^e} \{q^e\}^T [B]^T [E] [B] \{q^e\} \, dV$$

$$- \int_{S^e} \{q^e\}^T [L]^T \{\bar{T}\} \, dS \tag{B.6}$$

We know that at equilibrium the potential energy of the system assumes a minimum value. Because of the summation principle expressed in Equation (B.5), we may carry out the minimization process element by element. We note that the potential energy of the discretized system assumes its minimum value when the first variation of the functional vanishes, that is,

$$\delta\pi_p(u,v) = \sum_{e=1}^{M} \delta\pi_e(u,v) = 0 \tag{B.7}$$

where

$$\delta\pi_e(u,v) = \sum_{i=1}^{r} \frac{\partial\pi_e}{\partial u_i}\,\delta u_i + \sum_{i=1}^{r} \frac{\partial\pi_e}{\partial v_i}\,\delta v_i = 0 \tag{B.8}$$

and r is the number of element nodes. But the ∂u_i and the ∂v_i are independent variables; hence, we must have

$$\frac{\partial\pi_e}{\partial u_i} = \frac{\partial\pi_e}{\partial v_i} = 0 \qquad i=1,2,\ldots,r \tag{B.9}$$

for every element e of the system. Thus, after performing this minimization process on Equation (B.6), it becomes

$$\int_{V^e} [B]^T[E][B]\{q^e\}\,dV - \int_{S^e} [L]^T\{\bar{T}\}\,ds = 0$$

or

$$[K^e]\{q^e\} - \{F^e\} = 0 \tag{B.10}$$

where

$$[K^e] = \int_{V^e} [B]^T [E] [B] \, dv \tag{B.11}$$

is the "element stiffness matrix," and

$$\{F^e\} = \int_{S^e} [L]^T \{\bar{T}\} \, ds \tag{B.12}$$

are the equivalent nodal forces for the element. The summation of the terms in Equation (B.10) over all the elements results in a system of equilibrium equations for the entire continuum. These equations are then solved by any standard technique to yield the nodal displacements {q}.

APPENDIX C
STRESS AND DISPLACEMENT EQUATIONS FOR NEAR CRACK TIP SOLUTION

The stress field near the crack tip in an anisotropic body, as was stated by Sih, Paris, and Irwin [32], can be divided into modes of deformation, but the degree of simplification thus achieved is less than for the isotropic case. This is because the crack surface displacements in general anisotropic media depend upon the directional properties of the material and do not necessarily occur in a planar fashion. However, the general state of stress and displacement near a crack tip can still be considered as the sum of three individual boundary problems, namely, those corresponding to inplane-symmetric loading, inplane-skewsymmetric loading, and antiplane shear.

The stresses and displacments equations in a small region surrounding the crack tip in plane deformation are obtained from the same reference [32] as follows:

1. Symmetric loading (crack opening, mode I):

$$\sigma_x = \frac{k_I}{\sqrt{2r}} \operatorname{Re}\left[\frac{\mu_1\mu_2}{\mu_1 - \mu_2}\left(\frac{\mu_2}{\sqrt{\cos\theta + \mu_2 \sin\theta}} - \frac{\mu_1}{\sqrt{\cos\theta + \mu_1 \sin\theta}}\right)\right]$$

$$\sigma_y = \frac{k_I}{\sqrt{2r}} \operatorname{Re}\left[\frac{1}{\mu_1 - \mu_2}\left(\frac{\mu_1}{\sqrt{\cos\theta + \mu_2 \sin\theta}} - \frac{\mu_2}{\sqrt{\cos\theta + \mu_1 \sin\theta}}\right)\right] \qquad \text{(C.1)}$$

$$\tau_{xy} = \frac{k_I}{\sqrt{2r}} \operatorname{Re}\left[\frac{\mu_1\mu_2}{\mu_1 - \mu_2}\left(\frac{1}{\sqrt{\cos\theta + \mu_1 \sin\theta}} - \frac{1}{\sqrt{\cos\theta + \mu_2 \sin\theta}}\right)\right]$$

and

$$u = k_I\sqrt{2r} \operatorname{Re}\left[\frac{1}{\mu_1 - \mu_2}\left(\mu_1 p_2\sqrt{\cos\theta + \mu_2 \sin\theta} - \mu_2 p_1\sqrt{\cos\theta + \mu_1 \sin\theta}\right)\right]$$

(C.2)

$$v = k_I\sqrt{2r} \operatorname{Re}\left[\frac{1}{\mu_1 - \mu_2}\left(\mu_1 r_2\sqrt{\cos\theta + \mu_2 \sin\theta} - \mu_2 r_1\sqrt{\cos\theta + \mu_1 \sin\theta}\right)\right]$$

2. Skew-symmetric loading (crack sliding, mode II):

$$\sigma_x = \frac{k_{II}}{\sqrt{2r}} \operatorname{Re}\left[\frac{1}{\mu_1 - \mu_2}\left(\frac{\mu_2^2}{\sqrt{\cos\theta + \mu_2 \sin\theta}} - \frac{\mu_1^2}{\sqrt{\cos\theta + \mu_1 \sin\theta}}\right)\right]$$

$$\sigma_y = \frac{k_{II}}{\sqrt{2r}} \operatorname{Re}\left[\frac{1}{\mu_1 - \mu_2}\left(\frac{1}{\sqrt{\cos\theta + \mu_2 \sin\theta}} - \frac{1}{\sqrt{\cos\theta + \mu_1 \sin\theta}}\right)\right] \qquad \text{(C.3)}$$

$$\tau_{xy} = \frac{k_{II}}{\sqrt{2r}} \operatorname{Re}\left[\frac{1}{\mu_1 - \mu_2}\left(\frac{\mu_1}{\sqrt{\cos\theta + \mu_2 \sin\theta}} - \frac{\mu_2}{\sqrt{\cos\theta + \mu_2 \sin\theta}}\right)\right]$$

and

$$u = k_{II}\sqrt{2r} \operatorname{Re}\left[\frac{1}{\mu_1 - \mu_2}\left(p_2\sqrt{\cos\theta + \mu_2 \sin\theta} - p_1\sqrt{\cos\theta + \mu_1 \sin\theta}\right)\right]$$

$$v = k_{II}\sqrt{2r} \operatorname{Re}\left[\frac{1}{\mu_1 - \mu_2}\left(r_2\sqrt{\cos\theta + \mu_2 \sin\theta} - r_1\sqrt{\cos\theta + \mu_1 \sin\theta}\right)\right] \qquad \text{(C.4)}$$

The stress distributions and the displacement field near the crack tip in an isotropic body can be expressed in the following due to the work of Irwin [38] and Westergaard [39]:

1. Symmetric loading (crack opening, mode I):

$$\sigma_x = \frac{k_I}{\sqrt{2r}} \cos \theta/2(1 - \sin \theta/2 \sin 3\theta/2)$$

$$\sigma_y = \frac{k_I}{\sqrt{2r}} \cos \theta/2(1 + \sin \theta/2 \sin 3\theta/2) \qquad \text{(C.5)}$$

$$\tau_{xy} = \frac{k_I}{\sqrt{2r}} \cos \theta/2 \sin \theta/2 \cos 3\theta/2$$

and

$$u = \frac{k_I}{2E}\sqrt{\frac{r}{2}} (1+\nu)[(2\kappa - 1) \cos \theta/2 - \cos 3\theta/2]$$

$$v = \frac{k_I}{2E}\sqrt{\frac{r}{2}} (1+\nu)[(2\kappa + 1) \sin \theta/2 - \sin 3\theta/2] \qquad \text{(C.6)}$$

2. Skew-symmetric loading (crack sliding, mode II):

$$\sigma_x = -\frac{k_{II}}{\sqrt{2r}} \sin \theta/2 \, (2 + \cos \theta/2 \cos 3\theta/2)$$

$$\sigma_y = \frac{k_{II}}{\sqrt{2r}} \sin \theta/2 \cos \theta/2 \cos 3\theta/2$$

$$\tau_{xy} = \frac{k_{II}}{\sqrt{2r}} \cos \theta/2 \, (1 - \sin \theta/2 \sin 3\theta/2)$$

and

$$u = \frac{k_{II}}{2E} \sqrt{\frac{r}{2}} \, (1 + \nu)[(2\kappa + 3) \sin \theta/2 + \sin 3\theta/2]$$

$$v = -\frac{k_{II}}{2E} \sqrt{\frac{r}{2}} \, (1 + \nu)[(2\kappa - 3) \cos \theta/2 - \cos 3\theta/2]$$

where $\kappa = (3 - \nu)/(1 + \nu)$ for plane stress.

APPENDIX D

DERIVATION OF EQUATION (4.1)

Starting from the modified complementary energy functional of Chapter 3 and then adding and subtracting the term

$$\int_{S_{\sigma_n}} \overline{T}_i \, \tilde{u}_i \, dS$$

to Equation (3.8) with multipliers λ_i replaced by their physical meaning $\tilde{u}_i$, interelement boundary displacements, Equation (3.8) we derive

$$(\pi_c)_m = \sum_{n=1}^{M} \left\{ \int_{A_n} \frac{1}{2} C_{ijk\ell} \, \sigma_{ij} \, \sigma_{k\ell} \, dA - \int_{S_n} T_i \, \tilde{u}_i \, dS \right.$$

$$- \int_{S_{\sigma_n}} \overline{T}_i \, \tilde{u}_i \, dS - \int_{S_{u_n}} T_i \, \overline{u}_i \, dS$$

$$\left. + \int_{S_{\sigma_n}} \overline{T}_i \, \tilde{u}_i \, dS \right\} \qquad (D.1)$$

let

$$\int_{\partial A} T_i \tilde{u}_i \, dS = \int_{S_n} T_i \tilde{u}_i \, dS + \int_{S_{\sigma_n}} \bar{T}_i \tilde{u}_i \, dS + \int_{S_{u_n}} T_i \bar{u}_i \, dS \tag{D.2}$$

where $\partial A = S_n + S_{\sigma_n} + S_{u_n}$ is the entire boundary of an element A_n

$$\left.\begin{aligned} \tilde{u}_i &= \bar{u}_i \qquad \text{on } S_{u_n} \\ T_i &= \bar{T}_i \qquad \text{on } S_{\sigma_n} \end{aligned}\right\} \tag{D.3}$$

Also let

$$(\pi_c)_m = \sum_{n=1}^{M} \pi \tag{D.4}$$

where π now denotes the complementary energy functional for one element A with boundary ∂A.

Substitution of Equations (D.2), (D.3), and (D.4) into Equation (D.1) yields

$$\pi = \int_A \frac{1}{2} C_{ijk\ell} \sigma_{ij} \sigma_{k\ell} \, dA - \int_{\partial A} T_i \tilde{u}_i \, dS + \int_{S_\sigma} \bar{T}_i \tilde{u}_i \, dS \tag{D.5}$$

The Euler equations of the functional $(\pi_c)_m$ of Equation (3.8) of Chapter 3 are

$$C_{ijk\ell}\ \sigma_{k\ell} = \frac{1}{2}\ (u_{i,j} + u_{j,i}) \qquad \text{in A} \qquad \text{(D.6a)}$$

$$\sigma_{ij,j} = 0 \qquad \text{in A} \qquad \text{(D.6b)}$$

$$T_i = \sigma_{ij}\ \nu_j \qquad \text{on } \partial A \qquad \text{(D.6c)}$$

Now, with the help of Equation (D.6) and the divergence theorem, let us take a look at the first term on the right hand side of Equation (D.5) as the following

$$\int_A \frac{1}{2}\ C_{ijk\ell}\ \sigma_{ij}\ \sigma_{k\ell}\ dA = \frac{1}{2} \int_A \varepsilon_{k\ell}\ \sigma_{k\ell}\ dA$$

$$= \frac{1}{4} \int_A (\sigma_{ij}\ u_{i,j} + \sigma_{ij}\ u_{j,i})dA \qquad \text{(D.7)}$$

But

$$\int_A \sigma_{ij}\ u_{i,j}\ dA = \int_A [(\sigma_{ij}\ u_i)_{,j} - \sigma_{ij,j}\ u_i]dA$$

Now, applying the divergence theorem to the first term on the right hand side of the above equation, and cancelling the second term due to Equation (D.6b) leads to

$$\int_A \sigma_{ij}\ u_{i,j}\ dA = \int_{\partial A} \sigma_{ij}\ u_i\ \nu_j\ dS \qquad \text{(D.8)}$$

Inserting Equation (D.6c) into Equation (D.8), we get

$$\int_A \sigma_{ij}\, u_{i,j}\, dA = \int_{\partial A} T_i\, u_i\, dS \tag{D.9a}$$

and similarly

$$\int_A \sigma_{ij}\, u_{j,i}\, dA = \int_{\partial A} T_j\, u_j\, dS \tag{D.9b}$$

Insertion of Equations (D.9a) and (D.9b) into Equation (D.7) gives

$$\frac{1}{2}\int_A C_{ijk\ell}\, \sigma_{ij}\, \sigma_{k\ell}\, dV = \frac{1}{2}\int_{\partial A} T_i\, u_i\, dS \tag{D.10}$$

By replacing the first term of Equation (D.5) with its expression from Equation (D.10) we obtain the following:

$$\pi = \frac{1}{2}\int_{\partial A} T_i\, u_i\, dS - \int_{\partial A} T_i\, \tilde{u}_i\, dS + \int_{S_\sigma} \overline{T}_i\, \tilde{u}_i\, dS$$

but the term

$$\int_{S_\sigma} \overline{T}_i\, \tilde{u}_i\, dS = 0$$

because of the free traction on the crack surfaces.

APPENDIX E
FINITE ELEMENT COMPUTER PROGRAM

On the following pages appears a complete listing of the finite elements computer program which has been developed and used in this research. This program was written in a standard FORTRAN language and is applicable to FORTRAN compiler G and all other modified versions of the FORTRAN compilers.

The listing of the matrix inversion and the plot subroutines are not included here. The matrix inversion subroutine was taken from the Standard International Mathematical and Statistical Libraries (IMSL), while the plot subroutines were taken from the Gould plot. Both of these subroutines were installed by the Northeast Regional Data Center (NRDC), State University System of Florida.

This finite elements computer code handles the two-dimensional elasticity problem (plane stress) in fracture mechanics. This code calculates stress intensity factors (K_I,K_{II}) near the crack tip in the presence of a single or mixed mode fracture for either isotropic or anisotropic material. In addition it calculates the energy release rate for the case of rectilinear anisotropic materials.

```
      IMPLICIT REAL*8(A-H,O-Z)
      COMPLEX ZMU1,ZMU2,RMU1,RMU2
      REAL*4  YOUNG1,YOUNG2,POIS12,G12,THICK,SP(6),XTIP(2),YTIP(2)
     $       ,ROTR(4),ROTI(4)
      DIMENSION COORD(72,2),LNODS(46,9),ASDIS(144),NOFIX( 2),
     ,IFPRE( 2,2),PRESC( 2,2) ,ELOAD(46,18),NDFRO(72),BCRT(2,2,18)
     $  ,CRD(72,2),SIF(4)
      COMMON/WORK/SHAP(4),DERIV(2,4),BMATX(3,8),POSGP(3)
     ,      ,WEIGP(3),QBMAT(3,8),GPCOD(2,9),SMATX(3,8,9)
      COMMON/MATRIL/YOUNG1,YOUNG2,POIS12,G12,IANGL,ISTRFC,THICK
      COMMON/SUPER/ISUPR1,ISUPR2,KEY1,KEY2,XTIP,YTIP
C
      REWIND 1
      REWIND 2
      PI=4.0$DATAN(1.0D0)
      READ(5,900)NPOIN,NELEM,NVFIX, NGAUS,NNODE,ISUPR1,ISUPR2,KEY1,KEY2
      WRITE(6,905)NPOIN,NELEM,NVFIX,NGAUS,NNODE,ISUPR1,ISUPR2,KEY1,KEY2
      NTOTV=2*NPOIN
C.....Read all the element nodal coordinate (x,y) .....
      DO  5  I=1,NPOIN,6
      I2=I+5
      READ(5,930)((COORD(KK,JJ),JJ=1,2),KK=I,I2)
    5 CONTINUE
      DO  3  I=1,NELEM
      DO  3  J=1,NNODE
    3 LNODS(I,J)=0
      DO  10  I=1,NELEM,4
      K=I+3
      IF(I.EQ.45) K=46
      READ(5,925)((LNODS(KK,J),J=1,4),KK=I,K)
   10 CONTINUE
      READ(5,926)(LNODS(ISUPR1,I),I=5,9)
      READ(5,926)(LNODS(ISUPR2,I),I=5,9)
      WRITE(6,915)
      DO  20  IELEM=1,NELEM
   20 WRITE(6,920) IELEM, (LNODS(IELEM,INODE),INODE=1,NNODE)
      WRITE(6,940)
```

```
      WRITE(6,945)
C.....Read and write the fixed values (Restrained nodes).....
      DO  60  IVFIX=1,NVFIX
      READ(5,950) NOFIX(IVFIX),(IFPRE(IVFIX,IDOFN),IDOFN=1,2)
     ,           ,(PRESC(IVFIX,IDOFN),IDOFN=1,2)
   60 WRITE(6,951) NOFIX(IVFIX),(IFPRE(IVFIX,IDOFN),IDOFN=1,2)
     ,           ,(PRESC(IVFIX,IDOFN),IDOFN=1,2)
C.....Set up the sample GAUSS point positions and Weighting Factors
C     for numerical integration.
      POSGP(1)=-0.774596669241483D0
      POSGP(2)=0.0D0
      POSGP(3)=-POSGP(1)
      WEIGP(1)=0.555555555555556D0
      WEIGP(2)=0.888888888888889D0
      WEIGP(3)=WEIGP(1)
C
      READ(5,960) YOUNG1,YOUNG2,POIS12,G12,IANGL,ISTRPC,THICK
      WRITE(6,965)YOUNG1,YOUNG2,POIS12,G12,IANGL,ISTRPC,THICK
C
C.....Read Crack Tip Dimensions
C     ========================
      READ(5,800) XTIP(1),YTIP(1),XTIP(2),YTIP(2)
      WRITE(6,805)XTIP(1),YTIP(1),XTIP(2),YTIP(2)
  800 FORMAT(4E10.0)
  805 FORMAT(3X,'XTIP(1)=',F7.3,4X,'YTIP(1)=',F7.3,4X,
     ;          'XTIP(2)=',F7.3,4X,'YTIP(2)=',F7.3,//)
C
      CALL CHECK(NELEM,NVFIX,NOFIX,LNODS,IFPRE,COORD,NPOIN,
     ,            MFRON,NDFRO)
C.....NEXT  CREAT  THE  ELEMENT  STIFFNESS FILE.....................
      CALL STIFFS(NELEM,NPOIN,NGAUS,COORD,LNODS,BCRT,SF,ROTR,ROTI)
C.....C O M P U T E   L O A D S
      CALL  LOADPS(NELEM,NPOIN,NGAUS,COORD,LNODS,ELOAD)
C.....SOLVE  THE  RESULTING  EQUATIONS  BY  THE  FRONTAL  SOLVER.......
C
      CALL  FRONT(NELEM,NPOIN,NVFIX,NTOTV,NGAUS,COORD,LNODS,ELOAD,
     ,           ASDIS,NOFIX,IFPRE,PRESC,BCRT,MFRON,CRD,SIF)
```

```
C.....CALCULATE ENERGY RELEASE RATE (ANISOTROPIC CASE).....
      IF(ISTRPC.EQ.1) GO TO  37
      ZMU1=CMPLX(ROTR(2),ROTI(2))
      ZMU2=CMPLX(ROTR(4),ROTI(4))
      RMU1=1.0/ZMU1
      RMU2=1.0/ZMU2
      TEMJ1=SIF(1)*AIMAG(RMU2+RMU1)+SIF(2)*(REAL(RMU1)*
     $      AIMAG(RMU2)+REAL(RMU2)*AIMAG(RMU1))
      ENG1=-0.5*PI*SIF(1)*SP(3)*TEMJ1
      TEMJ2=SIF(2)*AIMAG(ZMU1+ZMU2)+SIF(1)*(REAL(ZMU1)*AIMAG(ZMU2)+
     $      REAL(ZMU2)*AIMAG(ZMU1))
      ENG2=0.5*PI*SIF(2)*SP(1)*TEMJ2
      TOTAL=ENG1+ENG2
      WRITE(6,970) ENG1,ENG2,TOTAL
   37 CONTINUE
  970 FORMAT(//,3X,'J1=',E12.4,6X,'J2=',E12.4,//,
     $       10X,'ENERGY RELEASE RATE=',E12.4)
  900 FORMAT(9I5)
  905 FORMAT(//,8H NPOIN =,I4,4X,8H NELEM =,I4,4X,8H NVFIX =,I4
     ,,4X,8H NGAUS =,I4,4X,'NNODE=',I4,4X,'ISUPER1=',I3,4X,'ISUPER2=',
     $ I3,4X,'KEY1=',I3,4X,'KEY2=',I3,//)
  915 FORMAT(//,5X,8H ELEMENT,6X,13H NODE NUMBERS)
  920 FORMAT(1X,I5,6X,9I5)
  925 FORMAT(16I4)
  926 FORMAT(5I4)
  930 FORMAT(12D6.0)
  940 FORMAT(//,5X,17H RESTRAINED NODES)
  945 FORMAT(5H NODE,1X,4HCODE,6X,12HFIXED VALUES)
  950 FORMAT(1X,I4,3X,2I1,2D8.5)
  951 FORMAT(1X,I4,3X,2I1,2D14.5)
  960 FORMAT(4E7.0,2I7,E7.0)
  965 FORMAT(/,3X,'YOUNG1=',E10.3,5X,'YOUNG2=',E10.3,5X,'POIS12=',F7.5,
     ,6X,'G12=',E10.4,6X,'ANGLE=',I4,4X,'ISTRPC=',I1,4X,'THICK=',F5.2,/)
      STOP
      END
```

```
      SUBROUTINE CHECK(NELEM,NVFIX,NOFIX,LNODS,IFPRE,COORD,NPOIN,
     ,                 MFRON,NDFRO)
C     ************************************************************
      IMPLICIT REAL*8(A-H,O-Z)
      DIMENSION  NDFRO(NELEM),NOFIX(NVFIX),LNODS(NELEM,9),
     1           IFPRE(NVFIX,2),NEROR(8),COORD(NPOIN,2)
      REAL*4 XTIP(2),YTIP(2)
      COMMON/SUPER/ISUPR1,ISUPR2,KEY1,KEY2,XTIP,YTIP
      DO  10  I=1,NELEM
   10 NDFRO(I)=0
      DO  15  I=1,8
   15 NEROR(I)=0
C.....CHECK FOR ANY REPETITION OF A NODE NUMBER WITHIN AN ELEMENT
      DO  140  IPOIN=1,NPOIN
      KSTAR=0
      DO  90  I=1,NELEM
      KZERO=0
      NNODE=4
      IF(I.EQ.ISUPR1.AND.KEY1.EQ.1)NNODE=5
      IF(I.EQ.ISUPR1.AND.KEY1.EQ.2)NNODE=9
      IF(I.EQ.ISUPR2)NNODE=9
      DO  90  INODE=1,NNODE
      IF(LNODS(I,INODE).NE.IPOIN)  GO TO  90
      KZERO=KZERO+1
      IF(KZERO.GT.1) NEROR(1)=NEROR(1)+1
      IF(KSTAR.NE.0) GO TO  80
      KSTAR=I
C.....CALCULATE INCREASE OR DECREASE IN  FRONTWIDTH AT EACH ELEMENT STAGE.
      NDFRO(I)=NDFRO(I)+2
   80 CONTINUE
C.....AND CHANGE THE SIGN OF THE LAST APPREANCE OF EACH NODE
      KLAST=I
      NLAST=INODE
   90 CONTINUE
      IF(KLAST.EQ.0) GO TO  110
      IF(KLAST.LT.NELEM) NDFRO(KLAST+1)=NDFRO(KLAST+1)-2
```

```
      LNODS(KLAST,NLAST)=-IPOIN
      GO TO   140
C.....CHECK THAT COORDINATES FOR AN UNUSED NODE HAVE NOT BEEN SPECIFIED.
  110 WRITE(6,900) IPOIN
  900 FORMAT(/,3X,15H CHECK WHY NODE,I4,14H NEVER APPEARS)
      NEROR(2)=NEROR(2)+1
      SIGMA=0.0
      DO  120  IDIME=1,2
  120 SIGMA=SIGMA+DABS(COORD(IPOIN,IDIME))
      IF(SIGMA.NE.0.0)NEROR(3)=NEROR(3)+1
C.....CHECK THAT AN UNUSED NODE NUMBER IS NOT A RESTRAINED NODE
      DO  130  IVFIX=1,NVFIX
  130 IF(NOFIX(IVFIX).EQ.IPOIN)NEROR(4)=NEROR(4)+1
  140 CONTINUE
C.....CALCULATE THE LARGEST FRONTWIDTH.
      NFRON=0
      MFRON=0
      DO  150  I=1,NELEM
      NFRON=NFRON+NDFRO(I)
  150 IF(NFRON.GT.MFRON) MFRON=NFRON
      WRITE(6,905) MFRON
  905 FORMAT(3X,/,29H MAX FRONTWIDTH ENCOUNTERED =,I5,/)
C.....CONTINUE CHECKING THE DATA FOR THE FIXED VALUES.
      DO  171  IVFIX=1,NVFIX
      IF(NOFIX(IVFIX).LE.0.OR.NOFIX(IVFIX).GT.NPOIN)NEROR(6)
     ,               =NEROR(6)+1
      KOUNT=0
      DO  160  IDOFN=1,2
  160 IF(IFPRE(IVFIX,IDOFN).GT.0) KOUNT=1
      IF(KOUNT.EQ.0) NEROR(7)=NEROR(7)+1
      KVFIX=IVFIX-1
      IF(KVFIX.EQ.0)GO TO  171
      DO  170  JVFIX=1,KVFIX
  170 IF(IVFIX.NE.1.AND.NOFIX(IVFIX).EQ.NOFIX(JVFIX))NEROR(8)
     ,               =NEROR(8)+1
  171 CONTINUE
      KEROR=0
```

```
      DO  180  IEROR=1,8
      IF(NEROR(IEROR).EQ.0) GO TO  180
      KEROR=1
      WRITE(6,910)IEROR,NEROR(IEROR)
  910 FORMAT(//,3X,'***** DIAGNOSIS BY CHECK, ERROR ',I3,
     ,            18H ASSOCIATED NUMBER,I5)
  180 CONTINUE
      IF(KEROR.NE.0) GO TO  200
C.....RETURN ALL NODAL CONNECTION NUMBERS TO POSTIVE VALUES
      DO  190  I=1,NELEM
      NNODE=4
      IF(I.EQ.ISUPR1.AND.KEY1.EQ.1)NNODE=5
      IF(I.EQ.ISUPR1.AND.KEY1.EQ.2)NNODE=9
      IF(I.EQ.ISUPR2)NNODE=9
      DO  190  INODE=1,NNODE
  190 LNODS(I,INODE)=IABS(LNODS(I,INODE))
      RETURN
  200 STOP
      END
      SUBROUTINE SHAPE(S,T)
C     ====================
      IMPLICIT REAL*8(A-H,O-Z)
C
C.....CALCULATES SHAPE FUNCTIONS (SHAP) AND THEIR DERIVATIVES (DERIV)
C       FOR 2D  ISOPARAMATRIC QUADRILATERAL ELEMENT (4 NODES).
C
      DIMENSION SI(4),TI(4)
      DATA  SI,TI/-.5D0,.5D0,.5D0,-.5D0,-.5D0,-.5D0,.5D0,.5D0/
      COMMON/WORK/SHAP(4),DERIV(2,4),BMATX(3,8),POSGP(3)
     ,      ,WEIGP(3),QBMAT(3,8),GPCOD(2,9),SMATX(3,8,9)
C
C.....COMPUTE SHAPE FUNCTIONS AND DERIVATIVE IN NATURAL COORDINATES....
      DO  10  I=1,4
      SHAP(I)=(0.5D0+SI(I)*S)*(0.5D0+TI(I)*T)
      DERIV(1,I)=SI(I)*(0.5D0+TI(I)*T)
   10 DERIV(2,I)=TI(I)*(0.5D0+SI(I)*S)
      RETURN
```

```
      END
      SUBROUTINE JACOB(IELEM,DETJAC,NELEM,NPOIN,COORD,LNODS)
C     ============================================================
      IMPLICIT REAL*8(A-H,O-Z)
      COMMON/WORK/SHAP(4),DERIV(2,4),BMATX(3,8),POSGP(3)
     ,      ,WEIGP(3),QBMAT(3,8),GPCOD(2,9),SMATX(3,8,9)
      DIMENSION COORD(NPOIN,2),LNODS(NELEM,9),CARTD(2,4)
      REAL*8 JAC(2,2),JACINV(2,2)
C
C.....CALCULATES THE JACOBIAN MATRIX AND ITS DETERMINANT AND INVERSE
C
      DO 5  IDIME=1,2
      DO 5  JDIME=1,2
      JAC(IDIME,JDIME)=0.0D0
      DO  5  INODE=1,4
      KK=LNODS(IELEM,INODE)
      TEM=COORD(KK,JDIME)
      JAC(IDIME,JDIME)=JAC(IDIME,JDIME)+DERIV(IDIME,INODE)*TEM
    5 CONTINUE
C
C.....CALCULATE DETERMINANT AND INVERSE OF JACOBIAN MATRIX
C
      DETJAC=JAC(1,1)*JAC(2,2)-JAC(2,1)*JAC(1,2)
      IF(DETJAC.GT.0.0) GO TO   10
      WRITE(6,900)  IELEM,DETJAC
  900 FORMAT(//,24HPROGRAM HALTED IN JACOB ,/,11X,
     ,22H ZERO OR NEGATIVE AREA,/,10X,16H ELEMENT NUMBER ,I5,9X,F12.4)
      DO 7 INODE=1,4
      K=LNODS(IELEM,INODE)
    7 WRITE(6,901)K,(COORD(K,J),J=1,2)
  901 FORMAT(/,2X,I3,2F12.4)
      STOP
C
   10 JACINV(1,1)=JAC(2,2)/DETJAC
      JACINV(2,2)=JAC(1,1)/DETJAC
      JACINV(1,2)=-JAC(1,2)/DETJAC
      JACINV(2,1)=-JAC(2,1)/DETJAC
```

```
C
C.....CALCULAT CARTESIAN DERIVATIVES FOR THE SHAPE FUNCTION
C
      DO 15  IDIME=1,2
      DO 15  INODE=1,4
      CARTD(IDIME,INODE)=0.0D0
      DO 15 JDIME=1,2
      CARTD(IDIME,INODE)=CARTD(IDIME,INODE)+JACINV(IDIME,JDIME)*
     *DERIV(JDIME,INODE)
   15 CONTINUE
C
C.....CALCULATE THE ELEMENT STRAIN MATRIX 'B'.....
C
      N=0
      DO  20  INODE=1,4
      M=N+1
      N=M+1
      BMATX(1,M)=CARTD(1,INODE)
      BMATX(1,N)=0.D0
      BMATX(2,M)=0.D0
      BMATX(2,N)=CARTD(2,INODE)
      BMATX(3,M)=CARTD(2,INODE)
      BMATX(3,N)=CARTD(1,INODE)
   20 CONTINUE
      RETURN
      END
      SUBROUTINE STIFFS(NELEM,NPOIN,NGAUS,COORD,LNODS,BCRT,SP,ROTR,ROTI)
C     ================================================================
C.....THIS ROUTINE CALCULATES THE ELEMENT STIFFNESS MATRIX
      IMPLICIT REAL*8(A-H,O-Z)
      REAL*4 XC(9),YC(9),XT,YT,EK(18,18),BCR(2,18),YOUNG1,YOUNG2,
     ,       POIS12,G12,THICK,SP(6),XTIP(2),YTIP(2),ROTR(4),ROTI(4)
      DIMENSION ESTIF(18,18),COORD(NPOIN,2),LNODS(NELEM,9),GP(3,3)
     $          ,BCRT(2,2,18)
      COMMON/WORK/SHAP(4),DERIV(2,4),BMATX(3,8),POSGP(3)
     ,      ,WEIGP(3),QBMAT(3,8),GPCOD(2,9),SMATX(3,8,9)
      COMMON/MATRIL/YOUNG1,YOUNG2,POIS12,G12,IANGL,ISTRPC,THICK
```

```
      COMMON/SUPER/ISUPR1,ISUPR2,KEY1,KEY2,XTIP,YTIP
      DO  3  I=1,2
      DO  3  J=1,2
      DO  3  K=1,18
    3 BCRT(I,J,K)=0.0D0
      IF(ISTRPC.EQ.2) GO TO  5
C
C.....[QP] matrix for istropic plane stress problem.............
      DO  4  I=1,3
      DO  4  J=1,3
    4 QP(I,J)=0.D0
      CONST=YOUNG1/(1.0-POIS12*POIS12)*1.0D0
      QP(1,1)=CONST
      QP(2,2)=CONST
      QP(1,2)=CONST*POIS12
      QP(2,1)=CONST*POIS12
      QP(3,3)=CONST*(1.0-POIS12)/2.0
      GO TO  6
C
C.....[QP] Matrix for anisotropic plane stress problem.
    5 POIS21=POIS12*YOUNG2/YOUNG1
      Q11=YOUNG1/(1.D0-POIS12*POIS21)
      Q12=YOUNG2*POIS12/(1.D0-POIS12*POIS21)
      Q22=YOUNG2/(1.D0-POIS12*POIS21)
      Q66=G12
      ANGL=IANGL*DATAN(1.0D0)/45
      SIN1=DSIN(ANGL)
      COS1=DCOS(ANGL)
      SIN2=SIN1*SIN1
      COS2=COS1*COS1
      SIN4=SIN2*SIN2
      COS4=COS2*COS2
      SIN3=SIN2*SIN1
      COS3=COS2*COS1
      QP(1,1)=Q11*COS4+2*(Q12+2*Q66)*SIN2*COS2+Q22*SIN4
      QP(1,2)=(Q11+Q22-4*Q66)*SIN2*COS2+Q12*(SIN4+COS4)
      QP(2,2)=Q11*SIN4+2*(Q12+2*Q66)*SIN2*COS2+Q22*COS4
```

```
      QP(1,3)=(Q11-Q12-2*Q66)*SIN1*COS3+(Q12-Q22+2*Q66)*SIN3*COS1
      QP(2,3)=(Q11-Q12-2*Q66)*SIN3*COS1+(Q12-Q22+2*Q66)*SIN1*COS3
      QP(3,3)=(Q11+Q22-2*Q12-2*Q66)*SIN2*COS2+Q66*(SIN4+COS4)
      QP(2,1)=QP(1,2)
      QP(3,1)=QP(1,3)
      QP(3,2)=QP(2,3)
    6 CONTINUE
C.....LOOP OVER EACH ELEMENT.....................................
C
      DO  70  IELEM=1,NELEM
      NDPE=18
C     INITIALIZE THE ELEMENT STIFFNESS MATRIX
      DO  20  II=1,18
      DO  20  JJ=1,18
   20 ESTIF(II,JJ)=0.D0
      KGASP=0
      IF(IELEM.EQ.ISUPR1.OR.IELEM.EQ.ISUPR2) GO TO  68
C.....INTER LOOPS FOR AREA NUMERICAL INTEGRATION
      DO  50  IGAUS=1,NGAUS
      DO  50  JGAUS=1,NGAUS
      KGASP=KGASP+1
      EXISP=POSGP(IGAUS)
      ETASP=POSGP(JGAUS)
C.....EVALUATE THE SHAPE FUNCTIONS,ELEMENTAL VOLUME, ETC.
C
      CALL SHAPE(EXISP,ETASP)
      CALL JACOB(IELEM,DETJAC,NELEM,NPOIN,COORD,LNODS)
      DVOLU= DETJAC*WEIGP(IGAUS)*WEIGP(JGAUS)*THICK
C
C.....EVALUATE  {QP}{B}  MATRIX
      DO  10  II=1,3
      DO  10  JJ=1,8
      QBMAT(II,JJ)=0.0D0
      DO  10  KK=1,3
      QBMAT(II,JJ)=QBMAT(II,JJ)+QP(II,KK)*BMATX(KK,JJ)
   10 CONTINUE
C.....CALCULATE THE ELEMENT STIFFNESSES (UPPER TRIANGLE PORTION)
```

```
      DO  30  II=1,8
      DO  30  JJ=II,8
      DO  30   K=1,3
   30 ESTIF(II,JJ)=ESTIF(II,JJ)+BMATX(K,II)*QBMAT(K,JJ)*DVOLU
   50 CONTINUE
C.....CONSTRUCT THE LOWER TRIANGLE OF THE STIFFNESS MATRIX.............
      DO  60  II=1,8
      DO  60  JJ=1,8
   60 ESTIF(JJ,II)=ESTIF(II,JJ)
      GO TO 67
   68 CONTINUE
      IF(IELEM.EQ.ISUPR2) GO TO 24
      KEY=KEY1
      XT=XTIP(1)
      YT=YTIP(1)
      GO TO  23
   24 KEY=KEY2
      XT=XTIP(2)
      YT=YTIP(2)
   23 IF(KEY.EQ.1)  NDPE=10
      NNPE=NDPE/2
      DO 19  I=1,NNPE
      XC(I)=COORD(LNODS(IELEM,I),1)
      YC(I)=COORD(LNODS(IELEM,I),2)
   19 CONTINUE
      WRITE(6,40)XT,YT,KEY,NNPE
   40 FORMAT(/,3X,'XT=',F6.2,7X,'YT=',F6.2,7X,'KEY=',I2,7X,'NNPE=',I2,/)
      DO  42  I=1,NNPE
   42 WRITE(6,44)I,XC(I),I,YC(I)
   44 FORMAT(/,3X,'XC(',I1,')=',F7.3,10X,'YC(',I1,')=',F7.3,//)
      IF(ISTRPC.EQ.1) GO TO  55
      CALL HYBRD2(KEY,XC,YC,XT,YT,EK,BCR,NNPE,SP,ROTR,ROTI)
      KEY=2
      GO TO 57
   55 CALL HYBRD1(KEY,XC,YC,XT,YT,EK,BCR,NNPE)
```

```
      KOUNT=2
      IF(IELEM.EQ.ISUPR1) KOUNT=1
      DO  66  K=1,KEY
      DO  66  N=1,NDPE
   66 BCRT(KOUNT,K,N)=BCR(K,N)
      DO 69  I=1,NDPE
      DO 69  J=1,NDPE
   69 ESTIF(I,J)=EK(I,J)
   67 WRITE(1) ESTIF
   70 CONTINUE
      RETURN
      END
      SUBROUTINE  LOADPS(NELEM,NPOIN,NGAUS,COORD,LNODS,ELOAD)
C     ******************************************************
C.....THIS ROUTINE IS TO CALCULATE THE NODAL FORCES FOR EACH ELEMENT
      IMPLICIT REAL*8(A-H,O-Z)
      COMMON/WORK/SHAP(4),DERIV(2,4),BMATX(3,8),POSGP(3)
     ,      ,WEIGP(3),QBMAT(3,8),GPCOD(2,9),SMATX(3,8,9)
      DIMENSION   PGASH(2),DGASH(2),NOPRS(3),PRESS(3,2),
     ,  POINT(2),STRAN(3),STRES(3),COORD(NPOIN,2),LNODS(NELEM,9),
     ,   ELOAD(NELEM,18)
      DO  10  I=1,NELEM
      DO  10  J=1,18
   10 ELOAD(I,J)=0.D0
C.....READ  NODAL  POINT  LOADS
      READ(5,930) NEDGE
  930 FORMAT(I5)
      WRITE(6,935) NEDGE
  935 FORMAT(1HO,5X,21HNO. OF LOADING EDGES=,I5)
      WRITE(6,940)
  940 FORMAT(1HO,5X,38HLIST OF LOADED EDGES AND APPLIED LOADS,/)
      NODEG=2
C.....LOOP  OVER  EACH  LOADED  EDGE
      DO  160  IEDGE=1,NEDGE
C.....READ DATA LOCATING THE LOADED EDGE AND APPLIED LOAD.
      READ(5,945) NEASS,(NOPRS(IODEG),IODEG=1,NODEG)
  945 FORMAT(3I5)
```

```
      WRITE(6,950) NEASS,(NOPRS(IODEG),IODEG=1,NODEG)
 950  FORMAT(I10,5X,2I5)
      READ(5,955) ((PRESS(IODEG,IDOFN),IODEG=1,NODEG),IDOFN=1,2)
      WRITE(6,956)((PRESS(IODEG,IDOFN),IODEG=1,NODEG),IDOFN=1,2)
 955  FORMAT(4D10.3)
 956  FORMAT(3X,4F10.3)
      ETASP=-1.D0
C
C....INTER  LOOP  FOR  LINEAR  NUMERICAL  INTEGRATION.
      DO  160  IGAUS=1,NGAUS
      EXISP=POSGP(IGAUS)
C
C.....EVALUATE  THE  SHAPE  FUINCTIONS  AT  THE  SAMPLING POINTS.
      CALL  SHAPE(EXISP,ETASP)
C
C.....CALCULATE  COMPONANTS  OF  THE  EQUIVALENT  NODAL  LOADS.
C
      DO  110  IDOFN=1,2
      PGASH(IDOFN)=0.D0
      DGASH(IDOFN)=0.D0
      DO  110  IODEG=1,NODEG
      PGASH(IDOFN)=PGASH(IDOFN)+PRESS(IODEG,IDOFN)*SHAP(IODEG)
 110  DGASH(IDOFN)=DGASH(IDOFN)+COORD(NOPRS(IODEG),IDOFN)*
     ,             DERIV(1,IODEG)
      DVOLU=WEIGP(IGAUS)
      PXCOM=DGASH(1)*PGASH(2)-DGASH(2)*PGASH(1)
      PYCOM=DGASH(1)*PGASH(1)+DGASH(2)*PGASH(2)
C.....ASSOCIATE THE EQUIVALENT NODAL EDGE LOADS WITH AN ELEMENT.......
      DO  120  INODE=1,4
      NLOCA=LNODS(NEASS,INODE)
      IF(NLOCA.EQ.NOPRS(1)) GO TO  130
 120  CONTINUE
 130  JNODE=INODE+NODEG-1
      KOUNT=0
      DO  140  KNODE=INODE,JNODE
      KOUNT=KOUNT+1
      NGASH=(KNODE-1)*2+1
```

```
      MGASH=(KNODE-1)*2+2
      IF(KNODE.GT.4)  MGASH=1
      IF(KNODE.GT.4)  MGASH=2
      ELOAD(NEASS,NGASH)=ELOAD(NEASS,NGASH)+SHAP(KOUNT)*PXCOM*DVOLU
  140 ELOAD(NEASS,MGASH)=ELOAD(NEASS,MGASH)+SHAP(KOUNT)*PYCOM*DVOLU
  160 CONTINUE
      RETURN
      END
      SUBROUTINE HYBRD1(KEY,XC,YC,XT,YT,EK,BCR,NNPE)
C     ==============================================================
      COMPLEX*8 ZET,Z,FF2(18),FF3(18),ZET4,CZZ,ZETK,ZA,ZC,ZE,ZD,CI,CZK
      DIMENSION W(5),Y(5),G(18,18),XLCN(9),YLCN(9),VA(45),VB(45),
     *BCR(2,18),BK(18,18),EK(18,18),EK1(171),WK(63),H1(9,9),H2(9,9),
     *VINV1(45),VINV2(45),TEM(18,18),VVG(18,18),XC(9),YC(9)
      COMMON/MATRIL/YOUNG1,YOUNG2,POIS12,G12,IANGL,ISTRPC,THICK
      DATA W/.2369269,.4786287,0.5688889,0.4786287,0.2369269/
      DATA Y/-0.9061799,-0.5384693,0.0,0.5384693,0.9061799/
      CI=CMPLX(0.0,1.0)
      ETA=(3-POIS12)/(1+POIS12)
      SMU=0.5*YOUNG1/(1+POIS12)
      NT=KEY*9
      DO 1 I=1,45
      VB(I)=0.0
    1 VA(I)=0.0
      NDPE=NNPE*2
      DO 4 I=1,18
      DO  3  K=1,2
    3 BCR(K,I)=0.0
      DO 4 J=1,18
      EK(I,J)=0.0
      VVG(I,J)=0.0
    4 G(I,J)=0.0
C     Rotate coordinate to local system
      ES=SQRT((XC(1)-XT)**2+(YC(1)-YT)**2)
      SIN=(YC(1)-YT)/ES
      COS=(XC(1)-XT)/ES
      XLCT=XT*COS+YT*SIN
```

```
      YLCT=-XT*SIN+YT*COS
      DO  10  I=1,NNPE
      XLCN(I)=(XC(I)*COS+YC(I)*SIN-XLCT)/ES
      YLCN(I)=(-XC(I)*SIN+YC(I)*COS-YLCT)/ES
   10 CONTINUE
      DO 41 ISI=1,4
      UX=YLCN(ISI+1)-YLCN(ISI)
      UY=XLCN(ISI)-XLCN(ISI+1)
      DO 41 II=1,5
      XX=(XLCN(ISI+1)+XLCN(ISI)+(XLCN(ISI+1)-XLCN(ISI))*Y(II))/2.0
      YY=(YLCN(ISI+1)+YLCN(ISI)+(YLCN(ISI+1)-YLCN(ISI))*Y(II))/2.0
      Z=CMPLX(XX,YY)
      ZET=CSQRT(Z)
      ZET4=Z*Z
      CZZ=CONJG(Z)
      ZETK=1.0/ZET4
      KK=1
      IF(KEY.EQ.2)  GO TO  1011
      DO  1010  K=1,9
      FF2(K)=0.0
      ZETK=ZETK*ZET
      CZK=CONJG(ZETK)
      KK=-KK
      IF(ABS(UY).LE.0.1E-6)GO TO  1009
      ZD=CZK*CZZ-KK*ZETK*Z
      ZC=ZETK*(CZZ-Z)
      FF2(K)=(0.5*K*(K-2)*ZC+K*ZD)*UY/2.0
 1009 ZE=CZK*CZZ*(CZZ-Z)
      FF3(K)=(ETA*ZETK*ZET4+KK*CZK*CONJG(ZET4)+0.5*K*ZE)/4.0
      IF(ABS(UX).LE.0.1E-6)GO TO 1010
      IB=K+2+2*KK
      ZA=(K-2)*ZETK-2.0*CZK
      FF2(K)=-K*(CZZ*ZA-IB*ZETK*Z)*CI*UX/4.0+FF2(K)
 1010 CONTINUE
      GO TO  2000
 1011 DO  1012  K=1,9
      FF2(K)=0.0
```

```
      FF2(K+9)=0.0
      ZETK=ZETK*ZET
      CZK=CONJG(ZETK)
      KK=-KK
      IF(ABS(UY).LE.0.1E-6)GO TO  1014
      ZD=CZK*CZZ-KK*ZETK*Z
      ZC=ZETK*(CZZ-Z)
      FF2(K)=(0.5*K*(K-2)*ZC+K*ZD)*UY/2.0
      FF2(K+9)=(FF2(K)-K*ZD*UY)*CI
 1014 ZE=CZK*CZZ*(CZZ-Z)
      FF3(K)=(ETA*ZETK*ZET4+KK*CZK*CONJG(ZET4)+0.5*K*ZE)/4.0
      FF3(K+9)=(FF3(K)-.25*K*ZE)*CI
      IF(ABS(UX).LE.0.1E-6)GO TO 1012
      IB=K+2+2*KK
      ZA=(K-2)*ZETK-2.0*CZK
      FF2(K)=-K*(CZZ*ZA-IB*ZETK*Z)*CI*UX/4.0+FF2(K)
      IB=K+2-2*KK
      ZA=(K-2)*ZETK+2.0*CZK
      FF2(K+9)=K*(CZZ*ZA-IB*ZETK*Z)*.25*UX+FF2(K+9)
 1012 CONTINUE
 2000 KJ=0
      DO 41 K=1,9
      L=2*ISI-1
      DO  40  J=1,KEY
      I=J*9+K-9
      G(I,L)  =G(I,L  )+0.5*W(II)*AIMAG(0.5*(1.0-Y(II))*FF2(I))
      G(I,L+1)=G(I,L+1)+0.5*W(II)* REAL(0.5*(1.0-Y(II))*FF2(I))
      G(I,L+2)=G(I,L+2)+0.5*W(II)*AIMAG(0.5*(1.0+Y(II))*FF2(I))
  40  G(I,L+3)=G(I,L+3)+0.5*W(II)* REAL(0.5*(1.0+Y(II))*FF2(I))
      DO 41  J=1,K
      KJ=KJ+1
      VA(KJ)=VA(KJ)+0.5*W(II)*AIMAG(FF2(K)*FF3(J)+FF2(J)*FF3(K))/SMU
      IF(KEY.EQ.1) GO TO  41
      I=K+9
      L=J+9
      VB(KJ)=VB(KJ)+0.5*W(II)*AIMAG(FF2(I)*FF3(L)+FF2(L)*FF3(I))/SMU
  41  CONTINUE
```

```
      IF(KEY.EQ.1) GO TO  64
      DO  500  III=1,9
      G(III,2)=0.0
      G(III,1)=2.0*G(III,1)
      II=III+9
      G(II,2)=2.0*G(II,2)
      G(II,1)=0.0
      DO  455  J=1,4
      JU=J+1
      JL=10-J
      G(III,2*JL-1)=G(III,2*JU-1)
      G(III,2*JL)=-G(III,2*JU)
      G(II,2*JL-1)=-G(II,2*JU-1)
  455 G(II,2*JL)=G(II,2*JU)
  500 CONTINUE
      DO  501  I=1,18
  501 G(11,I)=0.0
      DO  63  I=1,45
      VA(I)=VA(I)*2.0
   63 VB(I)=VB(I)*2.0
      VB(2)=0.0
      VB(3)=1.0
      DO  62  I=3,9
   62 VB((I*I-I)/2+2)=0.0
   64 CONTINUE
      N=9
      CALL LINV2P(VA,N,VINV1,IDGT,D1,D2,WK,IER)
      IF(IER.NE.0)STOP
      IF(KEY.EQ.2) CALL LINV2P(VB,N,VINV2,IDGT,D1,D2,WK,IER)
      IF(IER.NE.0)STOP
C.....Calculate [H]inv.* [G]
C     ====================
      DO  111  J=1,NDPE
      DO  110  I=1,9
      II=I*(I-1)/2
      BK(I,J)=0.0
      DO  110  K=1,9
```

```
      IK=II+K
      IF(K.GT.I) IK=K*(K-1)/2+I
  110 BK(I,J)=BK(I,J)+VINV1(IK)*G(K,J)
      IF(KEY.EQ.1) GO TO  111
      DO  121  I=10,18
      M=I-9
      IJ=M*(M-1)/2
      BK(I,J)=0.0
      DO  121  K=1,9
      IK=IJ+K
      IF(K.GT.M) IK=K*(K-1)/2+M
  121 BK(I,J)=BK(I,J)+VINV2(IK)*G(K+9,J)
  111 CONTINUE
C.....Calculate Element Stiffness matrix and Stress Intensity Matrix :
C     ================================================================
      IJ=0
      DO  112  I=1,NDPE
      DO  112  J=1,I
      IJ=IJ+1
      EK1(IJ)=0.0
      DO  112  K=1,NT
  112 EK1(IJ)=EK1(IJ)+BK(K,J)*G(K,I)*THICK*YOUNG1
      E=SQRT(2.0/ES)
      DO  113  J=1,NDPE
      BCR(2,J)=0.0
      IF(KEY.EQ.2) BCR(2,J)=E*BK(10,J)
  113 BCR(1,J)=E*BK(1,J)
C     Rotate (BCR) matrix and element stiffness matrix to global system:
C     ==================================================================
      N=0
      DO  3001  I=1,NDPE
      DO  3000  J=1,I
      N=N+1
      TEM(I,J)=EK1(N)
 3000 TEM(J,I)=EK1(N)
      DO  3001  J=1,KEY
 3001 BK(J,I)=BCR(J,I)
```

```
      DO  3002  J=1,KEY
      DO  3002  I=2,NDPE,2
      IM1=I-1
      BCR(J,IM1)=BK(J,IM1)*COS-BK(J,I)*SIN
 3002 BCR(J,I)  =BK(J,IM1)*SIN+BK(J,I)*COS
      DO  79  J=2,NDPE,2
      I=J-1
      VVG(I,I)=COS
      VVG(J,J)=COS
      VVG(I,J)=SIN
   79 VVG(J,I)=-SIN
      DO  80  I=1,NDPE
      DO  80  J=1,NDPE
      DO  80  K=1,NDPE
      DO  80  N=1,NDPE
   80 EK(I,J)=EK(I,J)+VVG(K,I)*TEM(K,N)*VVG(N,J)
      RETURN
      END
      SUBROUTINE HYBRD2(KEY,XC,YC,XT,YT,EK,BCR,NNPE,SP,ROTR,ROTI)
C     ============================================================
      COMPLEX  ZMU1,ZMU2,P1,P2,Q1,Q2,Z1,Z2,ZET1,ZET2,ZETK1,ZETK2,
     $          ZTEM1,ZTEM2,ZMU1S,ZMU2S
      DIMENSION W(5),Y(5),G(18,18),XLCN(9),YLCN(9),VA(45),VB(45),
     $BCR(2,18),BK(18,18),EK(18,18),EK1(171),WK(63),BCRTEM(2,18),
     $VINV1(45),VINV2(45),TEM(18,18),VVG(18,18),XC(9),YC(9)
     $,ROTR(4),ROTI(4),SP(6),FF2(18),FF3(18),FF4(18),FF5(18)
     $,BST1(18),BST2(18),BND1(18),BND2(18)
      REAL  M11,M12,M21,M22
      COMMON/MATRIL/YOUNG1,YOUNG2,POIS12,G12,IANGL,ISTRPC,THICK
      DATA W/.2369269,.4786287,0.5688889,0.4786287,0.2369269/
      DATA Y/-0.9061799,-0.5384693,0.0,0.5384693,0.9061799/
      CI=CMPLX(0.0,1.0)
      NT=KEY*9
      DO 1 I=1,45
      VB(I)=0.0
    1 VA(I)=0.0
      NDPE=NNPE*2
```

```
      DO 4 I=1,18
      DO  3  K=1,2
      BCRTEM(K,I)=0.0
    3 BCR(K,I)=0.0
      DO 4 J=1,18
      BK(I,J)=0.0
      EK(I,J)=0.0
      VVG(I,J)=0.0
    4 G(I,J)=0.0
      CALL ROOTS(ROTR,ROTI,SP)
      ZMU1=CMPLX(ROTR(2),ROTI(2))
      ZMU2=CMPLX(ROTR(4),ROTI(4))
      ZMU1S=ZMU1*ZMU1
      ZMU2S=ZMU2*ZMU2
      WRITE(6,33)ZMU1,ZMU2
      P1=SP(1)*ZMU1S+SP(2)-SP(4)*ZMU1
      P2=SP(1)*ZMU2S+SP(2)-SP(4)*ZMU2
      Q1=(SP(2)*ZMU1S+SP(3)-SP(5)*ZMU1)/ZMU1
      Q2=(SP(2)*ZMU2S+SP(3)-SP(5)*ZMU2)/ZMU2
   33 FORMAT(//,3X,'ZMU1=',E12.5,'   i',E12.5,10X,
     $             'ZMU2=',E12.5,'   i',E12.5)
C
C     Rotate coordinate to local system
C     =================================
      ES=SQRT((XC(1)-XT)**2+(YC(1)-YT)**2)
      SINN=(YC(1)-YT)/ES
      COSS=(XC(1)-XT)/ES
      XLCT=XT*COSS+YT*SINN
      YLCT=-XT*SINN+YT*COSS
      DO  10  I=1,NNPE
      XLCN(I)=(XC(I)*COSS+YC(I)*SINN-XLCT)/ES
      YLCN(I)=(-XC(I)*SINN+YC(I)*COSS-YLCT)/ES
   10 CONTINUE
      DO 42 ISI=1,4
      UX=YLCN(ISI+1)-YLCN(ISI)
      UY=XLCN(ISI)-XLCN(ISI+1)
      DO 41 II=1,5
```

```
      XX=(XLCN(ISI+1)+XLCN(ISI)+(XLCN(ISI+1)-XLCN(ISI))*Y(II))/2.0
      YY=(YLCN(ISI+1)+YLCN(ISI)+(YLCN(ISI+1)-YLCN(ISI))*Y(II))/2.0
      THETA1=ATAN2(ROTI(2)*YY , (XX+ROTR(2)*YY))
      THETA2=ATAN2(ROTI(4)*YY , (XX+ROTR(4)*YY))
      R1=SQRT((XX+ROTR(2)*YY)**2+(ROTI(2)*YY)**2)
      R2=SQRT((XX+ROTR(4)*YY)**2+(ROTI(4)*YY)**2)
      XR1=R1*COS(THETA1)
      YI1=R1*SIN(THETA1)
      XR2=R2*COS(THETA2)
      YI2=R2*SIN(THETA2)
      Z1=CMPLX(XR1,YI1)
      Z2=CMPLX(XR2,YI2)
      ZET1=CSQRT(Z1)
      ZET2=CSQRT(Z2)
      ZETK1=1.0/Z1
      ZETK2=1.0/Z2
      KK=1
      IF(KEY.EQ.2)  GO TO  1011
      DO  1010  K=1,9
      FF2(K)=0.0
      FF4(K)=0.0
      ZETK1=ZETK1*ZET1
      ZETK2=ZETK2*ZET2
      ZTEM1=ZETK1*Z1
      ZTEM2=ZETK2*Z2
      KK=-KK
      IF(KK.EQ.1) GO TO  13
      M11=-ROTI(2)/ROTI(4)
      M12=(ROTR(4)-ROTR(2))/ROTI(4)
      M21=0.0
      M22=-1.0
      GO TO  14
   13 M11=-1.0
      M12=0.0
      M21=(ROTR(2)-ROTR(4))/ROTI(4)
      M22=-ROTI(2)/ROTI(4)
   14 CONTINUE
```

```
      CJ=ROTR(2)*REAL(ZETK1)+(ROTR(4)*M11-ROTI(4)*M21)*REAL(ZETK2)
     $  -ROTI(2)*AIMAG(ZETK1)-(ROTR(4)*M21+ROTI(4)*M11)*AIMAG(ZETK2)
      IF(ABS(UY).LE.0.1E-6)GO TO  1009
      BJ=REAL(ZETK1)+M11*REAL(ZETK2)-M21*AIMAG(ZETK2)
      FF2(K)=-K*CJ*UY
      FF4(K)= K*BJ*UY
 1009 FF3(K)=REAL(P1)*REAL(ZTEM1)-AIMAG(P1)*AIMAG(ZTEM1)
     $       +M11*(REAL(P2)*REAL(ZTEM2)-AIMAG(P2)*AIMAG(ZTEM2))
     $       -M21*(REAL(P2)*AIMAG(ZTEM2)+AIMAG(P2)*REAL(ZTEM2))
      FF5(K)=REAL(Q1)*REAL(ZTEM1)-AIMAG(Q1)*AIMAG(ZTEM1)
     $       +M11*(REAL(Q2)*REAL(ZTEM2)-AIMAG(Q2)*AIMAG(ZTEM2))
     $       -M21*(REAL(Q2)*AIMAG(ZTEM2)+REAL(ZTEM2)*AIMAG(Q2))
      IF(ABS(UX).LE.0.1E-6)GO TO 1010
      AJ=REAL(ZMU1S)*REAL(ZETK1)-AIMAG(ZMU1S)*AIMAG(ZETK1)
     $  +M11*(REAL(ZMU2S)*REAL(ZETK2)-AIMAG(ZMU2S)*AIMAG(ZETK2))
     $  -M21*(REAL(ZMU2S)*AIMAG(ZETK2)+REAL(ZETK2)*AIMAG(ZMU2S))
      FF2(K)=K*AJ*UX+FF2(K)
      FF4(K)=-K*CJ*UX+FF4(K)
 1010 CONTINUE
      GO TO  2000
 1011 DO  1012  K=1,9
      FF2(K)=0.0
      FF2(K+9)=0.0
      FF4(K)=0.0
      FF4(K+9)=0.0
      ZETK1=ZETK1*ZET1
      ZETK2=ZETK2*ZET2
      ZTEM1=ZETK1*Z1
      ZTEM2=ZETK2*Z2
      KK=-KK
      IF(KK.EQ.1) GO TO  15
      M11=-ROTI(2)/ROTI(4)
      M12=(ROTR(4)-ROTR(2))/ROTI(4)
      M21=0.0
      M22=-1.0
      GO TO  16
  15  M11=-1.0
```

```
      M12=0.0
      M21=(ROTR(2)-ROTR(4))/ROTI(4)
      M22=-ROTI(2)/ROTI(4)
   16 CONTINUE
      CJ=ROTR(2)*REAL(ZETK1)+(ROTR(4)*M11-ROTI(4)*M21)*REAL(ZETK2)
     $  -ROTI(2)*AIMAG(ZETK1)-(ROTR(4)*M21+ROTI(4)*M11)*AIMAG(ZETK2)
      CJN=(ROTR(4)*M12-ROTI(4)*M22)*REAL(ZETK2)-ROTI(2)*REAL(ZETK1)
     $   -(ROTI(4)*M12+ROTR(4)*M22)*AIMAG(ZETK2)
     $   -ROTR(2)*AIMAG(ZETK1)
      IF(ABS(UY).LE.0.1E-6)GO TO  1014
      BJ=REAL(ZETK1)+M11*REAL(ZETK2)-M21*AIMAG(ZETK2)
      BJN=M12*REAL(ZETK2)-AIMAG(ZETK1)-M22*AIMAG(ZETK2)
      FF2(K)  =-K*CJ *UY
      FF2(K+9)=-K*CJN*UY
      FF4(K)  = K*BJ *UY
      FF4(K+9)= K*BJN*UY
 1014 FF3(K)  =REAL(P1)*REAL(ZTEM1)-AIMAG(P1)*AIMAG(ZTEM1)
     $       +M11*(REAL(P2)*REAL(ZTEM2)-AIMAG(P2)*AIMAG(ZTEM2))
     $       -M21*(REAL(P2)*AIMAG(ZTEM2)+AIMAG(P2)*REAL(ZTEM2))
      FF5(K)  =REAL(Q1)*REAL(ZTEM1)-AIMAG(Q1)*AIMAG(ZTEM1)
     $       +M11*(REAL(Q2)*REAL(ZTEM2)-AIMAG(Q2)*AIMAG(ZTEM2))
     $       -M21*(REAL(Q2)*AIMAG(ZTEM2)+REAL(ZTEM2)*AIMAG(Q2))
      FF3(K+9)=M12*(REAL(P2)*REAL(ZTEM2)-AIMAG(P2)*AIMAG(ZTEM2))
     $         -M22*(REAL(P2)*AIMAG(ZTEM2)+REAL(ZTEM2)*AIMAG(P2))
     $         -REAL(P1)*AIMAG(ZTEM1)-REAL(ZTEM1)*AIMAG(P1)
      FF5(K+9)=M12*(REAL(Q2)*REAL(ZTEM2)-AIMAG(Q2)*AIMAG(ZTEM2))
     $         -M22*(REAL(Q2)*AIMAG(ZTEM2)+REAL(ZTEM2)*AIMAG(Q2))
     $         -REAL(Q1)*AIMAG(ZTEM1)-REAL(ZTEM1)*AIMAG(Q1)
      IF(ABS(UX).LE.0.1E-6)GO TO 1012
      AJ=REAL(ZMU1S)*REAL(ZETK1)-AIMAG(ZMU1S)*AIMAG(ZETK1)
     $  +M11*(REAL(ZMU2S)*REAL(ZETK2)-AIMAG(ZMU2S)*AIMAG(ZETK2))
     $  -M21*(REAL(ZMU2S)*AIMAG(ZETK2)+REAL(ZETK2)*AIMAG(ZMU2S))
      AJN=M12*(REAL(ZMU2S)*REAL(ZETK2)-AIMAG(ZMU2S)*AIMAG(ZETK2))
     $   -M22*(REAL(ZMU2S)*AIMAG(ZETK2)+REAL(ZETK2)*AIMAG(ZMU2S))
     $   -REAL(ZMU1S)*AIMAG(ZETK1)-REAL(ZETK1)*AIMAG(ZMU1S)
      FF2(K)  = K*AJ *UX+FF2(K)
      FF2(K+9)= K*AJN*UX+FF2(K+9)
```

```
      FF4(K)  =-K*CJ *UX+FF4(K)
      FF4(K+9)=-K*CJN*UX+FF4(K+9)
 1012 CONTINUE
 2000 KJ=0
      DO 41 K=1,9
      L=2*ISI-1
      DO  40  J=1,KEY
      I=J*9+K-9
      G(I,L)  =G(I,L  )+0.5*W(II)*(0.5*(1.0-Y(II))*FF2(I))
      G(I,L+1)=G(I,L+1)+0.5*W(II)*(0.5*(1.0-Y(II))*FF4(I))
      G(I,L+2)=G(I,L+2)+0.5*W(II)*(0.5*(1.0+Y(II))*FF2(I))
  40  G(I,L+3)=G(I,L+3)+0.5*W(II)*(0.5*(1.0+Y(II))*FF4(I))
C
      DO 41  J=1,K
      KJ=KJ+1
      VA(KJ)=VA(KJ)+0.5*W(II)*(FF2(K)*FF3(J)+FF2(J)*FF3(K)
     $       +FF4(K)*FF5(J)+FF4(J)*FF5(K))
      IF(KEY.EQ.1) GO TO  41
      I=K+9
      L=J+9
      VB(KJ)=VB(KJ)+0.5*W(II)*(FF2(I)*FF3(L)+FF2(L)*FF3(I)
     $       +FF4(I)*FF5(L)+FF4(L)*FF5(I))
  41  CONTINUE
  42  CONTINUE
      IF(KEY.EQ.1) GO TO  64
      DO  500  III=1,9
      G(III,2)=0.0
      G(III,1)=2.0*G(III,1)
      II=III+9
      G(II,2)=2.0*G(II,2)
      G(II,1)=0.0
      DO  455  J=1,4
      JU=J+1
      JL=10-J
      G(III,2*JL-1)=G(III,2*JU-1)
      G(III,2*JL)=-G(III,2*JU)
      G(II,2*JL-1)=-G(II,2*JU-1)
```

```
 455  G(II,2*JL)=G(II,2*JU)
 500  CONTINUE
      DO  501  I=1,18
 501  G(11,I)=0.0
      DO  63  I=1,45
      VA(I)=VA(I)*2.0
  63  VB(I)=VB(I)*2.0
      VB(2)=0.0
      VB(3)=1.0
      DO  62  I=3,9
  62  VB((I*I-I)/2+2)=0.0
  64  CONTINUE
      N=9
      CALL LINV2P(VA,N,VINV1,IDGT,D1,D2,WK,IER)
      IF(IER.NE.0)WRITE(6,82)
      IF(IER.NE.0)STOP
  82  FORMAT(//,9X,'CHECK MATRIX H1',//)
      IF(KEY.EQ.2) CALL LINV2P(VB,N,VINV2,IDGT,D1,D2,WK,IER)
      IF(IER.NE.0)WRITE(6,83)
  83  FORMAT(//,9X,'CHECK MATRIX H2',//)
      IF(IER.NE.0)STOP
C.....Calculate [H]inv.* [G]
C     ====================
      DO  111  J=1,NDPE
      DO  110  I=1,9
      II=I*(I-1)/2
      BK(I,J)=0.0
      DO  110  K=1,9
      IK=II+K
      IF(K.GT.I) IK=K*(K-1)/2+I
 110  BK(I,J)=BK(I,J)+VINV1(IK)*G(K,J)
      IF(KEY.EQ.1) GO TO  111
      DO  121  I=10,18
      M=I-9
      IJ=M*(M-1)/2
      BK(I,J)=0.0
      DO  121  K=1,9
```

```
      IK=IJ+K
      IF(K.GT.M) IK=K*(K-1)/2+M
  121 BK(I,J)=BK(I,J)+VINV2(IK)*G(K+9,J)
  111 CONTINUE
C.....Calculate Element Stiffness matrix and Stress Intensity Matrix :
C     ================================================================
      IJ=0
      DO  112  I=1,NDPE
      DO  112  J=1,I
      IJ=IJ+1
      EK1(IJ)=0.0
      DO  112  K=1,NT
  112 EK1(IJ)=EK1(IJ)+BK(K,J)*G(K,I)*THICK
      E=SQRT(2.0/ES)
      T1=1-ROTI(2)/ROTI(4)
      T2=(ROTR(4)-ROTR(2))/ROTI(4)
      T3=ROTR(2)-ROTR(4)*ROTI(2)/ROTI(4)
      T4=ROTI(4)-ROTI(2)+ROTR(4)*T2
      DO  113  J=1,NDPE
      BST1(J)=E*T1*BK(1,J)
      BND1(J)=-E*T3*BK(1,J)
      IF(KEY.EQ.1) GO TO 23
      BST2(J)= E*T2*BK(10,J)
      BND2(J)=-E*T4*BK(10,J)
      BCR(1,J)=BST1(J)+BST2(J)
      BCR(2,J)=BND1(J)+BND2(J)
      GO TO 113
   23 BCR(1,J)=BST1(J)
      BCR(2,J)=BND1(J)
  113 CONTINUE
C     Rotate {BCR} matrix and element stiffness matrix to global system:
C     ==================================================================
      N=0
      DO  3001  I=1,NDPE
      DO  3000  J=1,I
      N=N+1
      TEM(I,J)=EK1(N)
```

```
3000 TEM(J,I)=EK1(N)
     DO  3001  J=1,2
3001 BCRTEM(J,I)=BCR(J,I)
     DO  3002  J=1,2
     DO  3002  I=2,NDPE,2
     IM1=I-1
     BCR(J,IM1)=BCRTEM(J,IM1)*COSS-BCRTEM(J,I)*SINN
3002 BCR(J,I)  =BCRTEM(J,IM1)*SINN+BCRTEM(J,I)*COSS
     DO  79  J=2,NDPE,2
     I=J-1
     VVG(I,I)=COSS
     VVG(J,J)=COSS
     VVG(I,J)=SINN
  79 VVG(J,I)=-SINN
     DO  80  I=1,NDPE
     DO  80  J=1,NDPE
     DO  80  K=1,NDPE
     DO  80  N=1,NDPE
  80 EK(I,J)=EK(I,J)+VVG(K,I)*TEM(K,N)*VVG(N,J)
     RETURN
     END
     SUBROUTINE ROOTS(ROR,ROI,SPP)
     DIMENSION XCO(5),SPP(6),CO(5),ROOOTR(4),ROOOTI(4),ROR(4),ROI(4)
     COMMON/MATRIL/YOUNG1,YOUNG2,POIS12,G12,IANGL,ISTRPC,THICK
     M=4
     S11=1/YOUNG1
     S12=-POIS12*S11
     S22=1/YOUNG2
     S66=1/G12
C.....Calculate the coefficients of the charactaristic equation.
     IF(IANGL.EQ.0.OR.IANGL.EQ.90) GO TO  2
     ANGL=IANGL*ATAN(1.0)/45
     SIN1=SIN(ANGL)
     COS1=COS(ANGL)
     SIN2=SIN1*SIN1
     COS2=COS1*COS1
     SIN4=SIN2*SIN2
```

```
      COS4=COS2*COS2
      SIN3=SIN2*SIN1
      COS3=COS2*COS1
      SPP(1)=S11*COS4+(2*S12+S66)*SIN2*COS2+S22*SIN4
      SPP(2)=S12*(SIN4+COS4)+(S11+S22-S66)*SIN2*COS2
      SPP(3)=S11*SIN4+(2*S12+S66)*SIN2*COS2+S22*COS4
      SPP(4)=(2*S11-2*S12-S66)*SIN1*COS3-(2*S22-2*S12-S66)*SIN3*COS1
      SPP(5)=(2*S11-2*S12-S66)*SIN3*COS1-(2*S22-2*S12-S66)*SIN1*COS3
      SPP(6)=2*(2*S11+2*S22-4*S12-S66)*SIN2*COS2+S66*(SIN4+COS4)
      WRITE(6,8)(SPP(I),I=1,6)
    8 FORMAT(2X,'SPP(I)=',6E14.6,//)
      XCO(1)=SPP(3)
      XCO(2)=-2*SPP(5)
      XCO(3)=2*SPP(2)+SPP(6)
      XCO(4)=-2*SPP(4)
      XCO(5)=SPP(1)
      GO TO  6
    2 XCO(2)=0.0
      XCO(3)=2*S12+S66
      XCO(4)=0.0
      SPP(2)=S12
      SPP(4)=0.0
      SPP(5)=0.0
      SPP(6)=S66
      IF(IANGL.EQ.90) GO TO  4
      SPP(1)=S11
      SPP(3)=S22
      XCO(1)=S22
      XCO(5)=S11
      GO TO  6
    4 XCO(1)=S11
      XCO(5)=S22
      SPP(1)=S22
      SPP(3)=S11
    6 WRITE(6,12)(XCO(I),I=1,5)
   12 FORMAT(5X,'XCO(I)=',5E14.6,//)
C.....Calculate the roots of the charactaristic equation.
```

```
      CALL POLRT(XCO,CO,M,ROOOTR,ROOOTI,IER)
      DO  7  I=1,4
    7 WRITE(6,10) I,ROOOTR(I),I,ROOOTI(I)
   10 FORMAT(5X,'ROOTR(',I1,')=',F10.5,6X,'ROOTI(',I1,')=',F10.5,'i',/)
      DO 14 I=1,4
      ROI(I)=ROOOTI(I)
      IF(IANGL.EQ.0.OR.IANGL.EQ.90) GO TO 13
      ROR(I)=ROOOTR(I)
      GO TO 14
   13 ROR(I)=0.0
   14 CONTINUE
      RETURN
      END
      SUBROUTINE POLRT(XCOF,COF,M,ROOTR,ROOTI,IER)
      DIMENSION XCOF(1),COF(1),ROOTR(1),ROOTI(1)
      IFIT=0
      N=M
      IER=0
      IF(XCOF(N+1))10,25,10
   10 IF(N) 15,15,32
   15 IER=1
   20 RETURN
   25 IER=4
      GO TO 20
   30 IER=2
      GO TO 20
   32 IF(N-36) 35,35,30
   35 NX=N
      NXX=N+1
      N2=1
      KJ1 = N+1
      DO 40 L=1,KJ1
      MT=KJ1-L+1
   40 COF(MT)=XCOF(L)
   45 XO=.00500101
      YO=0.01000101
      IN=0
```

```
50 X=XO
   XO=-10.0*YO
   YO=-10.0*X
   X=XO
   Y=YO
   IN=IN+1
   GO TO 59
55 IFIT=1
   XPR=X
   YPR=Y
59 ICT=0
60 UX=0.0
   UY=0.0
   V =0.0
   YT=0.0
   XT=1.0
   U=COF(N+1)
   IF(U) 65,130,65
65 DO 70 I=1,N
   L =N-I+1
   TEMP=COF(L)
   XT2=X*XT-Y*YT
   YT2=X*YT+Y*XT
   U=U+TEMP*XT2
   V=V+TEMP*YT2
   FI=I
   UX=UX+FI*XT*TEMP
   UY=UY-FI*YT*TEMP
   XT=XT2
70 YT=YT2
   SUMSQ=UX*UX+UY*UY
   IF(SUMSQ) 75,110,75
75 DX=(V*UY-U*UX)/SUMSQ
   X=X+DX
   DY=-(U*UY+V*UX)/SUMSQ
   Y=Y+DY
78 IF(ABS(DY)+ABS(DX)-1.0E-05) 100,80,80
```

```
 80 ICT=ICT+1
    IF(ICT-500) 60,85,85
 85 IF(IFIT)100,90,100
 90 IF(IN-5) 50,95,95
 95 IER=3
    GO TO 20
100 DO 105 L=1,NXX
    MT=KJ1-L+1
    TEMP=XCOF(MT)
    XCOF(MT)=COF(L)
105 COF(L)=TEMP
    ITEMP=N
    N=NX
    NX=ITEMP
    IF(IFIT) 120,55,120
110 IF(IFIT) 115,50,115
115 X=XPR
    Y=YPR
120 IFIT=0
122 IF(ABS(Y)-1.0E-4*ABS(X)) 135,125,125
125 ALPHA=X+X
    SUMSQ=X*X+Y*Y
    N=N-2
    GO TO 140
130 X=0.0
    NX=NX-1
    NXX=NXX-1
135 Y=0.0
    SUMSQ=0.0
    ALPHA=X
    N=N-1
140 COF(2)=COF(2)+ALPHA*COF(1)
145 DO 150 L=2,N
150 COF(L+1)=COF(L+1)+ALPHA*COF(L)-SUMSQ*COF(L-1)
155 ROOTI(N2)=Y
    ROOTR(N2)=X
    N2=N2+1
```

```
      IF(SUMSQ) 160,165,160
  160 Y=-Y
      SUMSQ=0.0
      GO TO 155
  165 IF(N) 20,20,45
      END
      SUBROUTINE FRONT(NELEM,NPOIN,NVFIX,NTOTV,NGAUS,COORD,LNODS,
     ,      ELOAD,ASDIS,NOFIX,IFPRE,PRESC,BCRT,MFRON,CRD,SIF)
C     ============================================================
      IMPLICIT REAL*8(A-H,O-Z)
      DIMENSION COORD(NPOIN,2),LNODS(NELEM,9),ELOAD(NELEM,18),
     ,QV(18),ASDIS(NTOTV),NOFIX(NVFIX),IFPRE(NVFIX,2),PRESC(NVFIX,2)
     $  ,CRD(NPOIN,2),QV1(18),SIF(4)
      REAL*4 XTIP(2),YTIP(2)
      COMMON/WORK/SHAP(4),DERIV(2,4),BMATX(3,8),POSGP(3)
     ,      ,WEIGP(3),QBMAT(3,8),GPCOD(2,9),SMATX(3,8,9)
      COMMON/SUPER/ISUPR1,ISUPR2,KEY1,KEY2,XTIP,YTIP
C
      DIMENSION  FIXED(368),EQUAT(60),VECRV(60),GLOAD(60),LOCEL(18),
     ,GSTIF(1830),ESTIF(18,18),IFFIX(368),NACVA(60),NDEST(18),
     $ BCRT(2,2,18)
      NFUNC(I,J)=I+(J*(J-1))/2
C
      MSTIF=MFRON*(MFRON+1)/2
C
C.....Interpret fixity data in vector from.....................
C
      DO  100  I=1,NTOTV
      IFFIX(I)=0
  100 FIXED(I)=0.DO
      DO  110  I=1,NVFIX
      NLOCA=2*(NOFIX(I)-1)
      DO  110  J=1,2
      NGASH=NLOCA+J
      IFFIX(NGASH)=IFPRE(I,J)
  110 FIXED(NGASH)=PRESC(I,J)
C
```

```
C.....Change the sign of last appearance of each node.....
      DO  140  I=1,NPOIN
      KLAST=0
      DO  120  IELEM=1,NELEM
      NNODE=4
      IF(IELEM.EQ.ISUPR1.AND.KEY1.EQ.1)NNODE=5
      IF(IELEM.EQ.ISUPR1.AND.KEY1.EQ.2)NNODE=9
      IF(IELEM.EQ.ISUPR2)NNODE=9
      DO  120  INODE=1,NNODE
      IF(LNODS(IELEM,INODE).NE.I) GO TO  120
      KLAST=IELEM
      NLAST=INODE
 120  CONTINUE
      IF(KLAST.NE.0)LNODS(KLAST,NLAST)=-I
 140  CONTINUE
C
C.....I N I T I A L I Z A T I O N.....
      DO  150  ISTIF=1,MSTIF
 150  GSTIF(ISTIF)=0.D0
      DO  160  IFRON=1,MFRON
      GLOAD(IFRON)=0.D0
      EQUAT(IFRON)=0.D0
      VECRV(IFRON)=0.D0
 160  NACVA(IFRON)=0
C
C.....PREPARE FOR DISC READING AND WRITING OPERATIONS
      REWIND 1
      REWIND 2
C
C.....ENTER MAIN ELEMENT ASSEMBLY - REDUCTION LOOP.....
      NFRON=0
      KELVA=0
      DO  380  I=1,NELEM
      NNODE=4
      IF(I.EQ.ISUPR1.AND.KEY1.EQ.1)NNODE=5
      IF(I.EQ.ISUPR1.AND.KEY1.EQ.2)NNODE=9
      IF(I.EQ.ISUPR2)NNODE=9
```

```
      NEVAB=NNODE*2
      KEVAB=0
      READ(1) ESTIF
      DO  165  IEVAB=1,NEVAB
 165  LOCEL(IEVAB)=0
      DO  170  J=1,NNODE
      DO  170  K=1,2
      NPOSI=(J-1)*2+K
      LOCNO=LNODS(I,J)
      IF(LOCNO.GT.0) LOCEL(NPOSI)=(LOCNO-1)*2+K
      IF(LOCNO.LT.0) LOCEL(NPOSI)=(LOCNO+1)*2-K
 170  CONTINUE
C
C.....START BY LOOKING FOR EXISTING DESTINATIONS
C
      DO  210  IEVAB=1,NEVAB
      NIKNO=IABS(LOCEL(IEVAB))
      IF(NIKNO.EQ.0)  GO TO  210
      KEXIS=0
      IF(NFRON.EQ.0) GO TO  181
      DO  180  IFRON=1,NFRON
      IF(NIKNO.NE.NACVA(IFRON)) GO TO  180
      KEVAB=KEVAB+1
      KEXIS=1
      NDEST(KEVAB)=IFRON
 180  CONTINUE
 181  CONTINUE
      IF(KEXIS.NE.0) GO TO 210
C
C.....WE NOW SEEK NEW EMPTY PLACES FOR DESTINATION VECTOR
C
      DO  190  IFRON=1,MFRON
      IF(NACVA(IFRON).NE.0) GO TO  190
      NACVA(IFRON)=NIKNO
      KEVAB=KEVAB+1
      NDEST(KEVAB)=IFRON
      GO TO  200
```

```
 190  CONTINUE
C
C.....THE NEW PLACES MAY DEMAND AN INCREASE IN CURRENT FRONTWIDTH
C
 200  IF(NDEST(KEVAB).GT.NFRON) NFRON=NDEST(KEVAB)
 210  CONTINUE
C.....Asseable element loads.............................
      DO  240  II=1,NEVAB
      IF(LOCEL(II).EQ.0)  GO  TO  240
      IDEST=NDEST(II)
      GLOAD(IDEST)=GLOAD(IDEST)+ELOAD(I,II)
C.....Asseable the element stiffnesses but not in resolution.....
      DO  220  JJ=1,II
      JDEST=NDEST(JJ)
      NGASH=NFUNC(IDEST,JDEST)
      NGISH=NFUNC(JDEST,IDEST)
      IF(JDEST.GE.IDEST)GSTIF(NGASH)=GSTIF(NGASH)+ESTIF(II,JJ)
      IF(JDEST.LT.IDEST)GSTIF(NGISH)=GSTIF(NGISH)+ESTIF(II,JJ)
 220  CONTINUE
 240  CONTINUE
C.....Re-Examin each element node to enquire which can be eliminated...
      DO  370  II=1,NEVAB
      NIKNO= -LOCEL(II)
      IF(NIKNO.LE.0) GO TO  370
C.....Find positions of variables ready for elimination.............
      DO  350  IFRON=1,NFRON
      IF(NACVA(IFRON).NE.NIKNO)GO TO  350
C.....Extract the cofficients of the new equation for elimination...
      DO  250  JFRON=1,NFRON
      IF(IFRON.LT.JFRON) NLOCA=NFUNC(IFRON,JFRON)
      IF(IFRON.GE.JFRON) NLOCA=NFUNC(JFRON,IFRON)
      EQUAT(JFRON)=GSTIF(NLOCA)
 250  GSTIF(NLOCA)=0.D0
C.....And extract the correspondins risht hand sides.............
      EQRHS=GLOAD(IFRON)
      GLOAD(IFRON)=0.D0
      KELVA=KELVA+1
```

```
C.....Write equations to DISC or to TAPE ......
      WRITE(2) EQUAT, EQRHS, IFRON, NIKNO
C.....Deal  with  Pivot .....................................
      PIVOT=EQUAT(IFRON)
      EQUAT(IFRON)=0.D0
C.....Enquire whether present variable is free or prescribed.....
      IF(IFFIX(NIKNO).EQ.0) GO TO  300
C.....Deal with a prescribed displacement.....................
      DO  290  JFRON=1,NFRON
 290  GLOAD(JFRON)=GLOAD(JFRON)-FIXED(NIKNO)*EQUAT(JFRON)
      GO TO  340
C.....Eliminate a free variable - deal with the right hand side first...
 300  DO  330  JFRON=1,NFRON
      GLOAD(JFRON)=GLOAD(JFRON)-EQUAT(JFRON)*EQRHS/PIVOT
C.....Now deal with the coefficients in core.................
      IF(EQUAT(JFRON).EQ.0.0) GO TO   330
      NLOCA=NFUNC(0,JFRON)
      DO  310  LFRON=1,JFRON
      NGASH=LFRON+NLOCA
 310  GSTIF(NGASH)=GSTIF(NGASH)-EQUAT(JFRON)*EQUAT(LFRON)/PIVOT
 330  CONTINUE
 340  EQUAT(IFRON)=PIVOT
C.....Record the new vacant space, and reduce frontwidth if possible.....
      NACVA(IFRON)=0
      GO TO  360
C.....Complete the element loop in the forward elimination.....
 350  CONTINUE
 360  IF(NACVA(NFRON).NE.0)GO TO  370
      NFRON=NFRON-1
      IF(NFRON.GT.0) GO TO  360
 370  CONTINUE
 380  CONTINUE
C.....Enter back-substitution phase, loop backwords throusth variables...
      DO  410  IELVA=1,KELVA
C.....Read a new equation.....................................
      BACKSPACE 2
      READ(2) EQUAT, EQRHS, IFRON, NIKNO
```

```
      BACKSPACE 2
C.....Prepare to back - substitute from the current equation.......
      PIVOT=EQUAT(IFRON)
      IF(IFFIX(NIKNO).EQ.1) VECRV(IFRON)=FIXED(NIKNO)
      IF(IFFIX(NIKNO).EQ.0) EQUAT(IFRON)=0.DO
C.....Back-substitute in the current equation.................
      DO  400  JFRON=1,MFRON
  400 EQRHS=EQRHS-VECRV(JFRON)*EQUAT(JFRON)
C.....Put the final values where they belong..................
      IF(IFFIX(NIKNO).EQ.0) VECRV(IFRON)=EQRHS/PIVOT
      IF(IFFIX(NIKNO).EQ.1) FIXED(NIKNO)=-EQRHS
      ASDIS(NIKNO)=VECRV(IFRON)
  410 CONTINUE
      WRITE(6,900)
  900 FORMAT(//,15X,13HDISPLACEMENTS)
      WRITE(6,905)
  905 FORMAT(1HO,5X,4HNODE,6X,7HX-DISP.,7X,7HY-DISP.)
      DO  450  IPOIN=1,NPOIN
      NGASH=IPOIN*2
      NGISH=NGASH-1
      CRD(IPOIN,1)=COORD(IPOIN,1)-ASDIS(NGISH)
      CRD(IPOIN,2)=COORD(IPOIN,2)-ASDIS(NGASH)
  450 WRITE(6,920)IPOIN,(ASDIS(IGASH),IGASH=NGISH,NGASH),(CRD(IPOIN,
     $    M),M=1,2)
  920 FORMAT(I10,2E14.6,2F15.6)
      WRITE(6,925)
  925 FORMAT(1HO,15X,9HREACTIONS)
      WRITE(6,935)
  935 FORMAT(1HO,5X,4HNODE,5X,7HX-FORCE,7X,7HY-FORCE)
      DO  510  IPOIN=1,NPOIN
      NLOCA=(IPOIN-1)*2
      DO  490  IDOFN=1,2
      NGUSH=NLOCA+IDOFN
      IF(IFFIX(NGUSH).GT.0) GO TO  500
  490 CONTINUE
      GO TO 510
  500 NGASH=NLOCA+2
```

```
      NGISH=NLOCA+1
      WRITE(6,945) IPOIN, (FIXED(IGASH),IGASH=NGISH,NGASH)
  510 CONTINUE
  945 FORMAT(/,I10,3E14.6)
C.....Post FRONT - Reset all elemenet connection number to positive
C     values for subseauent use in stress calculation.
      DO  520  I=1,NELEM
      DO  520  J=1,9
  520 LNODS(I,J)=IABS(LNODS(I,J))
      DO  30  I=2,18,2
      J=I/2
      QV1(I-1)=ASDIS(LNODS(ISUPR1,J)*2-1)
      QV1(I) =ASDIS(LNODS(ISUPR1,J)*2)
      QV(I-1)=ASDIS(LNODS(ISUPR2,J)*2-1)
   30 QV(I)  =ASDIS(LNODS(ISUPR2,J)*2)
      DO  32  K=1,4
   32 SIF(K)=0.0D0
C.....Calculate the stress intensity factor for Super-Element number  '1'
      DO  36  I=1,18
      SIF(1)=SIF(1)+QV1(I)*BCRT(1,1,I)
      SIF(2)=SIF(2)+QV1(I)*BCRT(1,2,I)
      SIF(3)=SIF(3)+QV(I) *BCRT(2,1,I)
   36 SIF(4)=SIF(4)+QV(I) *BCRT(2,2,I)
      WRITE(6,922)ISUPR1
      WRITE(6,923) SIF(1) , SIF(2)
      WRITE(6,922)ISUPR2
      WRITE(6,923) SIF(3) , SIF(4)
  922 FORMAT(///,23X,'STRESS INTENSITY FACTOR FOR SUPER-ELEMENT #',I3,/)
  923 FORMAT(/,12X,'S.I.F. (OPENING MODE)=',E12.4,10X,
     $            'S.I.F. (SHEAR MODE)=',E12.4,///)
      RETURN
      END
```

APPENDIX F

STRESS-CONCENTRATION COMPUTER PROGRAM

The following computer program is based on Savin's closed-form analytical solution of Chapter 2. It is used to obtain all tables and figures in the first section of Chapter 5.

The subroutine (POLRT) which is used to calculate the roots of the characteristic equation of Chapter 2, Equation (2.11), is not listed here since it is already listed in one of the finite-element computer subroutines in Appendix E. The only modification of the subroutine POLRT needed is to convert it from single precision to double precision in order to be applicable to the following computer program.

```
      IMPLICIT REAL*8(A-H,O-Z)
      DIMENSION  XCOF(5),SP(6),COF(5),ROOTR(4),ROOTI(4)
      REAL*4 SS(183),XX(183)
      CALL PLOTS(10.0,12.0,0,0.5,1.5)
      XX(182)=0.0
      XX(183)=20.0
      SS(182)=-3.0
      SS(183)= 10.0
      CALL LINEWT(-1)
      CALL AXIS(0.0,0.0,'ANGLE',-5,9.0,0.0,XX(182),XX(183),20.0)
      CALL AXIS(0.0,0.0,'STRESS-CONCENTRATION FACTORS',28,
     *6.0,90.0,SS(182),SS(183),20.0)
      CALL PLOT(9.0,0.0,3)
      CALL PLOT(9.0,6.0,2)
      CALL PLOT(0.0,6.0,2)
      CALL SYM(4.6,-0.4,.17,280,0.0,-1)
      CALL SYM(-0.3,4.6,0.17,'14S17I4YI814/11P',90.0,16)
      CALL SYM(0.3,5.5,0.15,'10CJ11ISOTROPIC',0.0,15)
      CALL SYM(0.3,5.2,0.17,'10 J13Q=010=',0.0,11)
      CALL SYM(0.3,4.9,0.17,'10AJ13Q=3010=',0.0,13)
      CALL SYM(0.3,4.6,0.17,'10BJ13Q=4510=',0.0,13)
      CALL SYM(0.3,4.3,0.17,'10EJ13Q=6010=',0.0,13)
      CALL SYM(0.3,4.0,0.17,'10DJ13Q=9010=',0.0,13)
      DO  95  K=1,6
      M=4
      IF(K.EQ.6) GO TO 18
      RATIO=9.0D0
      READ(5,1005) YOUNG1,YOUNG2,POIS12,G12,ANGL
      WRITE(6,1006)YOUNG1,YOUNG2,POIS12,G12,ANGL
      S11=1/YOUNG1
      S12=-POIS12*S11
      S22=1/YOUNG2
      S66=1/G12
C.....
      ANGL=ANGL*DATAN(1.0D0)/45
      SIN1=DSIN(ANGL)
```

```
      COS1=DCOS(ANGL)
      SIN2=SIN1*SIN1
      COS2=COS1*COS1
      SIN4=SIN2*SIN2
      COS4=COS2*COS2
      SIN3=SIN2*SIN1
      COS3=COS2*COS1
      SP(1)=S11*COS4+(2*S12+S66)*SIN2*COS2+S22*SIN4
      SP(2)=S12*(SIN4+COS4)+(S11+S22-S66)*SIN2*COS2
      SP(3)=S11*SIN4+(2*S12+S66)*SIN2*COS2+S22*COS4
      SP(4)=(2*S11-2*S12-S66)*SIN1*COS3-(2*S22-2*S12-S66)*SIN3*COS1
      SP(5)=(2*S11-2*S12-S66)*SIN3*COS1-(2*S22-2*S12-S66)*SIN1*COS3
      SP(6)=2*(2*S11+2*S22-4*S12-S66)*SIN2*COS2+S66*(SIN4+COS4)
      WRITE(6,8)(SP(I),I=1,6)
 8    FORMAT(2X,'SP(I)=',6E14.6,//)
      XCOF(1)=SP(3)
      XCOF(2)=-2*SP(5)
      XCOF(3)=2*SP(2)+SP(6)
      XCOF(4)=-2*SP(4)
      XCOF(5)=SP(1)
1005  FORMAT(5D12.0)
1006  FORMAT(/,3X,'YOUNG1=',F12.3,8X,'YOUNG2=',F12.3,8X,'POIS12=',F7.5,
     , 6X,    'G12=',F12.3,6X,'ANGLE=',F6.1,//)
      CALL POLRT(XCOF,COF,M,ROOTR,ROOTI,IER)
      DO  7  I=1,4
 7    WRITE(6,10) ROOTR(I),ROOTI(I)
 10   FORMAT(5X,F10.5,6X,F10.5,'i',/)
      U=ROOTR(2)*ROOTR(4)-ROOTI(2)*ROOTI(4)
      V=ROOTR(2)*ROOTI(4)+ROOTR(4)*ROOTI(2)
      X=ROOTR(2)+ROOTR(4)
      Y=ROOTI(2)+ROOTI(4)
      IF(K.LT.6) GO TO  19
 18   U=-1.0D0
      V=0.0D0
      X=0.0D0
      Y=2.0D0
```

```
19  U2=U*U
    V2=V*V
    X2=X*X
    Y2=Y*Y
    Z1=2-U-X2-Y2
    Z2=2*X*U-2*X+2*Y*V
    Z3=1+2*U-U2-V2
    DO  20  I=1,181
    THETA=(I-1)*DATAN(1.0D0)/45
    IF((I-1).EQ.180) GO TO  25
    A=DSIN(THETA)
    GO TO  26
25  A=0.0D0
26  A2=A*A
    A3=A*A2
    A4=A*A3
    A5=A*A4
    IF((I-1).EQ.90) GO TO  30
    BP=DCOS(THETA)
    GO TO  31
30  BP=0.0D0
31  B=RATIO*BP
    B2=B*B
    B3=B*B2
    B4=B*B3
    B5=B*B4
    Z4=A2*Y-A*B*V
    Z5=A2-A*B*X+B2*U
    Z52=Z5*Z5
    Z6=(B*V-A*Y)*B
    Z62=Z6*Z6
    Z7=A2+B2
    Z72=Z7*Z7
    Z8=A*B4*X-B5*U
    ZZ=A5*X+A4*B*Z1+A3*B2*Z2+A2*B3*Z3-Z8
    STR=(A2+RATIO*(BP*ZZ+Z4*Z72)/(Z52+Z62))/Z7
```

```
      XX(I)=I-1
      SS(I)=STR
20    CONTINUE
      DO  97  I=1,185,10
      II=I+9
      IF(I.GT.180) II=183
97    WRITE(6,96)(XX(IN),IN=I,II)
      DO 98 I=1,185,10
      II=I+9
      IF(I.GT.180) II=183
98    WRITE(6,96)(SS(IN),IN=I,II)
96    FORMAT(3X,10F10.3,/)
      KKK=K-1
      CALL LINE(XX,SS,181,1,5,KKK)
95    CONTINUE
      CALL PLOT(0.0,0.0,999)
      STOP
      END
```

LIST OF REFERENCES

1. Karlsson, A., and Backlund, J., "Summary of SIF Design Graphs for Cracks Emanating from Circular Holes," International Journal of Fracture, Vol. 14, No. 6, Dec. 1978, pp. 585-596.

2. Sih, G.C., and H. Liebowitz, "Mathematical Theories of Brittle Facture." In Fracture, an Advanced Treatise (ed. H. Liebowitz), Vol. 2. Academic Press, New York, 1968.

3. Sih, G.C., and Chen, E.P., "Fracture Analysis of Unidirectional Composites," Journal of Composite Materials, Vol. 7, 1973, pp. 230-244.

4. Nuismer, J., "An Energy Release Rate Criterion for Mixed Mode Fracture," International Journal of Fracture Mechanics, Vol. 11, No. 2, April 1975, pp. 245-250.

5. Gross, B., Srawley, J.E., and Brown, W.F., Jr., "Stress Intensity Factors for a Single-Edge-Notch Tension Specimen by Boundary Collocation of Stress Function," NASA TN-D2395, NASA, Washington, D.C., 1964, pp. 1-11.

6. Newman, J.C., Jr., "An Improved Method of Collocation for the Stress Analysis of Cracked Plates with Various Shaped Boundaries," NASA TN-D6376, NASA, Washington, D.C., 1971, pp. 1-45.

7. Gandhi, K.R., "Analysis of an Inclined Crack Centrally Placed in an Orthotropic Rectangular Plate," AMMRC TR 71-31, Army Material and Mechanics Research Center, Watertown, Mass. 1971, pp. 1-19.

8. Bowie, O.L., "Analysis of an Infinite Plate Containing Radial Cracks Originating at the Boundary of an Internal Circular Hole," Journal of Mathematics and Physics, Vol. 35, No. 1, April 1956, pp. 60-71.

9. Shivakumar, V., and Forman, R.G., "Green's Function for a Crack Emanating from a Circular Hole in an Infinite Sheet," International Journal of Fracture, Vol 16, No. 4, Aug. 1980, pp. 305-316.

10. Gallagher, R.H., "A Review of Finite Element Techniques in Fracture Mechanics," Proc. 1st Int. Conf. on Numerical Methods in Fracture Mechanics, Swansea, 1978, pp. 1-25.

11. Oladimeji, M.K., "Crack Emanating from a Circular Hole under Biaxial Load," Engineering Fracture Mechanics, Vol. 15, Nos. 3-4, 1981, pp. 391-405.

12. Bowie, O.L., and Freese, C.E., "Central Crack in Plane Orthotropic Rectangular Sheet," International Journal of Fracture Mechanics, Vol. 8, No. 1, March 1972, pp. 49-52.

13. Hsu, Y.C., "The Infinite Sheet with Cracked Cylindrical Hole under Inclined Tension or In-Plane Shear," International Journal of Fracture, Vol. 11, No. 4, Aug. 1975, pp. 571-581.

14. Tirosh, J., "The Mixed Mode Fracture of Unidirectional Fibrous Composites," Enginerring Fracture Mechanics, Vol. 13, 1980, pp. 119-127.

15. Wang, S.S., and Yau, J.F., "An Analysis of Cracks Emanating from a Circular Hole in Unidirectional Fiber-Reinforced Composites," Engineering Fracture Mechanics, Vol. 13, 1980, pp. 57-67.

16. Savin, G.N., "Some Problems in the Theory of the Elasticity of Anisotropic Media," Doklady Akademii Nauk SSSR, Vol. 23, No. 3, 1939, pp. 217-220.

17. Savin, G.N., Stress Concentration around Holes, Pergamon Press, Oxford, England, 1961.

18. Lekhnitskii, S.G., Theory of Elasticity of an Anisotropic Elastic Body, translated by P. Fern, Holden-Day, Inc., San Francisco, Calif., 1963.

19. Sokolinikoff, I.S., Mathematical Theory of Elasticity, Second Edition, McGraw-Hill, New York, 1956.

20. Muskhelishvili, N.I., Some Basic Problems of the Mathematical Theory of Elasticity, P. Noordhoff Ltd., Groningen, Holland, 1963.

21. Timoshenko, S.P., and Goodier, J.N., Theory of Elasticity, Third Edition, McGraw-Hill, New York, 1970.

22. Desai, C.S., and Abel, J.F., Introduction to the Finite Element Method, Van Nostrand Reinhold Co., New York, 1972.

23. Day, M.L., "A Mixed Variational Principle for Finite Element Analysis," Ph.D. Dissertation, Purdue University, 1981.

24. Spiering, R., and de Pater, C., "On the Cracked Element Approach for the Computation of Stress Intensity Factors," Trans. 4th SMIRT Conf., Vol. 6, Paper G5/7, 1977, pp. 1-12.

25. Pian, T.H.H., and Tong, P., "Basis of Finite Element Methods for Solid Continua," International Journal for Numerical Methods in Engineering, Vol. 1, 1969, pp. 3-28.

26. Tong, P., "New Displacement Hybrid Finite Element Models for Solid Continua," International Journal for Numerical Methods in Engineering, Vol. 2, 1970, pp. 73-80.

27. Apostal, M.C., Lee, Q.C., Braun, F.W., and Jordan, S., "Anisotropic Hybrid Displacement Singularity Element," Proc. ASCE, Journal of the Structural Division, Vol. 103, No. ST2, 1977, pp. 335-354.

28. Tong, P., Pian, T.H.H., and Larsy, S.J., "A Hybrid-Element Approach to Crack Problems in Plane Elasticity," International Journal for Numerical Methods in Engineering, Vol. 7, 1973, pp. 297-308.

29. Tong, P., "A Hybrid Crack Element for Rectilinear Anisotropic Material," International Journal for Numerical Methods in Engineering, Vol. 11, 1977, pp. 377-382.

30. Gallagher, R.H., Finite Element Analysis: Fundamentals, Prentice-Hall Book Co., Englewood Cliffs, N.J., 1975.

31. Tong, P., and Pian, T.H.H., "On the Convergence of the Finite Element Methods for Problems with Sinfularity," International Journal of Solids and Structures, Vol. 9, 1973, pp. 313-321.

32. Sih, G.C., Paris, P.C., and Irwin, G.R., "On Cracks in Rectilinearly Anisotropic Bodies," International Journal of Fracture Mechanics, Vol. 1, 1965, pp. 189-203.

33. Greszczuk, L.B., "Stress Concentrations and Failure Criteria for Orthotropic and Anisotropic Plates with Circular Openings," ASTM STP 497, American Society for Testing Materials, 1972, pp. 363-381.

34. Collazo, J.F., "Study of Delamination of Composite Laminates under Axial Compressive Loads," Master's Thesis, University of Florida, 1982.

35. Sun, C.T., and Sierakowski, R.L., "Fracture Characterization of Chopped Fiber Glass Composites," SAMPE Quarterly, July 1980, pp. 15-21.

36. International Mathematical and Statistical Libraries, Inc., Houston, Tex., IMSL Reference Manual, Vol. 2, 1979.

37. Jones, R.M., Mechanics of Composite Materials, McGraw-Hill, New York, 1975.

38. Irwin, G.R., "Analysis of Stresses and Strains Near the End of a Crack Traversing a Plate," Journal of Applied Mechanics, Vol. 79, 1957, pp. 361-364.

39. Westergaard, H.M., "Bearing Pressures and Cracks," Journal of Applied Mechanics, Vol. 61, 1939, pp. A49-A53.

BIOGRAPHICAL SKETCH

Said Abdel-Maaboud Khalil was born in Alexandria, Egypt, on October 19, 1946. He graduated from Alexandria Industrial High School in June 1964. He received his high school diploma with the highest ranked grade in the nation (about 900 students had taken the same examinations). He next enrolled to the Higher Industrial Institute, Cairo, Egypt. After five years majoring in mechanical engineering, he received his bachelor's degree in June 1969 with the highest ranking grade of all graduates (about 80 students) in the Mechanical Engineering Department.

In August 1969 he was employed by the Ministry of Higher Education to hold an instructor (teaching assistant) position in the same institute from which he received his undergraduate degree. From late 1970 through the end of 1972 he served in the Egyptian army. From 1973 through 1975 he took graduate courses leading to a master's degree. In 1976 he was awarded a scholarship through a nationwide competition to continue higher education in the United States. In January 1977 he attended Stanford University and graduated in June 1978 with a Master of Science degree in engineering mechanics.

In January 1980 he joined the graduate program in the Department of Engineering Sciences, University of Florida, Gainesville, Florida. Since that time, Mr. Khalil has been pursuing the doctorate degree in the fields of composite materials and fracture mechanics. After he received the degree of Doctor of Philosophy in December 1984, he returned home to work for the same college he attended for undergraduate study--College of Engineering and Technology, Helowan University, Cairo, Egypt.

Mr. Khalil was married to Nadia H. Ali in 1976 and they have one son, Hythem.

I certify that I have read this study and that in my opinion it conforms to acceptable standards of scholarly presentation and is fully adequate, in scope and quality, as a dissertation for the degree of Doctor of Philosophy.

C. T. Sun

C. T. Sun, Chairman
Professor of Engineering Sciences

I certify that I have read this study and that in my opinion it conforms to acceptable standards of scholarly presentation and is fully adequate, in scope and quality, as a dissertation for the degree of Doctor of Philosophy.

L. E. Malvern

L. E. Malvern, Co-Chairman
Professor of Engineering Sciences

I certify that I have read this study and that in my opinion it conforms to acceptable standards of scholarly presentation and is fully adequate, in scope and quality, as a dissertation for the degree of Doctor of Philosophy.

U. H. Kurzweg

U. H. Kurzweg
Professor of Engineering Sciences

I certify that I have read this study and that in my opinion it conforms to acceptable standards of scholarly presentation and is fully adequate, in scope and quality, as a dissertation for the degree of Doctor of Philosophy.

M. H. Clarkson

M. H. Clarkson
Professor of Engineering Sciences

I certify that I have read this study and that in my opinion it conforms to acceptable standards of scholarly presentation and is fully adequate, in scope and quality, as a dissertation for the degree of Doctor of Philosophy.

R. Reed-Hill

R. Reed-Hill
Professor of Materials Science
and Engineering

This dissertation was submitted to the Graduate Faculty of the College of Engineering and to the Graduate School, and was accepted as partial fulfillment of the requirements for the degree of Doctor of Philosophy.

December 1984

Herbert A. Beaver

Dean, College of Engineering

Dean for Graduate Studies
and Research